REACH-SCALE CONTROLS OF A POOL-RAPID CHANNEL DURING AN EXTREME FLOOD EVENT: SABIE RIVER, SOUTH AFRICA

Simon Edmund SHERRINGTON

School of Environment and Life Sciences,
University of Salford, Salford, UK

Submitted in Partial Fulfilment of the
Requirements of the Degree of Master of Science
by Research, March 2016

List of Contents

List of figures

List of tables

Acknowledgements

I would first of all like to thank my supervisor Dr. Neil Entwistle, who has supported me throughout my entire period in higher education, displaying honest advice, fairness with feedback and showing a great amount of patience with me, which I know can be extremely testing even to the calmest of personnel. I would also like to thank him for convincing me to attend the AGU fall meeting in San Francisco, which not only broadened my mind to different methods that could be used in my own work but also in future projects. The food was terrific as well! I would also like to thank the research team at the Kruger National Park for allowing me to use the Lidar data collected on the Sabie River and JBA Consulting for JFlow outputs. Additionally I would also wish to thank Claire Bitthal of JBA Consulting Ltd for implementing the JFlow model.

I would also like to thank Prof. David Collins for his support and advice. His advice enabled me to question everything and really made me think outside the box. I would also like to thank him for the help he gave me between my undergraduate and postgraduate courses, as I would not have survived without him. I would also like to thank him for lending me money on the last day in San Francisco as the bank blocked my card… typical.

Acknowledgements that are more personal include my parents, whose unquestioned love and support made it possible to have the confidence to quit my dead-end call centre job and go for a degree in the first place. They also gave me the support to do my postgraduate both through advice and finances; I definitely would not have been able to do this without them. I would additionally like to thank my father for helping me proofread my work, which was challenging but necessary.

To all my friends and family who I have annoyed for nearly three years saying, thank you for all your support and I can safely say I'm done… for now.

Declaration

I certify that this thesis consist of my own original work. All quotations from published and unpublished sources are acknowledged as such in the text. Material derived from other sources is also indicated.

Total number of words: 16249

Name: Simon E. Sherrington

Signature: _____

Date: _____

For Mum and Dad

“Run when you can, walk if you have to, crawl if you must; just never give up”

- Dean Karnazes

Abstract

The Sabie River exhibits a unique macrochannel incised 10 – 20 m into the Cainozoic planar surface, producing a mixed-bedrock-alluvial system draining a semi-arid catchment of 7096 km^2. The channel sequences between bedrock outcrops alternating with alluvial features and are influenced by rare, high magnitude flood events, which act as a major control to riparian landscape maintenance. Pool-rapid channels found in the Sabie River are particularly influenced by large floods because of their vulnerability to both sedimentation and scour brought on by non-uniform hydraulics. Through an aerial LiDAR survey within Kruger National Park, Mpumalanga, 50km of 1 m spatial data were investigated to isolate a single reach consisting of a pool-rapid channel and an anastomosing channel immediately upstream. These data were used to create a 2D flow model (JFlow) simulating high magnitude discharge scenarios up to ~5000 m^3s^{-1}, incorporated with post-processed spatial data including channel velocity, depth, water surface elevations. Further analysis occurred through the development of spatial models comprised of Froude numbers and bed shear stress. In addition, observations of time sequenced aerial photographs involving multiple channels similar to and including the study area were scrutinised for obvious alterations in morphology following both Cyclone's Eline and Dando. Model outputs indicate comparably reduced longitudinal flow velocity, Froude and bed shear stress as flow passes through an area of increased gradient of the anastomosing channel prior to the pool-rapid during increased discharge. Substantial rises in cross-sectional area following the upstream pool-rapid boundary (control point one) as a result of island networks becoming submerged, greatly influenced Froude numbers and bed shear stress as macro-channel settings within this area allowed floodwater to spread much wider than elsewhere in the reach. Further downstream at subsequent control points representative of individual rapid units, channel hydraulics displayed an irregular template of relative highs and lows associated with differential slope and geometric characteristics at each control point. Geometric settings situated both upstream and downstream of each control point also influenced the hydraulic nature of the channel during extreme discharge, in addition to other features associated with the channel (e.g. tributary confluences and alluvial bedforms). Geomorphic response is mixed because of such irregular hydraulics, however deposition is much more prevalent, with progressive aggradation occurring years following 2012's Cyclone Dando as seen in photography leading up to 2015. Such conditions allow for areas of refugia for riparian species such as *Combretum erythrophyllum* (River Bushwillow) to develop, enabling pool-rapids in the Sabie River to possess a unique platform for riparian habitat recovery.

1. Introduction

Determination of river channel form depends on two external controls; gravity and flow resistance (Leopold *et al.,* 1964), with documentation of such controls mostly focussed upon temperate perennial-alluvial channels (Heritage *et al.,* 1999; Heitmuller *et al*., 2015). Despite their commonality, literature-outlining controls upon bedrock-alluvial channels are in stark contrast to temperate perennial-alluvial systems (Ashley *et al.,* 1988; Howard *et al*., 1994; Meshkova and Carling, 2012), however bedrock-alluvial rivers can be found throughout each continent including: Colorado River, USA; Narmada River, India; Burdekin Gorge, Australia; Nahal Paran, Israel and River Sabie, South Africa (Heritage *et al*., 1999).

Mixed bedrock-alluvial channels differ to temperate perennial-alluvial systems as they consist of exposed ancient bedrock substratum with a discontinuous coating of alluvium as seen in figure 1.1 (Howard *et al*., 1994; Nittrouer *et al*., 2011). Commonly structured on a channel-in-channel basis (Gupta *et al*., 1999), a mixed-bedrock alluvial system's active channel evolution is restricted within a larger macrochannel (Van Niekerk *et al*., 1999). As limitations in lateral migration of active channels occur within resistant bedrock walls, erosion of bedrock-alluvial channels take place through exploitation of joints and fractures within the primary channel (Tooth and McCarthy, 2004; Heitmuller *et al*., 2015). Consequently, substratum erosion within the macrochannel produced diverse expanses of alluvium that fully covered areas of bedrock (Heritage *et al*., 2000), which once mobilised, contributes further to active channel development through plucking and abrasion actions (Howard, 1998). Therefore, combinations of both lithological controls (bedrock channels) and sediment-transport processes (alluvial channels) dominate geomorphic settings found at mixed bedrock-alluvial channels (Ashley *et al*., 1988).

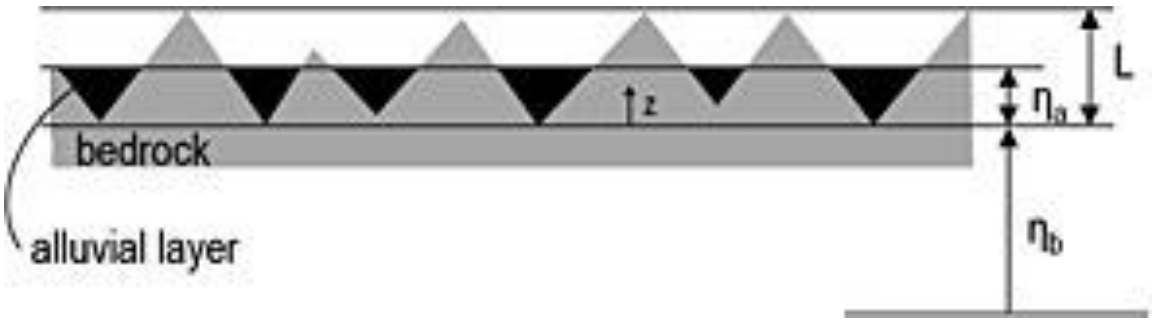

Figure 1.1. Definition diagram of a mixed bedrock-alluvial channel, here η_a is the alluvial layer thickness, L is bedrock macroroughness height, η_b is the bottom surface bedrock elevation, Z is above the bottom of the bedrock (Inoue et al., 2014).

Through a combination of lateral confinement and irregular, yet progressive alluviation found at mixed bedrock-alluvial channels such as River Sabie, a continuum of channel types range from entirely bedrock to fully alluvial units (Ashley *et al*., 1988; Heritage *et al*., 2000). Multiple channel types arise because of resistant bedrock outcrops that steepen subsequent regions of the macrochannel (Van Niekerk *et al*., 1999), whilst increased joint and fracture exploitation during alternative flow settings produce numerous channel pathways (Tooth and McCarthy, 2004). Through such diversity in channel units and their specific wetted perimeter, mixed bedrock alluvial networks became associated with channel types such as, anastomosing, braided, single-thread and pool-rapids (Moon *et al*., 1997).

Mixed bedrock-alluvial systems found mostly in semi-arid environments are heavily influenced by seasonal high flows, as well as much lower frequency high-magnitude flood events (Van Niekerk *et al*., 1999). Deeply cut and confined settings found at macrochannels typical of bedrock-alluvial rivers restrict floodwater, thus velocity and depth significantly increased producing extreme levels of flood power (Kale *et al*., 1994). Influences of high-magnitude flood events translate as phases of sedimentation and stripping of softer sediments (Rountree *et al*., 2001), thus, mixed bedrock-alluvial channels found in semi-arid regions reveal sharp sensitivity towards local climate variation (Yair and Kossovsky, 2002).

High-magnitude floods that completely fill a macrochannel are comparatively rare therefore difficult to observe, with investigations into sediment mobility thresholds at Sandy Creek Gorge, SE Central Australia demonstrated that flows capable of filling the channel and reformatting its structure could be spaced by several centuries (Jansen, 2006). Further to the evidence provided by Jansen (2006), multiple authors (Baker and Pickup, 1987; Whittaker, 1987; Grant *et al*., 1990) concluded that high-magnitude flood events capable of reworking mixed bedrock-alluvial channels through substantial levels of discharge generally have a reoccurrence interval of 50 - 100 years. However, exceptions to this include River Sabie where two extreme floods occurred within 12 years, which due to the river's immense size, flows capable of filling its macrochannel would need to be in excess of 3000 m^3s^{-1} (Van Niekerk *et al*., 1999).

Flow conditions at extreme flood events are important to channel evolution at systems such as River Sabie as they control both bedrock and alluvial reaches (Gupta *et al*., 1999). Strong flow conditions produced during high-magnitude floods potentially restructure bedforms located within reaches comprised of exposed substratum through wear (Tinkler, 1993), with examples found following Cyclone Eline (February, 2000), which returned to a basic configuration of exposed lithological templates previously seen after a flood event in 1996 (Rountree *et al*., 2001). Events such as Cyclone Eline are very important to the evolution of active channels found at mixed bedrock-alluvial rivers, however, they are also detrimental to short-term biodiversity through destruction of fully developed riparian habitats (Parsons *et al*., 2005).

1.1. Pool-Rapids

Historical research at River Sabie focused mostly upon anastomosed channels, including research involving their morphology and hydrodynamics (Van Niekerk *et al*., 1999), hydraulic control and sediment distribution (Entwistle *et al*., 2014), and observations of stage-discharge relationships found within them (Broadhurst and Heritage, 1998). Whilst other research involved general analysis of channel types within the River Sabie including, geomorphic classifications of channel types (Van Niekerk *et al*., 1995), comparative examinations on high-magnitude flood impacts on channel types (Heritage *et al*., 2001; Heritage *et al*., 2014), and linkages between channel type and riparian vegetation (Van coller *et al*., 2000). Therefore, this thesis will focus upon the knowledge gap regarding pool-rapids at the Sabie River and its controls upon hydraulics during a high-magnitude flood event.

A pool-rapid is characteristically consistent with multiple backwater pools separated by shallow and steep bedrock dominated rapids (Van Niekerk *et al*., 1995; Parsons *et al*., 2005). Leopold's (1969) documentation of pool-rapids found throughout the Colorado River found at the Grand Canyon originally described them as stepped channels as seen in figure 1.2, although as simple as this definition seems, pool-rapids are more complex than one would anticipate. Further analysis of River Sabie's pool-rapid channels highlighted their diverse geomorphic template consistent with additional bedrock and alluvial features (Heritage *et al*., 1999).

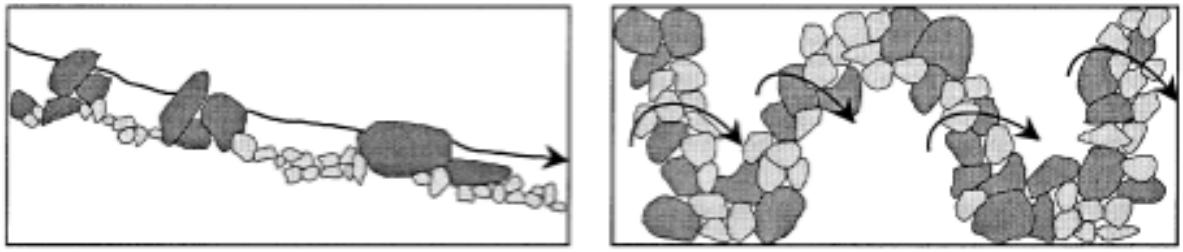

Figure 1.2. Stepped channel sequence typical of those found at pool-rapids (Halwas and Church, 2002).

Geomorphic rapids consist of ribs approximately positioned perpendicular to a given channel (Grant *et al*., 1990; Charlton, 2007), which are generally large and potentially numerous enough to break water surface (Graf, 1979). Rapid composition is dependent on the channel itself with alluvial pathways comprised of coarse cobbles and boulders, or through irregularities found in channel lithology (Halwas and Church, 2002), with evidence from the Sabie River indicated that mixed bedrock-alluvial channels contained rapids of either setting. However, in contrast, the Colorado River contains over 400 rapid channels each comprised of large boulder deposits (Graf, 1978), which occur through tributary flash floods, pre-historic boulder bars and mass-movement of coarse sediment (Graf, 1980). Therefore, Colorado River's pool-rapid channels differ considerably to those found at River Sabie, which despite evidence suggesting the presence of boulder rapids at the latter, it remains more commonly associated with rapids derived from knickpoints within the ancient substratum (Phillips *et al*., 2010).

Bedrock channel rapids are a product of relative hard rock surfaces exposed through sediment removal during a flood (Van Coller *et al*., 1997), where channel lithology is a common and major aspect of rapid development and river erosion in bedrock systems (Ortega *et al*., 2014). Rapids developed through lithological irregularities owe their development to exposed igneous intrusions, paleo-lava flows or metamorphic protuberances that act as a barrier against flow, breaking water surfaces through constriction (Maner, 2010; Van Hinsberg *et al*.,

2010; Meshkova and Carling, 2012). As a result, knickpoints associated with rapids at bedrock channels produce locally abrupt and steepened gradients on the channel's long profile (Crosby and Whipple, 2006; Phillips *et al*., 2010).

Rapids remain a geometrically smaller physical feature within the overall pool-rapid channel (Heritage *et al*., 1999), whilst pools are features associated with distinct geomorphic and hydraulic characteristics. Generally, pools consist of tranquil flow lacking in free surface instability due to their lower gradients (Graf, 1979; Grant *et al*., 1990; Moon and Heritage, 2001), which contrast to more turbulent and rapid flows typical of a rapid's slope characteristics. Pools are also consistent with minimal visibility of coarse material at low flow dissimilar to adjacent rapid channels, where exposed sediment contributes to its broken water surfaces (Death and Joy, 2004).

Pool development results from local interactions between flow and sediment transport (Montgomery *et* al., 1995), with Moon (1939) describing pools as habitats associated with deposition. However, erosion within the active channel can also develop settings favourable to a pool (Frissel *et al*., 1986). The majority of obstructions along a fluvial system (for example, bedrock outcrops, larger boulders, large woody debris, etc.) can create flow convergence, resulting in a heavily scoured channel bed or a plunge pool as seen in figure 1.3 (Montgomery *et al*., 1995). Contrary to arguments describing a pool consisting of tranquil flow (Grant *et al*., 1990), pools can inherent higher velocities immediately downstream of rapids (Bisson *et al.*, 1982). Minor units such as plunge pools tend to consist of a varied substrate, with deeper water located immediately after a rapid consistent with higher velocities that gradually becoming shallower with sediment accumulation (Halwas and Church, 2002). The river Sabie is a great example of sedimentation presented within pool

environments, as pools there display a diverse range of alluvial features from medial to laterally deposited bars (Heritage *et al*., 1999).

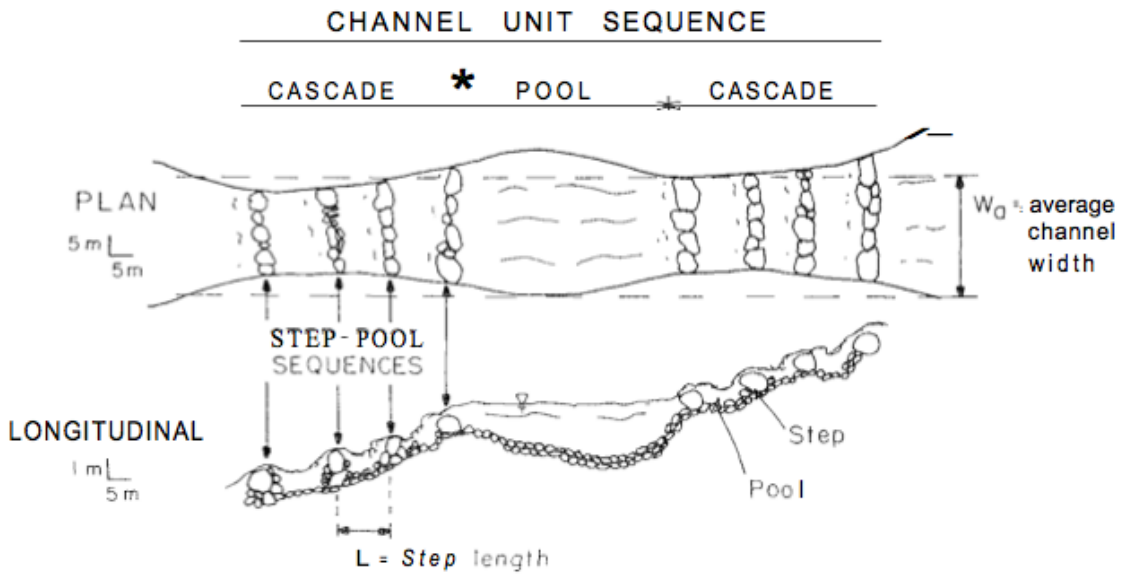

Figure 1.3. Alternative schematic of a stepped channel consistent with plunge pools between each outcrop, whilst the pool begins with a plunge pool but progressively builds up as it approaches another rapid section (Grant et al., 1990).

General analysis on pool-rapid characteristics are analogous to riffle-pool channels coherent with gravel-bed rivers (Graf, 1978), with both channel types showing similar turbulence patterns over comparatively shallow and resistant strata adjacent to neighbouring deeper pools (Lisle, 1982; Busulwas and Bailey, 2004). Some rapid types also share similarities with riffles including their slope and geomorphic characteristics as seen in figure 1.4 (Chin, 2002), as Richards (1976) identified that pool-riffles consist of similar topographic settings as pool-rapids consistent of both positive (riffles) and negative (pools) residual profiles. In addition, both rapids and riffles are of vital importance to ecology, as they provide oxygenation to a given channel through flow turbulence (Busulwa and Bailey, 2004). Despite their similarities, differences occur between both channel types as coarse sediment placement is more organised within rapids than riffles as also seen in figure 1.4 (Grant *et al*., 1990). Whilst Grant et al

(1990) also highlighted significant size differences between riffles and rapids, with the latter consisting of much higher volumes of surface area (~15 – 50%).

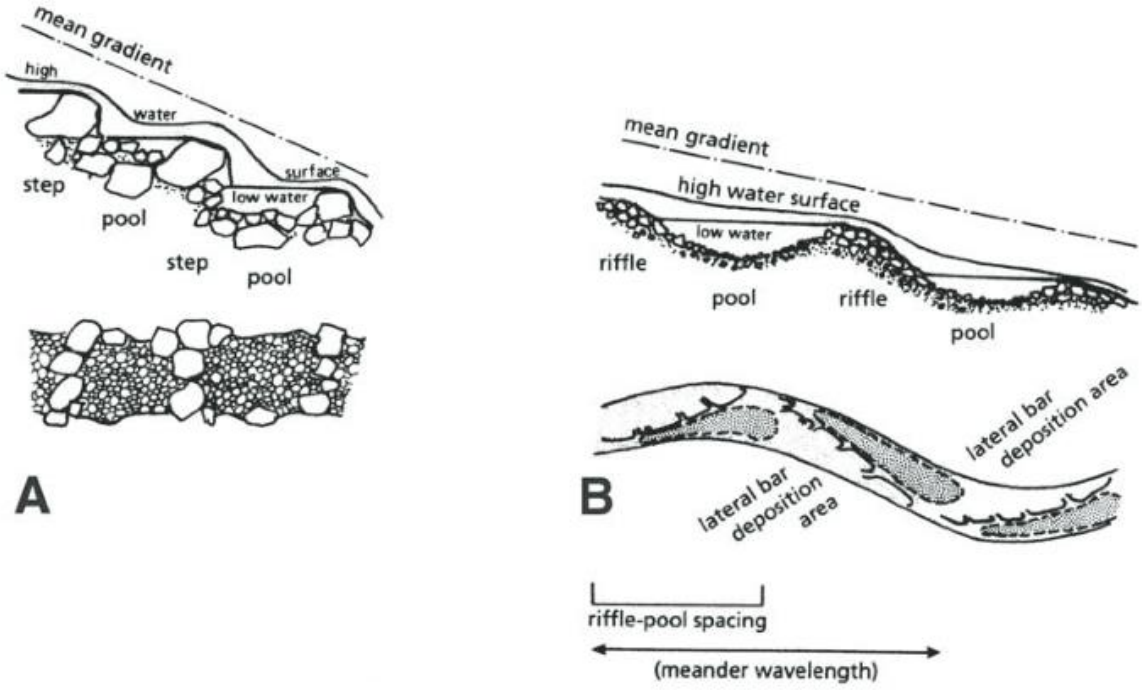

Figure 1.4. Step-pool/ pool-rapid (A) and Pool-riffle (B) morphologies (Church, 1992).

1.2. Aims of Thesis

Very limited literature exists to investigate pool-rapid channels and relate them to other channel types, for example anastomosing channels. This lack of research is the focus for this thesis, where the overarching aim is to expand knowledge concerning pool-rapid hydraulic controls and channel form. The geographic location for this research is the Sabie River, in the Kruger National Park, South Africa. Hydraulic controls are investigated following a high magnitude flood event (cyclone Dando). To address the overarching aim of this research, several objectives are investigated (as listed in table 1.1).

Table 1.1. Objectives addressing the predominant aim of this thesis.

	Core Scientific Objectives	Method	Reference chapter (s)
Objective 1	Validate a two-dimension simulation model of the River Sabie reach to facilitate the thesis research.	Analyse differences in distance between simulated water surface extent and field derived dGPS points.	4
Objective 2.	Analyse pool-rapid and anastomosed geomorphic form changes following cyclone-driven flood events through aerial photography.	Observe changes to channel form through time series schematics, of before and progressively after cyclone events (cyclone Eline and Dando).	5, 6
Objective 3	Investigate pool-rapid and anastomosed hydraulic response following a high-magnitude flood event through simulation.	Analyse two-dimensional river simulation models of alternative variables during progressive discharge scenarios.	5, 6
Objective 4	Scrutinise topographical conditions found at a pool-rapid channel and the influence on hydraulics during a high-magnitude flood event.	Combined analysis of two-dimensional river simulations and one-dimensional models at individual control points during differing discharge scenarios.	4, 5, 6
Objective 5	Investigate how active channel geometry influences hydraulics throughout a pool-rapid during floods displaying extreme levels of discharge.	Scrutinise two-dimensional river simulation models and one-dimensional cross-sections at progressive discharge scenarios.	4, 5, 6
Objective 6	Develop a conceptual model of how the pool-rapid and anastomosing reaches respond hydraulic control and the influence on geomorphic change.	Through findings associated with previous objectives, develop a plan view and cross-sectional model consistent of geomorphic changes at differential stages of an extreme flood.	6

1.3. Layout of thesis

The stimulus behind how this thesis's structure is based on the type of data used for analysis as seen in figure 1.5, with separate chapters and sections placed within a traditional results-discussion-conclusion layout for photographic evidence. Further separation regarding hydraulic changes occurred within the results dependent on variables used their relation to each other, whilst one-dimensional extractions are set out in both results and methods as a means to display channel settings, before they are combined in the discussion based on influences on hydraulics and linkages between hydraulic changes and geomorphic response to flooding.

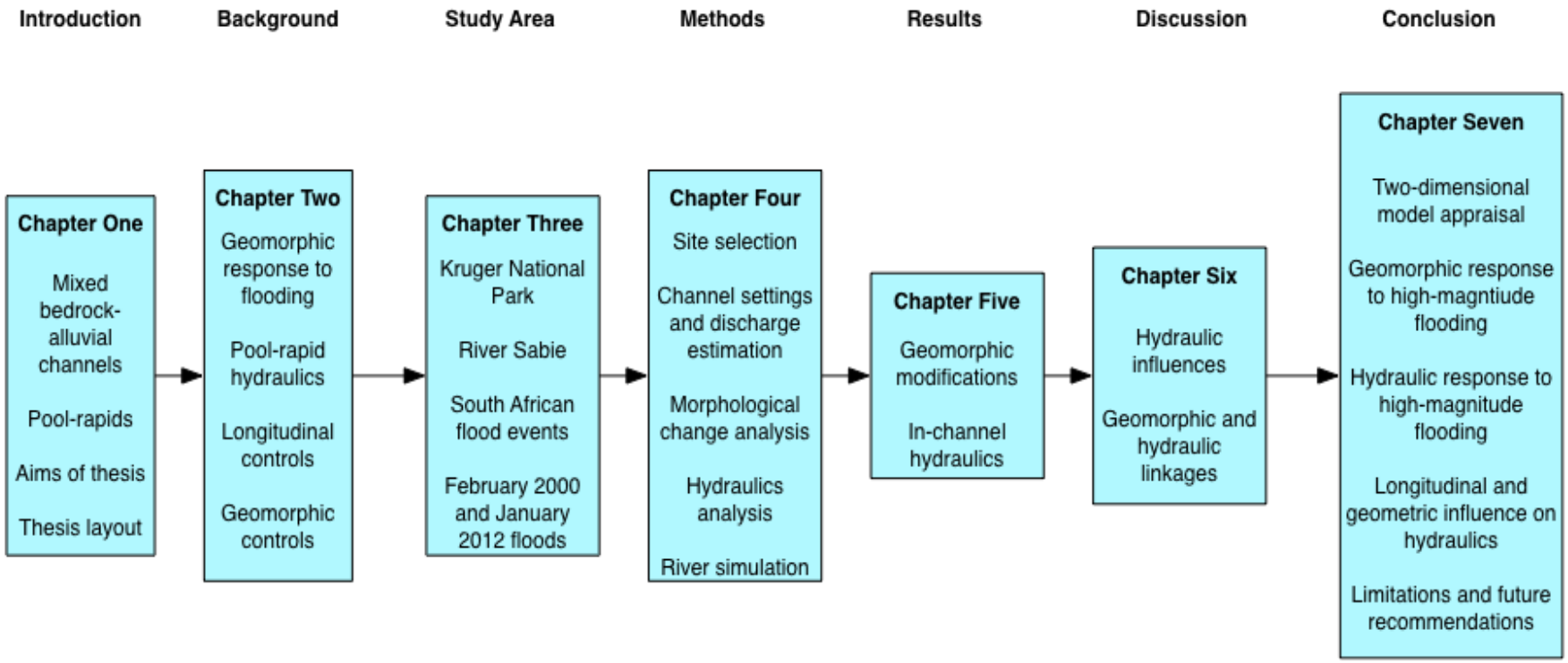

Figure 1.5. Layout of thesis including chapters that address objectives set in table 1.1.

2. Background

This current chapter involved a review of literature regarding pool-rapids and how they relate to objectives set for research on the Sabie River. Initial discussions involved the geomorphic response of pool-rapids following periods of flooding (section 2.1), which is then followed by a detailed review on literature regarding hydraulics found at pool-rapids (section 2.2 and 2.3). The review of literature based upon hydraulics found within a pool-rapid occurred in two alternate sections, with section 2.2 giving a background on general hydraulics found at pool-rapids including longitudinal (section 2.2.1) and geometric controls (section 2.2.2), whilst 2.3 discussed how those hydraulics altered during a flood.

2.1. Flood impacts on pool-rapid geomorphology

As literature on pool-rapids is sparse, difficulties arise in addressing the physical controls on erosional processes found acting upon them (Lamb and Dietrich, 2004), however, such literature revealed how stream power typical of a high magnitude flood strips finer sediment and transports coarse boulders (Baker, 1984; Charlton, 2007). Mobilisation of such uncohesive sediments occurred because critical shear stress acted upon the channel as stream power and flow resistance reach equilibrium (Knighton, 1998). Fine sediment entrainment was also evident at pool-rapids within the Sabie River, as Parsons *et al*. (2005) and Heritage *et al*. (2001) detailed changes to geomorphic units in the form of loose sediment removal at their steeper segments (i.e. rapids). These high-gradient segments have an increased possibility of sediment entrainment as shear stresses, which is a product of channel velocity and bed gradient, are typically higher at rapids (Kirchner *et al.*, 1990). Further investigations into Southern African river systems, with emphasis on palaeo-channels by Hattingh and Rust (1999), also determined that loose sediment removal was common following extreme flood events, which lead to steeper gradients favourable to rapid units. In addition to fine sediments

and coarse clasts, which are found at pool-rapids being subjected to critical shear stresses (Baker and Kale, 1998), particularly those that remain unprotected by riparian vegetation such as common reeds at the Sabie River (Tooth, 2000; Van Coller *et al.*, 2000).

Rapids are durable during a flood event despite removal of loose sediment previously located on top of them, with only high-magnitude flooding leaving any remnants of change due to a rapids tolerance towards increased stream power (Gupta *et al*., 1999). In regards to the River Sabie, destruction of ribs associated with pool-rapids are not documented, with changes to them only occurring in relation to the removal or deposition of soft sediment following a high magnitude flood event (Heritage *et al*., 2014). Additionally, Leopold (1969) and Graf (1979) hypothesised that rapids were almost permanent features, whilst Graf (1979) discussed the durability of rapid channels, as research from Colorado River exhibited their persistence through erosive processes associated with relatively high-magnitude floods.

Pools were also significantly affected by stream power typical of large flood events, for example Leopold (1969) highlighted how deep scours associated with pools found immediately downstream of rapids developed during peak flows. Plunge pool development could also be associated with macro-turbulent plucking of bedrock fractures associated with flows representative of high-magnitude floods (Bretz, 1924; Meshkova and Carling, 2002). Other types of pools also displayed evidence of erosion to alluvial features situated within them, as Parsons *et al*. (2006) found concentrations of uncohesive sediment removal at areas of general deposition within pool-rapid channels at the Sabie River. Despite sediment removal at alluvial features such as bars and islands during a high-magnitude flood, most of these features remained relatively stable, with erosion almost solely occurring at poorly vegetated bedforms (Heritage *et al*., 2004).

Deposition, as well as erosion is a key response to high-magnitude flood events, particularly during latter stages of the flood (i.e. a flood hydrograph's falling limb), for example mixed-bedrock alluvial channels displayed sedimentation as flows associated with flood events began to reduce (Leopold, 1969; Gupta *et al.,* 1999; Van Niekerk *et al*., 1999). In relation to rapids, deposition also occurred as discharge fell, particularly in regions of tranquil flow found at pools downstream of them (Torrente-vilara, 2011). Findings of uncohesive sediment accumulation were also frequently evident along a 50 km reach of River Sabie following cyclone Dando in 2012 (Heritage *et al*., 2014), with a number of pool-rapids experiencing mass deposition that transformed them to alluvial-braided channels (Parsons *et al*, 2006). Therefore, pool-rapids did not display a singular response to flooding at the Sabie River but demonstrated a dynamic retort dependant on conditions present within each specific reach (Heritage *et al*., 2004).

2.2. Pool-rapid hydraulics

The irregular physical structure (i.e. varied gradients) of pool-rapids produced hydraulics rarely seen elsewhere within a river system, as Maddock *et al*. (2005) described them as channels characterised by stretches of regulated, almost tranquil flows (pools) interjected by unregulated, turbulent waters (rapids). Such a highly varied hydraulic template is mostly visible during periods of low to intermediate flow (Church, 2002), where rapids displayed increased flows translated through broken and undulating wave features consistent of increased water surface turbulence (Wadeson and Rountree, 1998; Pastuchova *et al*., 2010). Contrasting to rapids, pools are comprised of relatively flatter, unbroken water surfaces occurring over a greater distance (Magirl *et al*., 2005), however they can still consist of increased flow through upstream rapids (Bisson *et al*, 1982; Azzelino and Vismara, 2001).

Diverse water surface conditions that include varied gradients and turbulence aid to distinguish pool-rapid morphology that serves as a critical influence on river systems because of their ability to regulate flow resistance (Lamarre and Roy, 2008). Flow resistance serves as key control throughout pool-rapids at the Sabie River (Heritage, Moon *et al*., 2004), as diverse interchanges found between flow resistance characteristics enabled pool-rapids to display such a varied hydraulic and physical template. Rapids generally displayed greater flow resistance than pools, as evidence produced by both Moon *et al*. (2001) and Zimmermann and Church (2002) exhibited increased water surface turbulence because of higher levels of flow resistance within small mountain stepped channels. However, increased flow resistance is also present within much larger bedrock-alluvial channels (Halwas and Church, 2002), with Heritage *et al*. (2004) demonstrating that bedrock-dominated rapids located at the Sabie River displayed significantly high levels of flow resistance, as a result of outcrops breaking up water surfaces and increasing channel roughness. Research into such flow resistance characteristics found at rapids can be extremely useful, whether resistance is produced at bedrock-dominated rapids such as those at River Sabie or clast derived rapids, as such research acts as a key method in evaluating the stability of a pool-rapid channel (Graf, 1980).

As pool-rapids are consistent with non-uniform hydraulics, variations in channel roughness and flow resistance typical of them can help in keeping their geomorphic structure stable through producing energy dissipation phenomena such as hydraulic jumps as seen in figure 2.1 (Grant, 1997; Heritage *et al*., 2004). A hydraulic jump occurs where flow resistance becomes much greater than adjacent regions of the channel (Pagliera *et al*., 2008), for example, rapids consistent with high levels of flow resistance produce such jumps in water surface (Wohl, 1992).

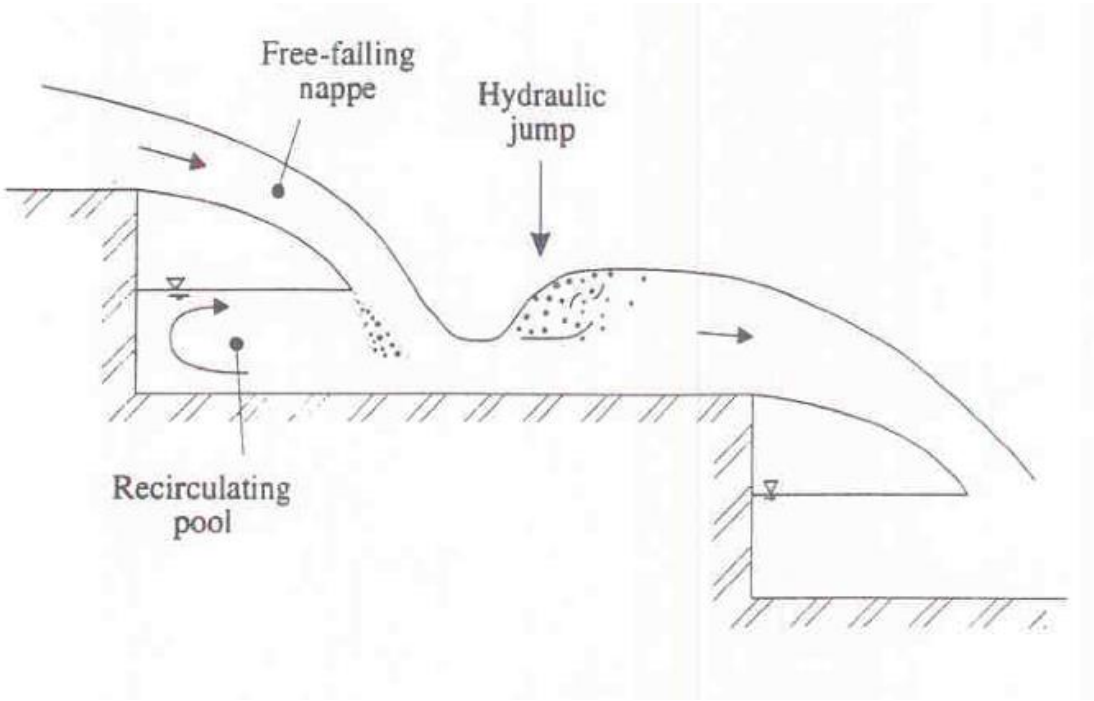

Figure 2.1. Localised flow mechanics within a stepped channel sequence (Chanson, 1996).

Analysis on energy dissipation that aids in stabilising a pool-rapid in the form of hydraulic jumps occurred through Froude numbers, which are representative of dimensionless velocity to depth ratios (Jowett, 1993). Froude numbers are also a precise method in distinguishing the ratio between internal and gravitational forces within flow making them ideal for hydraulic biotope identification (Heritage *et al*., 2010), which have been traditionally difficult to classify are now visible through alternative parameters present within Froude numbers as seen in figure 2.2 (Entwistle *et al*., 2010). In regards to Pool-rapids, particularly those at the Sabie River, hydraulic biotope classification has not occurred, however, pool-rapids found elsewhere demonstrated how their irregular bed topography is key to biotope diversity, specifically during periods of low flow due to the physical restrictions found at them (Heritage *et al*., 2010).

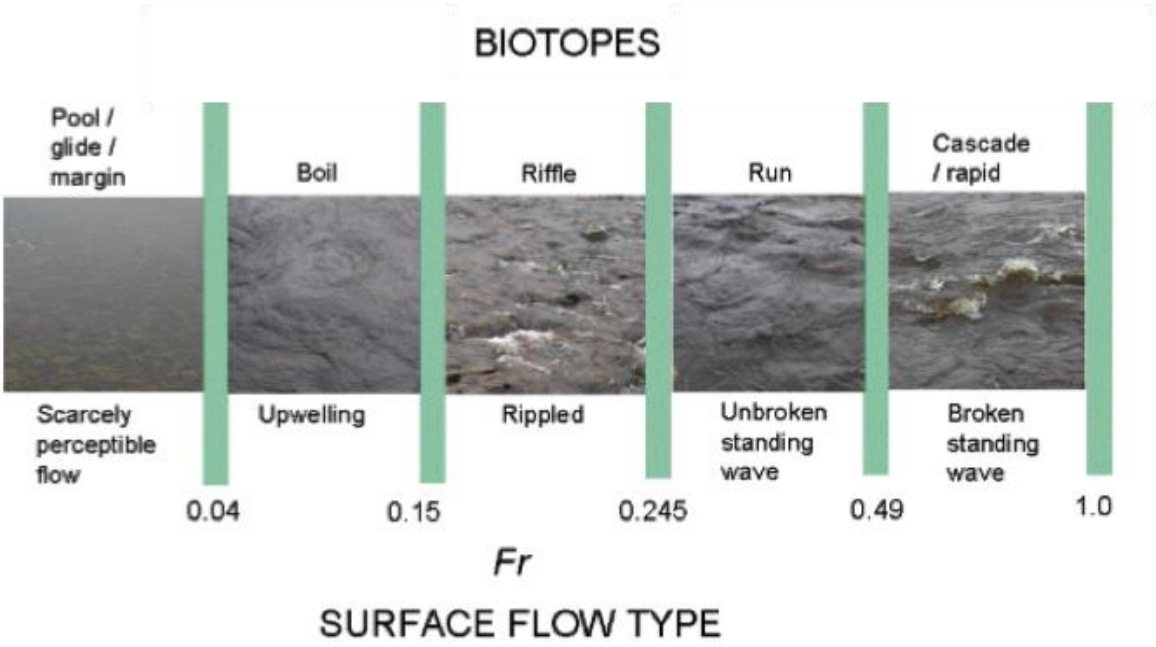

Figure. 2.2. Biotope classifications with altering Froude number (Fr) parameters indicating different biotopes (Entwistle et al., 2010).

2.2.1. Longitudinal controls on pool-rapid maintenance

Grant *et al.* (1990) described how longitudinal relationships found between hydraulic variables are influential at a pool-rapid. Gradient control on flow conditions particularly in pool-rapids can be made visible through Froude number models, Milan *et al*. (2010) found that Froude numbers demonstrated how flow is closely related to gradient found within pool-rapid channels because of their high levels of variation in bed topography. Ultimately due to gradient settings found at pool-rapids, longitudinal controls are instrumental in relation to local hydraulics and the potential for erosion or deposition as gravitational forces determine local stream power (Leopold *et al*., 1964; Kale *et al*., 1996).

In regards to individual channel units found at pool-rapids, longitudinal controls are distinct, for example high gradients found at rapids are consistent with considerably high levels of energy (Moon *et al*., 2001). Control upon hydraulics at rapids occurred as energy availability increased closer to the knickpoint, causing flow to become rapid in nature, therefore being

comprised of high levels of velocity and bed shear stress (Gardner, 1983). Gradient settings found before knickpoints or protuberances found at rapids can also have the opposite effect on flow conditions, for example tranquil flows typical of backwater pools can be a product of a rapid outcrop's ability to act as a natural dam (Gregory and Walling, 1973; Thompson, 2011). Whilst reduced gradients typical of pools immediately downstream of such rapid outcrops also have a significant effect on the energy availability through spill resistance that caused an 80% head loss to local stream power (Grant, 1997; D'Agostini and Michelini, 2015).

2.2.2. Geometric controls on pool-rapid maintenance

Geometric settings, similar to longitudinal controls produced contrasts in local velocity, bed shear stress and water surfaces typical of individual channel units within a pool-rapid; such contrasts are influenced by geometry through inverse relationships between these hydraulic variables and cross-sectional areas (Wohl, 1992; Sawyer *et al*., 2010). In addition to longitudinal influence, geometric settings found at a rapid unit also produced relatively higher levels of velocity and bed shear stress as its shallow and steep structure congested flow towards critical levels (Wohl, 1992; Magirl *et al*., 2005). Convergence of flow is somewhat typical of rapid channels as their relatively low cross-sectional areas maintain high levels in velocity and bed shears stress through considerable stream power (D'Angelo *et al*., 1993; Ferguson and Brierley, 1999). Whilst contrasts in cross-sectional area found commonly at pools resulted in relatively lower values in velocity and bed shear stress as their wider active channel dissipates energy (Leopold *et al*., 1969). Such diverse geometric settings demonstrated throughout literature on pool-rapids potentially give way to the Sabie River, which consists of a similar varied physical template to other pool-rapids in mixed bedrock-alluvial channels, as geomorphic classifications of its pool-rapid channels described them as generally wide-single channels, comprised of elongated pools.

2.3. Flood-induced hydraulics at a pool-rapid

As pool-rapids are consistent of diverse geometric and longitudinal settings, hydraulics typical of each individual channel unit should also remain diverse during a flood (Richards, 1978; Carling, 1991; Thompson *et al*., 1998). However, Heritage *et al.* (2004) discussed how pool-rapid channels found at the Sabie River responded differently at each pool-rapid, Whilst Wilcox *et* al. (2006) and Vieira (2015) demonstrated that flood-induced hydraulics at rapids are influenced by its specific size and gradient.

Evidence of a pool-rapids varied velocity and bed shear stress remained during a flood, as Wohl and Thompson (2000) and Schmidt *et al*., (2001) expressed that general velocity and shear stress models was consistent with rapids made up of higher levels of such than its adjacent pools. Furthermore, Gregory and Walling (1973) discussed how rapid influence increased during a flood, as turbulent and rapid flows found only at knickpoints during low flow expanded as discharge increased.

Flooding can also have a negative impact on hydraulic controls at a pool-rapid, as high-magnitude flows can render their longitudinal influence insignificant by making slopes representative of rapids hidden (Zimmermann and Church, 2001). During extreme flood events, stage can be generally higher than characteristic outcrops making up rapids, thus reducing flow resistance produced by such protuberances (Graf, 1980; Robert, 2011). With reduced resistance, flow can travel freely over once restrictive features present within a pool-rapid (Leopold *et al*., 1964; Wohl and Thomson, 2000), as documented by D'Agostini and Michelini (2015) who found that spill resistance that can reduce head loss to stream power by 80% immediately following a rapid can be halved as stage increased during a flood. Thus, during extreme flood events, longitudinal controls usually prominent within a pool-rapid was

lost, as the distinction between bed shear stress and velocity at each channel unit reduced, therefore, leading to potential deposition as seen following such floods events at the Sabie River (Graf, 1980; Baker and Pickup, 1984; Booker *et al*., 2001).

With increased velocity and water surface elevations, floods also have a significant impact on hydraulic biotope templates found throughout a pool-rapid (Milner and Gilvear, 2012; Zavadil *et al*., 2012), as biotope complexity became progressively reduced as discharge increased, until flow conditions are dominated by larger, less energetic biotopes such as runs (Heritage *et al.,* 2009). Increased flow during a flood enabled energy availability within a channel to remain high, therefore rapid biotopes persist within the channel, however in channels as large and as deeply incised as the Sabie River, potential biotope sequences during floods could replace distinct hydraulic pool-rapid successions with those more typical of deeper waters, such as rapid-runs (Royall and Shoffner, 2008).

3. Study Area

The following describes conditions present within Kruger National Park, where research for this thesis took place in addition to conditions found at the Sabie River. Initial descriptions of Kruger National Park focus on its physical characteristics (i.e. size, border etc.) through narratives on its geological and climatic settings also. Section 3.2 described the Sabie River, including its catchment, route and its underlying geological conditions, whilst Section 3.3 and 3.4 described flood events that occurred their through two cyclone events in 2000 and 2012.

3.1. Kruger National Park

Situated at Mpumalanga in the Lowveld region of South Africa, Kruger National Park (figure 3.1) has been one of Africa's largest areas of wildlife preservation since 1926, where large river channels act as an important region for biodiversity and tourism (Van Wyk and Fairfall, 1969; Moon *et al.* 1997; Van Coller *et al.*, 1997; Eckhardt *et al*., 2000). Measuring at 386 km in length and 40-80 km wide, Kruger National Park covers an estimated area of ~19011 km^2 (Codd, 1951), which is bordered by Crocodile River in the south and Levvuhu river to the north (Van Wyk and Fairfell, 1969).

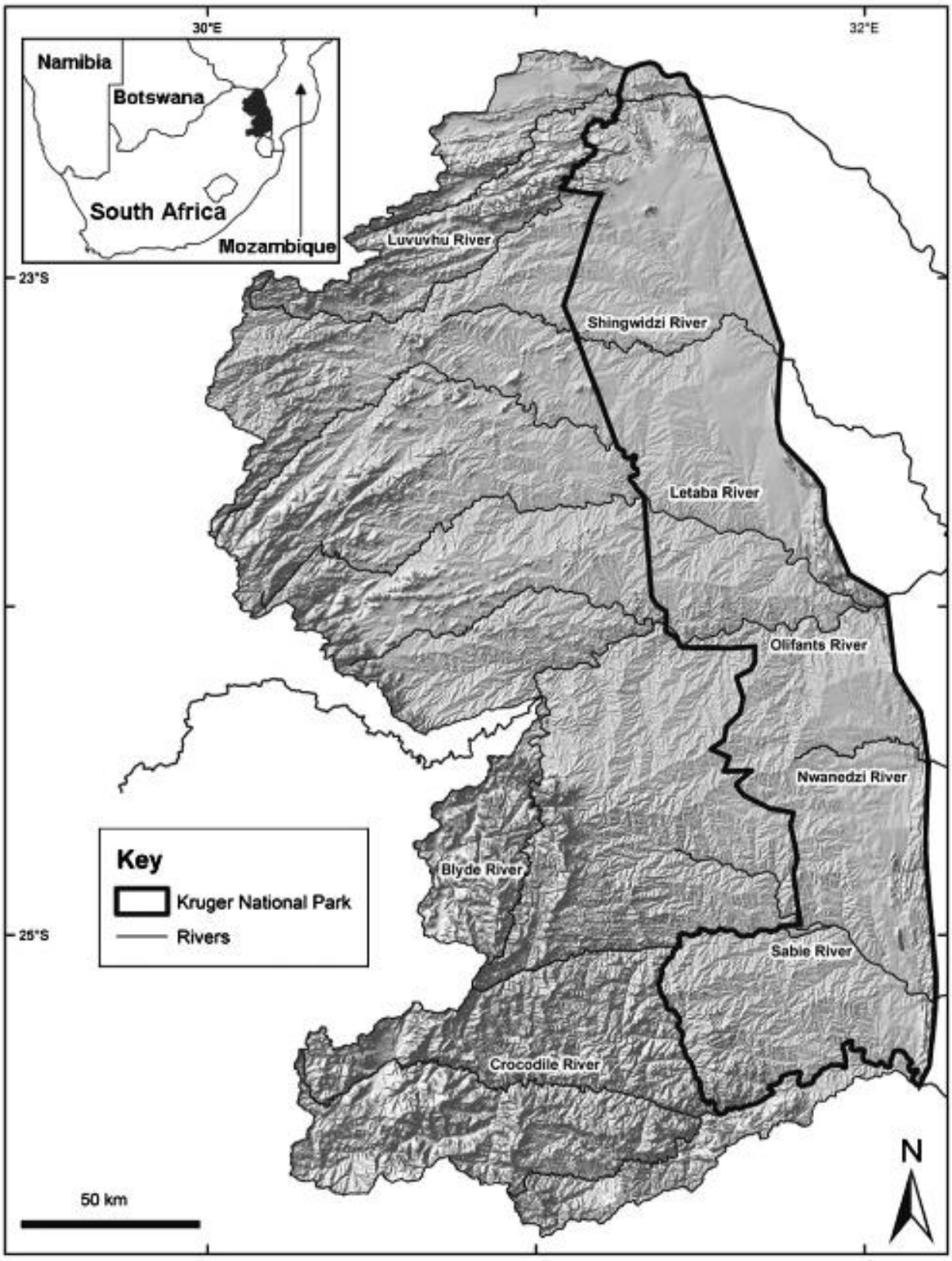

Figure 3.1. ***Kruger National Park and its river channels, with inset displaying the location of Kruger National Park within South Africa (Roux et al., 2008).***

Consistent with a varied topography, Kruger National Park displays mountainous landscapes in the west and accompanied by low-lying conditions towards the east, marked by a reef of subterranean sandstone (Van Wyk, and Fairfell, 1969). An outstanding feature found at Kruger National Park is the Lebombo Mountain range initiating from the River Shingwezi and traversing in a southerly direction along the Mozambique border (Schutte, 1986).

Geological conditions at Kruger National Park are highly diverse, with multiple rock types identified throughout figure 3.2. The park's Lowveld region is composed of granite, gneiss, schists, amphibolites, sediments, basalt and gabbros (Schutte, 1986), whilst additional rock sequences found in the area include alternative igneous rock types comprised of felsic and mafic qualities (Venter, 1986), as well as six Granitoid variants (Barton *et al.*, 1986). Sedimentary rock types are also present at Kruger National Park, including argillaceous rocks such as grey mudstone, shale, micaceous sand-and-siltstones and arenaceous rock-types composed of sandstones and quartzite (Venter, 1986). Kruger National Park is also rich in alluvium deposits and deep sandy soils, derived from sediments that date more recently than adjacent rock types more commonly representative of pre-Cambrian periods, whilst alternative sediment (i.e. alluvium deposits) date from both Tertiary and Quaternary periods (Venter, 1986).

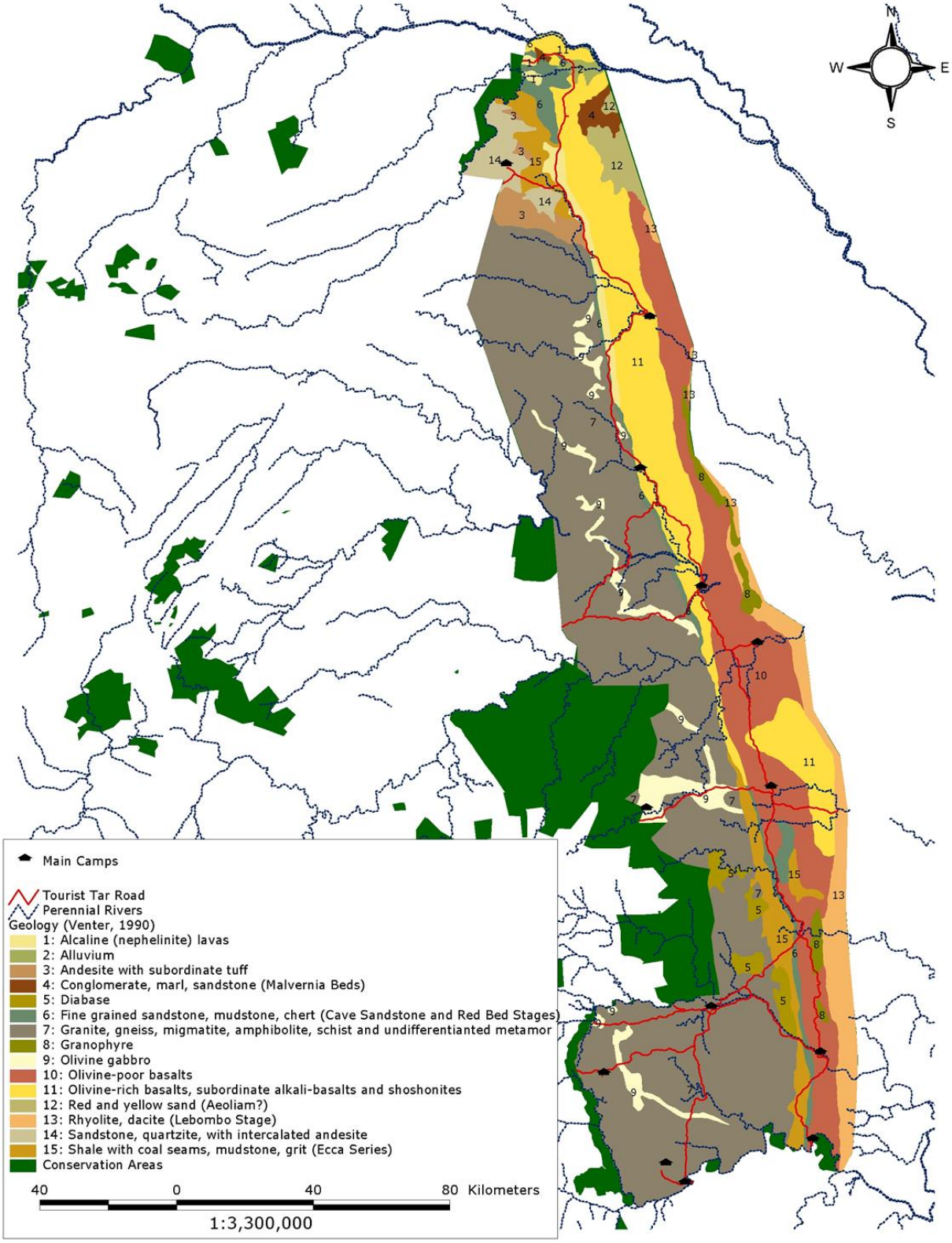

Figure. 3.2. Geological Map of Kruger National Park (Venter, 1990).

South Africa is characteristically high variability in rainfall seen through intraseasonal and interannual observations (Reason *et al.,* 2005), as precipitation at Kruger National Park varies between hot, humid and tropical conditions during summer months (December to February) consistent of precipatory peaks associated with cyclone events (Venter and Gertenbach, 1989; Codron *et al*., 1979). Whilst dry, mild, semi-arid settings associated with average rainfall of just 25mm during winter periods (June to September) (Coatzee *et al.* 1979; Venter and Gertenbach, 1986). Rainfall patterns vary throughout the park from North to South, as seen in figure 3.3 (Venter and Gertenbach, 1986), as Kruger National Park's geographic locality places it between two alternative climatic zones, both divided by the Olifants River. South of Olifants more humid conditions present an average annual rainfall between 500-700mma^{-1}; comparatively north of Olifants is more arid, with rainfall measuring between 300-500mma^{-1} (Codron *et al.* 2006). Monthly conditions also vary with Austral summer months of November to March experiencing considerably higher levels of precipitation (Codron *et al.,* 2006).

Variations in precipitation are also distinct at the Sabie River depending on the time of year and location, with highs mostly occurring within summer months (Moon *et al.* 1997; Heritage *et al.,* 2004). Rainfall collection ranges from 2000mma^{-1} in high altitude areas to 400mma^{-1} near the border of Mozambique (Moon *et al.* 1997). Some active channels found at the River Sabie can flow throughout the year, with winter flow inputs attributed to dolomitic aquifers found in mountainous areas upstream albeit such flow conditions are minimal (Heritage *et al.,* 2004).

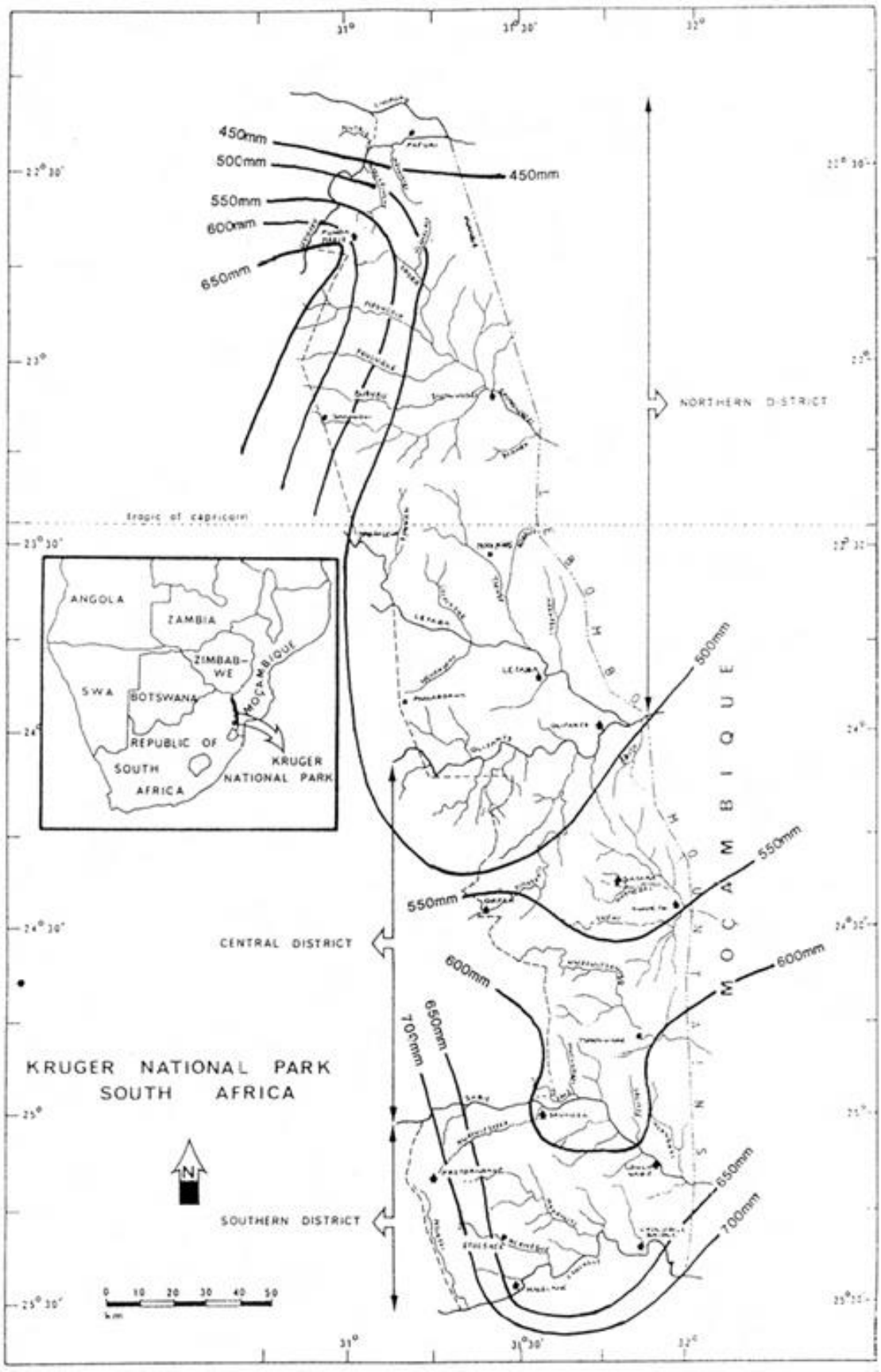

Figure 3.3. Rainfall map of Kruger National Park (Venter and Gertenbach, 1986).

3.2. River Sabie

The Sabie River drains a catchment area of 7096 km^2 before joining up with the Limpopo River in Mozambique (figure 3.2.1), with 6252 km^2 of Sabie's catchment located within South Africa (Moon *et al.,* 1997; Heritage *et al.,* 2004). The River Sabie's source rises in the high mountainous region of Drakensberg found at 1600 m.a.s.l, flowing down to Kruger National Park's Lowveld region at 400 m.a.s.l, until finally descending on to Lebombo at 200 m.a.s.l (Heritage *et al.,* 2004).

The river Sabie is characterised by an incised macrochannel that encloses alluvial deposits, riparian vegetation and areas of dominant bedrock features (Heritage, e*t al.,* 2001), with underlying geology comprised of multiple examples of sedimentary, metamorphic and igneous rock types incorporating both extrusive and intrusive structures (Heritage *et al.,* 2004). Within Kruger National Park, River Sabie runs over the Karro Sequence that consists of sandstones, basalts, rhyolites, and granitic basement rocks (Moon *et al.* 1997). Lithological controls on the Sabie River's longitudinal profile have evidently caused alterations in geomorphic form, enabling the river to consist of a multiple channel types such as a anastomosing and pool-rapids (Heritage *et al.,* 2004).

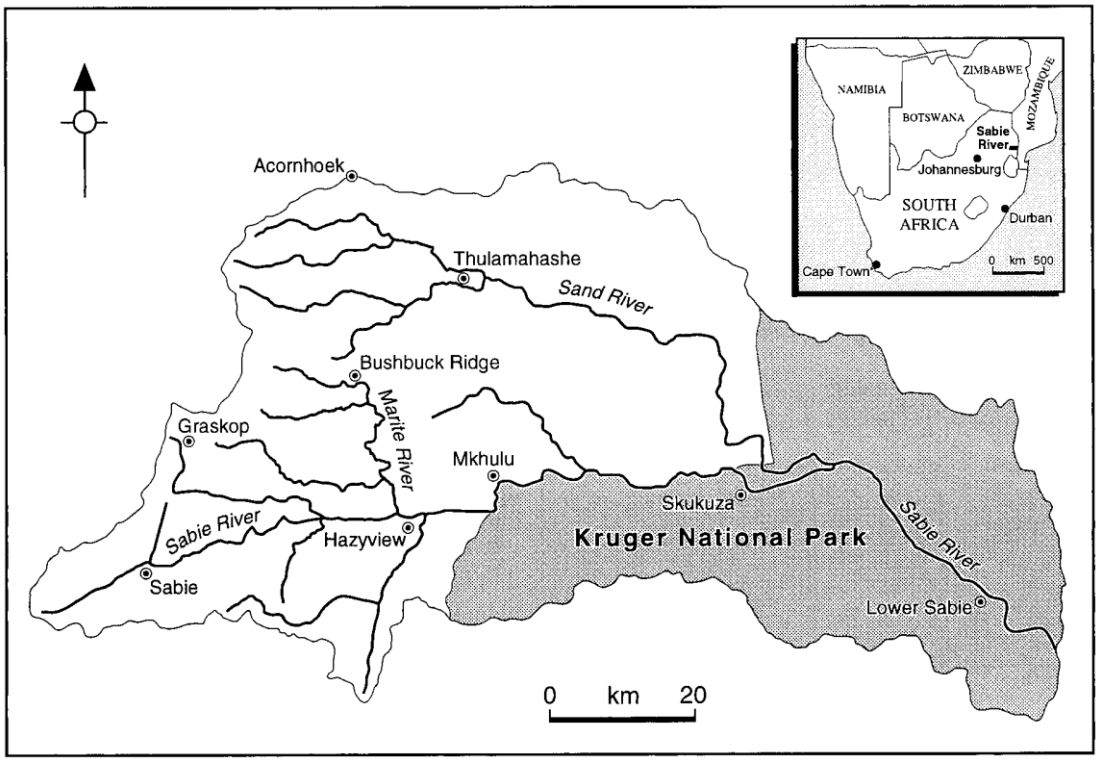

Figure 3.4. The River Sabie's catchment area (Heritage et al., 2004).

3.3. Southern African flooding events

Variability in precipitation not only within Kruger National Park but also throughout Southern Africa contributes to highly variable flow regimes prone to extreme flooding events (Rountree *et al.,* 2000; Reason *et al.,* 2006). North Eastern regions of South Africa that display semi-arid climates such as Kruger National Park display high levels of deviation in discharge, ranging between minor and moderate floods that occur seasonally to rare floods events comprised of extreme levels of discharge (Rountree *et al.,* 2001; Holmes *et al.,* 2005).

The River Sabie has experienced five flood events in the past 60 years causing flow to approach extreme levels in discharge, with the largest floods occurring in 1925, 2000 and 2012 (Holmes *et al.,* 2005). In addition to the Sabie River where unusually high levels of rainfall produced unprecedented flow regimes of up to 7000 m^3s^{-1}, the Karoo basin also experienced destructive ephemeral flash floods in January 1981, which saw water levels rise to approximately 12 m in 7 hours (Stear, 1985). Input from severe weather systems contribute to high variability in levels of precipitation found in South Africa (Reason *et al.,* 2006), such cyclone events correlate with extreme floods consistent with the highest mean annual runoff coefficient of any country (Holmes *et al.,* 2005).

3.4. February 2000 and January 2012 flood events

In February 2000, northeastern South Africa experienced very high levels of rainfall (Dyson and Van Heerden, 2001), which was a product of multiple tropical systems that dominated northeastern regions of Africa's subcontinent throughout February 2000 (Dyson and Van Heerden, 2001; Smithers *et al.* 2001). Two major tropical systems travelled over South Africa

between the 5th and 10th as well as the 22nd and 25th of February, with the latter of these systems being tropical cyclone Eline (Smithers *et al.* 2001; Reason and Keibel, 2004).

Cyclone Eline caused mass devastation to the northern regions of South Africa, wreaking havoc as it made landfall, producing high-magnitude flood events that killed >700 people, destroyed bridges and washed roads away as streams became violent torrents (Olivier and de Rautenbach, 2002; Reason and Keibel, 2004; Chikoore *et al*., 2015). Unusually cyclone Eline maintained a long lasting lifespan, it is recognised as the most enduring cyclone since records began in the Southwest Indian Ocean and travelled approximately 2000km across South Africa, penetrating its southwestern coast as seen in figure 3.5 (Reason and Keibel, 2004). The combined longevity of cyclone Eline and its resultant precipitation (25% of overall summer precipitation), in addition to increased soil moisture content from previous storms depressions resulted in widespread flooding (Smithers *et al.*, 2001; Williams and Kniveton, 2012). Flooding produced by cyclone Eline consequently caused high levels of damage throughout North Eastern South Africa as well as causing extensive damage in Mozambique and Zimbabwe (Dyson and Van Heerden, 2001; Heritage, Moon *et al.*, 2001; Reason and Keibler, 2004).

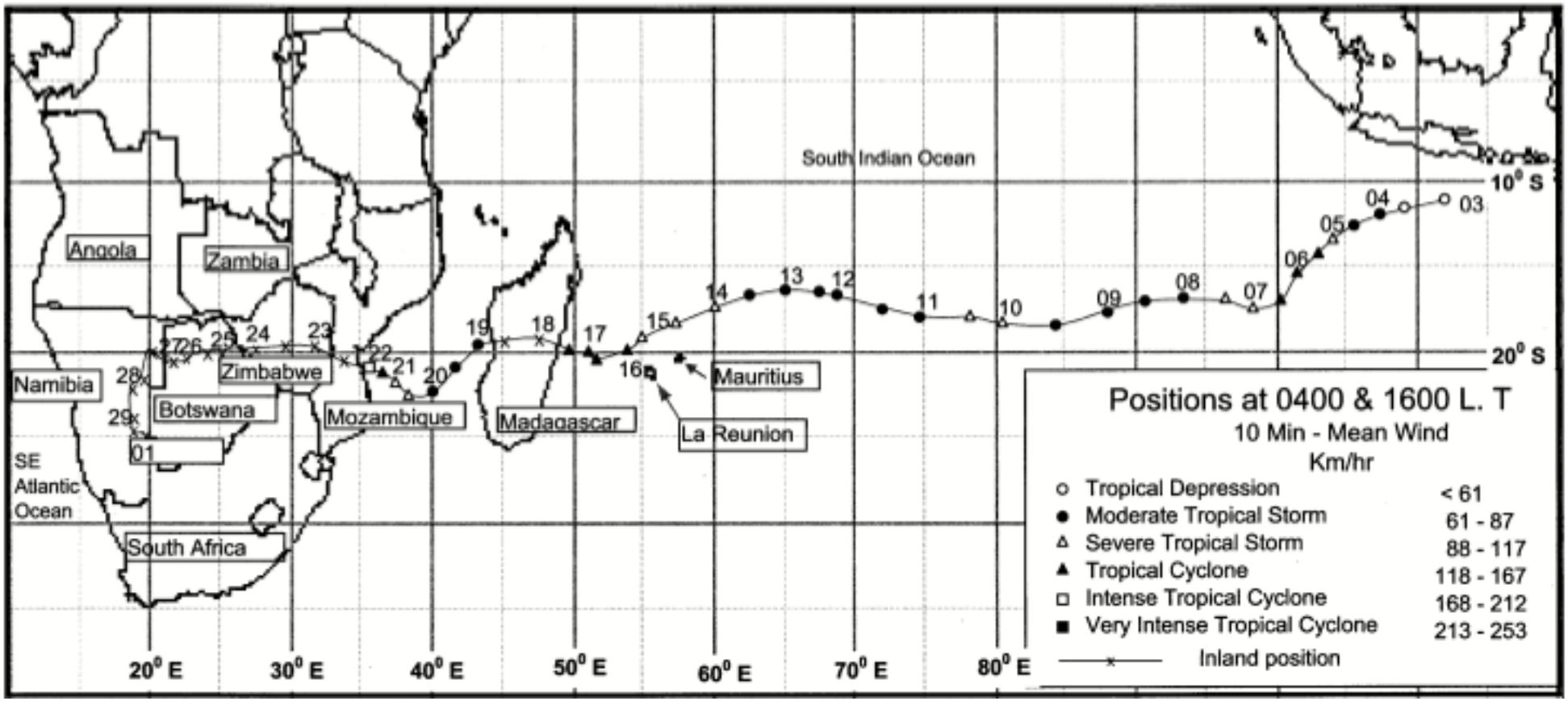

Figure 3.5. Track of Eline across the south Indian Ocean and southern African mainland with its position marked at 0400 and 1600 LT during the 3 Feb–1 Mar 2000 period. The wind speeds associated with south Indian Ocean storm categories are given in the legend (Reason and Keibel, 2004).

Records of extreme highs in discharge occurred at both Rivers Sabie and Letaba following cyclone Eline, with the former experiencing flow of ~3000 m^3s^{-1} at Kruger gate and ~7000 m^3s^{-1} at gauging stations nearby lower Sabie (Heritage *et al.,* 2001; Parsons *et al*., 2006). Discharges associated with cyclone-produced flood events were considerably higher higher than River Sabie's typical flow during summer months, which normally flow from 15 to 20 m^3s^{-1} (Parsons *et al.* 2006). High-magnitude floods at the Sabie River usually occur on a 60-year cycle, with arguments suggesting much larger cycles of 90 to 200 years (Heritage *et al.* 2001; Parsons *et al,* 2006), however in 2012 another cyclone-induced flood event occurred with flows similar to those recorded in 2000.

Cyclone Dando, another large tropical cyclone event disrupted Kruger National Park with its associated flood that destroyed roads, bridges and gauging stations, made landfall at Mozambique (figure 3.6), travelling in a north-westerly trajectory over South Africa from January 16th to January 18th (Gutro, 2012a; WMO, 2012). From satellite imagery and data collected via an Atmospheric infrared sounder, large storms were estimated with bulk rainfall found in southern regions of the cyclone over Kruger National Park as seen in figure 3.7 (Gutro, 2012a; Gutro, 2012b; Chikoore *et al*., 2015). The position of bulk precipitation found in cyclone Dando resulted in large quantities of rainfall over Kruger National Park, with ~450-500mm of rain falling in 48 hours (Milan *et al.,* 2012). Such considerable amounts of precipitation in such a short space of time resulted in a devastating flood coherent with flows ranging between ~2000 and ~4000m^3s^{-1} at River Sabie (Milan *et al.,* 2012).

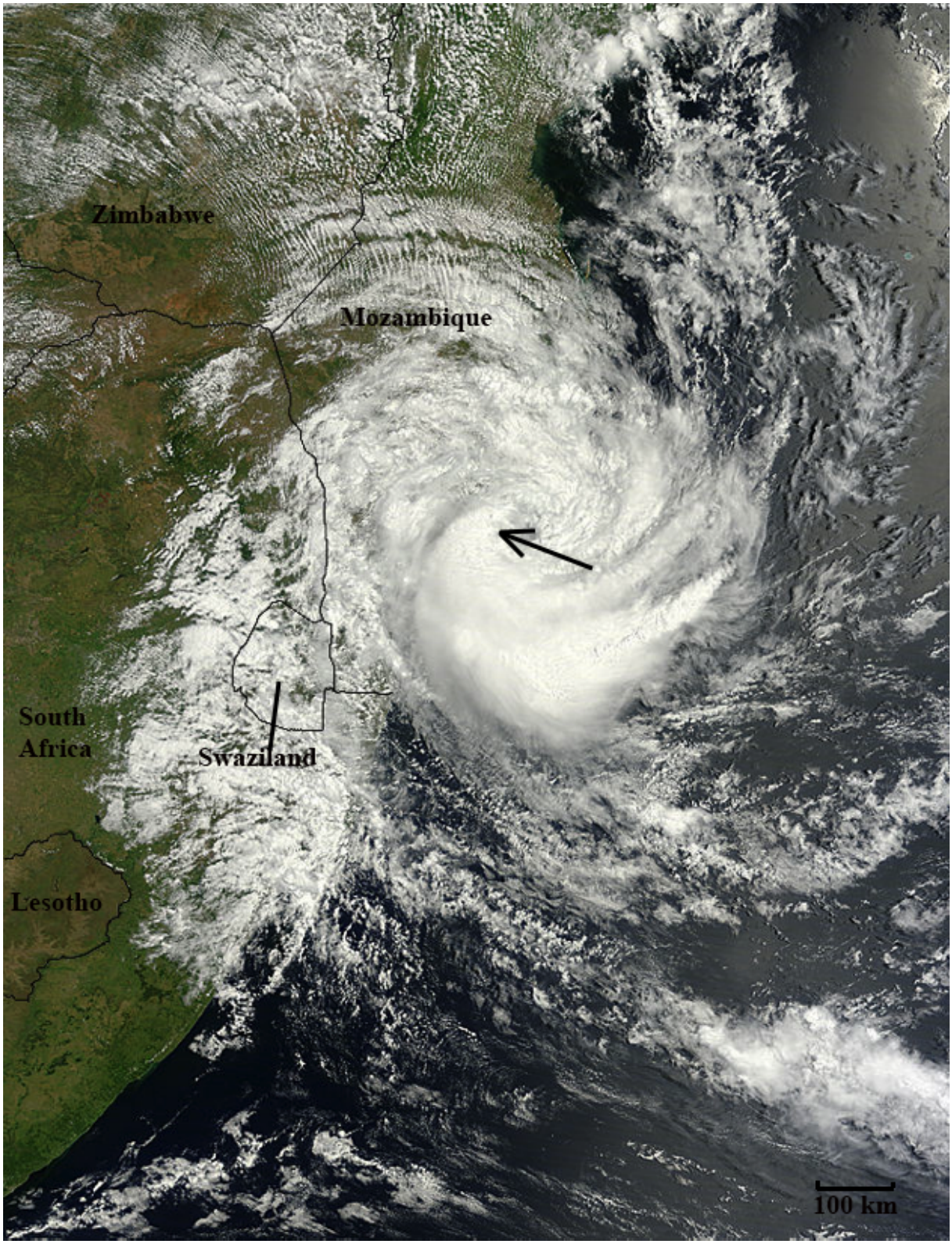

Figure 3.6. Cyclone Dando making landfall on the 17th January 2012, including its trajectory over Southern Africa (NASA, 2012).

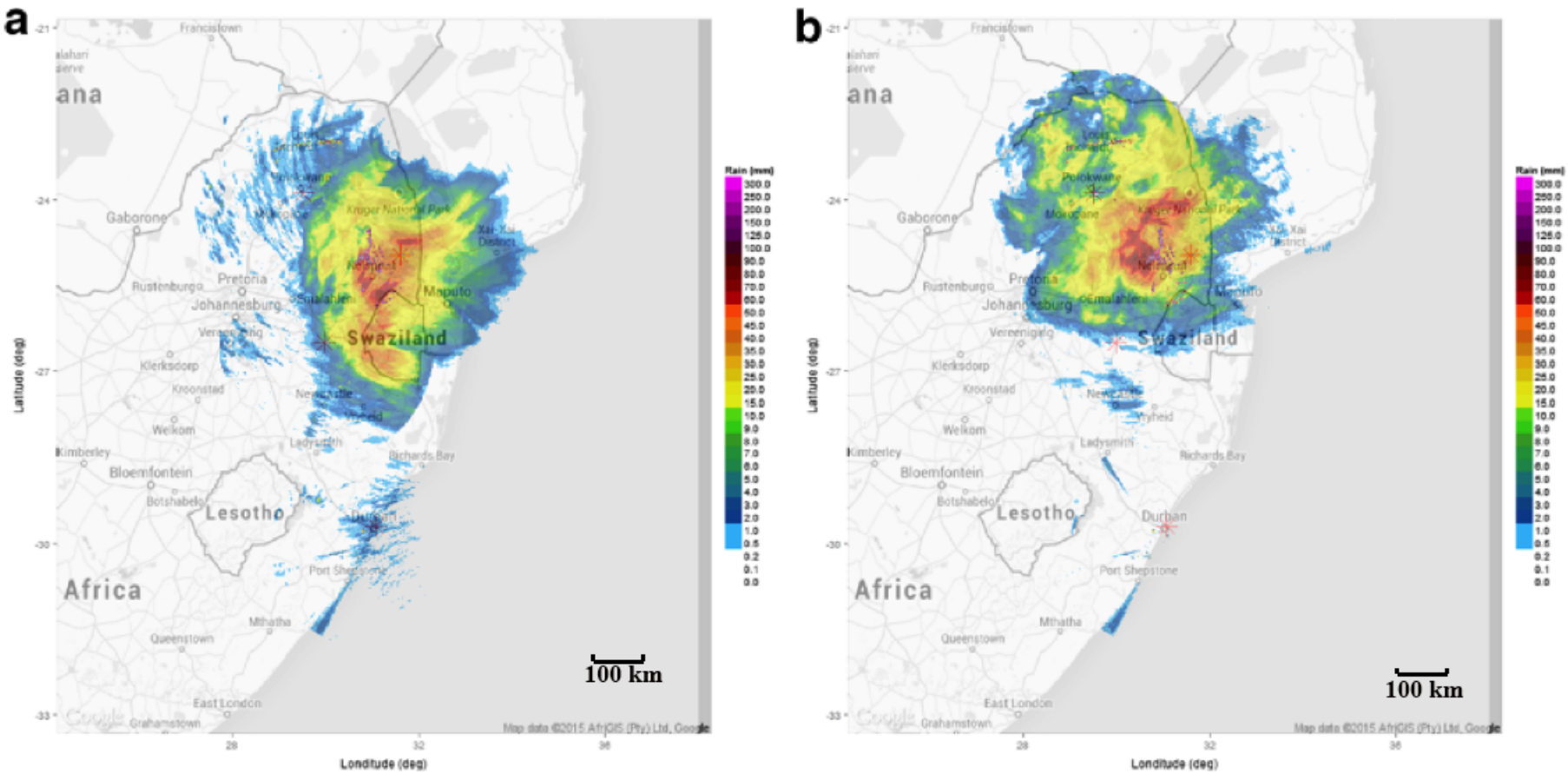

Figure 3.7. Dando 24-h cumulative rainfall based on South African Weather Service radar montage: a January 17, 2012, b January 18, 2012 (Chikoore et al., 2015).

4. Methods

In terms of analysing hydromorphic alterations found at River Sabie in response to an extreme flood event, this thesis employed the use of aerial photography and two-dimensional flow simulations. This chapter initially describes each study site in relation to their location and physical settings during section one. Section two then concentrated solely upon site one, describing the channel in more detail, discussing its diverse gradient template and geometric characteristics, particularly in relation to cross-sections extracted from river simulation models. Additionally, Cross-sectional extractions also gave rise to discussing to achieving discharge scenarios for each flow model. Geomorphic analysis, is later employed to tackle objective one is detailed in section 4.3, which is then followed by how in-channel hydraulics are analysed in relation to model development and analysis found within section 4.4. Such flow simulations used for hydraulic analysis is then validated to confidently discuss hydraulic variation in site one.

4.1. Site selection

Pool-rapid analysis occurred at two sites found along the River Sabie (figure 4.1), with analysis into flood induced hydraulics soley focused at site one (figure 4.2; Top), whilst geomorphic change occurred at both sites. Site one, located near to the villages of Cork, Belfast, Mkuhuhlu A and Oakley E, consisted of a varied geomorphic template consistent with two distinct chanel types; bedrock anastomosing and mixed pool-rapid channels. Much further downstream the second site close to Lower Sabie and Mozambique, comprised of a typical pool and rapid succession found occupied by forested in-channel islands laid between distributary passageways (figure 4.2; bottom).

Consideration of site one's geomorphic form generally found the reach to be an anastomosing channel (Parsons *et al*., 2006). However, geomorphic classifications provided by Van Niekerk *et al.* (1995) helped to identify a pool-rapid within site one, which demonstrated longitudinal alterations in gradient, in addition to a diverse channel geometry that coincides with vast shifts in its wetted perimeter. Both alternative channel types surround the bedrock-anastomosing segment of site one but most importantly, a pool-rapid succeeds it (figure 4.2: top). Distinguishing both anastomosing and pool-rapid channels within site one is relatively simple, as a visible line representing the boundary between both channel types found within aerial photographs. Such a boundary is more visible when analysing differences in elevation and gradient found between both anastomosing and pool-rapid, seen clearly in figure 4.3.

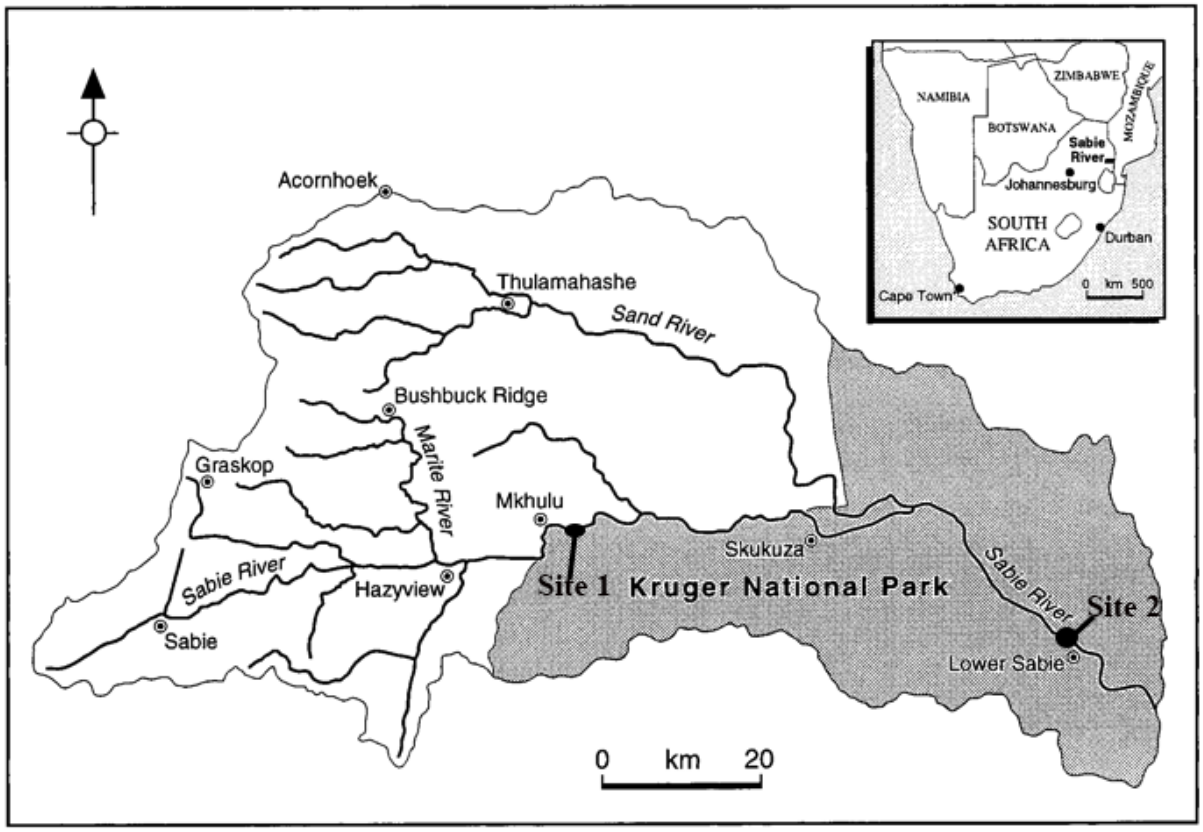

Figure 4.1. Schematic of the Sabie River including site locations (Heritage et al., 2004).

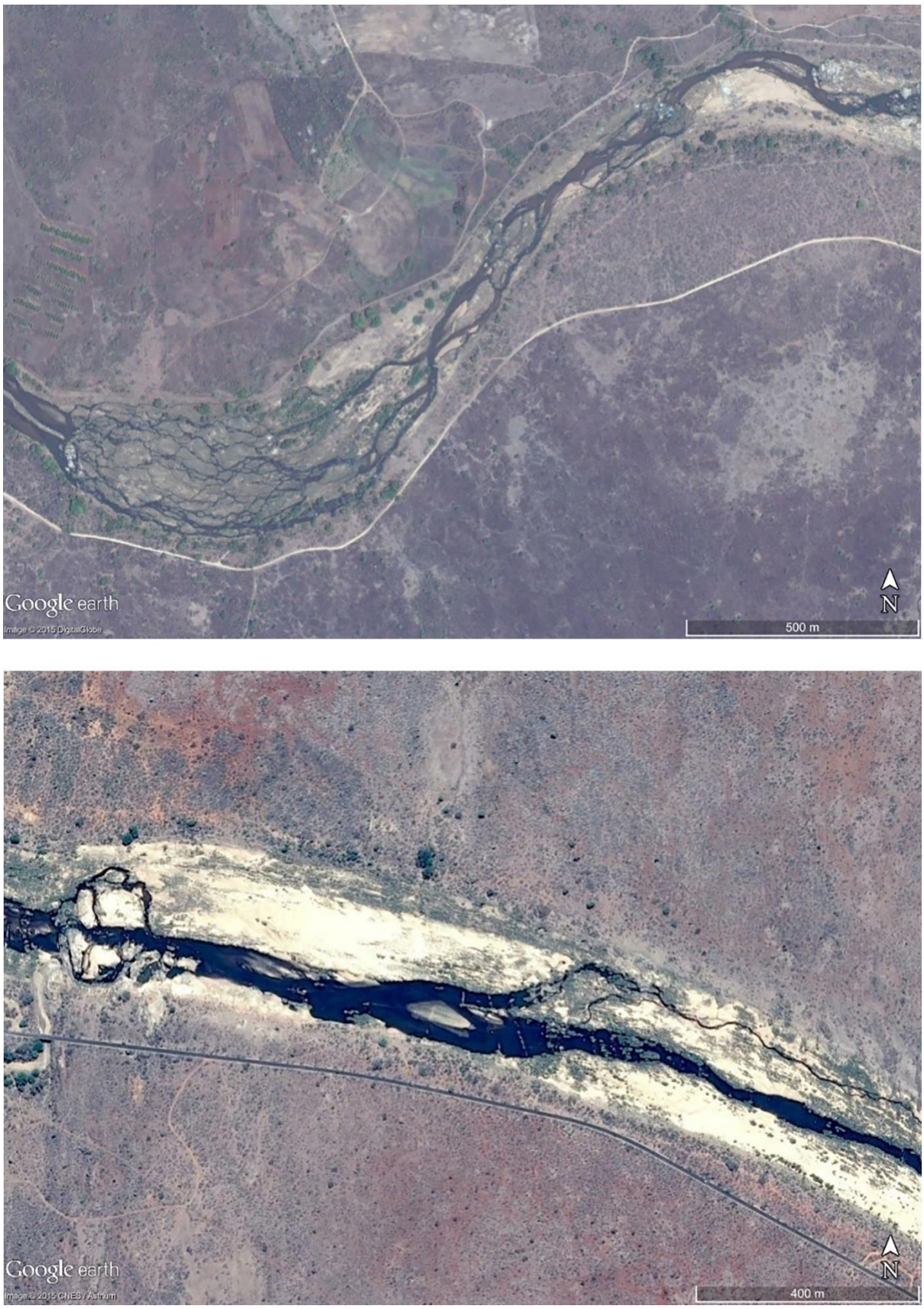

Figure 4.2. Site one used for both geomorphic and hydraulic examinations (top) and site two used solely for chronological geomorphic observations (bottom) (DigitalGlobe, 2014; CNES/Astrium, 2011).

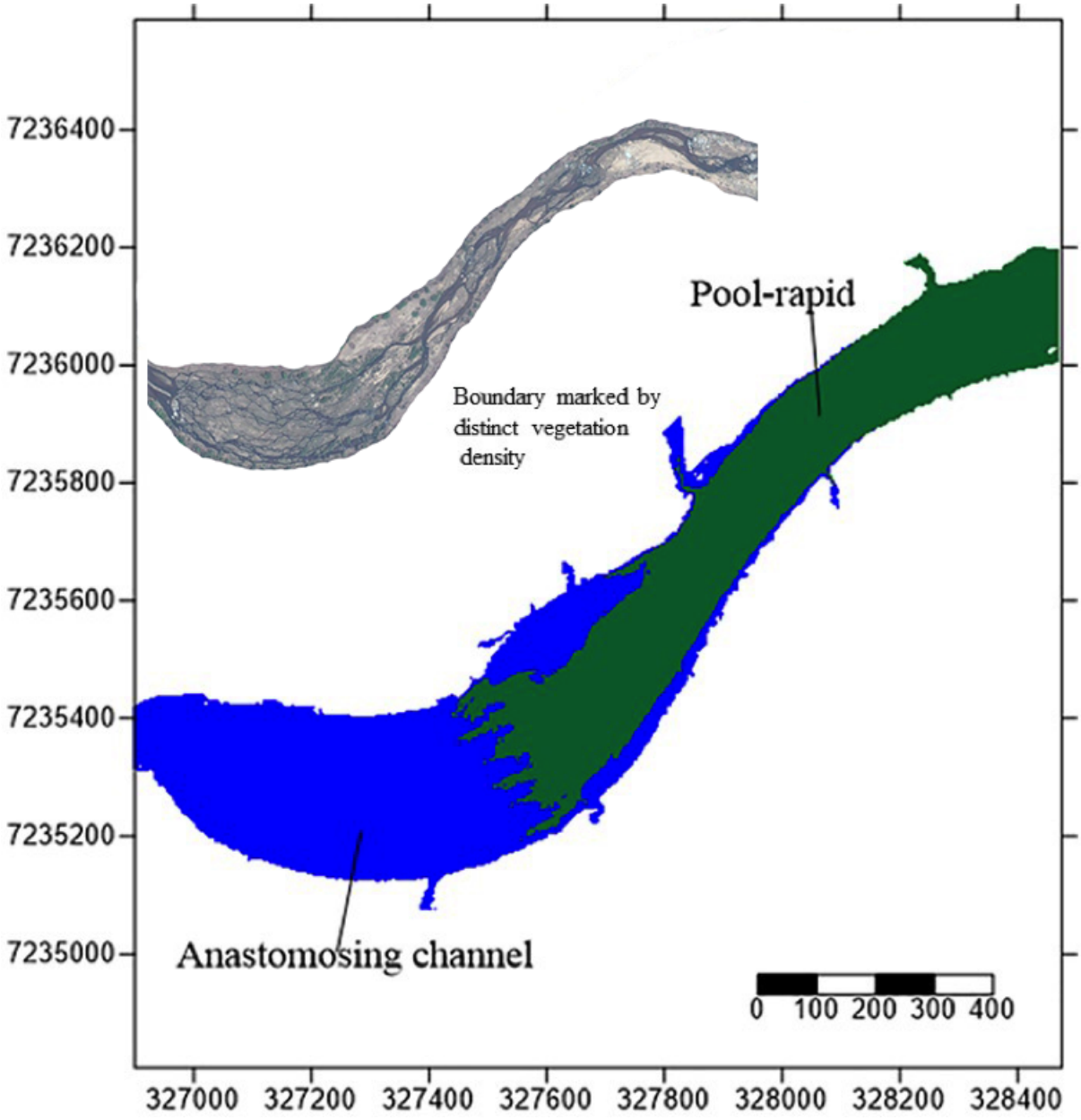

Figure 4.3. Channel boundary identification separating both anastomosing (blue) and pool-rapid (green) channels found at site one, accompanied by an aerial photograph highlighting the distinct vegetation boundary.

4.2. Channel settings and discharge estimation

Comparisons of gradients found between each channel type at site one indicate how bedrock dominated settings found at the anastomosing channel (0.01) produce much steeper slopes than those found throughout the pool-rapid (0.004). Contrasts are markedly visible in regards to longitudinal profiles representative of both anastomosing and pool-rapid channels. Anastomosing channels displayed a continuous slope consistent with relatively minor alterations in gradient, whereas pool-rapids exhibited a distinct topographic long profile comprised of a stepped morphology as seen in figure 4.4. Differences in topographic conditions are clearer when observing site one's study digital terrain model (DTM) found figure 4.4 (bottom). The DTM itself was not readily available for analysis, as its capture through aerial photogrammetry did not occur so far upstream, ceasing north of Skukuza. Therefore, subtraction of river simulation models exhibiting water depth from those simulating water surface elevations enabled the development of a digital terrain model.

Table 4.1 displays slope settings found at individual regions of the reach located at site one. Comparatively steeper slopes are typical of areas classed as rapid units, also known within this thesis as control points as they become highly influential towards hydraulic variables found within a pool-rapid. Analysis of rapid units within this reach identified four control points, however the first three of such remained as the focus within this thesis as control point four was cut off by the model's map limits. Each control point consisted of differing slopes, with much steeper slopes found at control points one and three. Control point two consists of a lesser slope, however it remained considerably steeper than adjacent pools that are comprised of a less significant gradient. Such varied gradient settings from relatively steep to more gentle slopes is the key reason for such the pool-rapid channel displaying a lesser slope of 0.004 compared to the anastomosing channel 0.01.

Table 4.1. Slope conditions at individual channel units found from upstream to downstream of the pool-rapid.

Channel unit	**Slope**
Control point one (rapid and channel boundary)	0.148
Initial pool-rapid segment (pool)	0.0008
Control point two (rapid)	0.008
Pool	0.0003
Control point three (rapid)	0.04

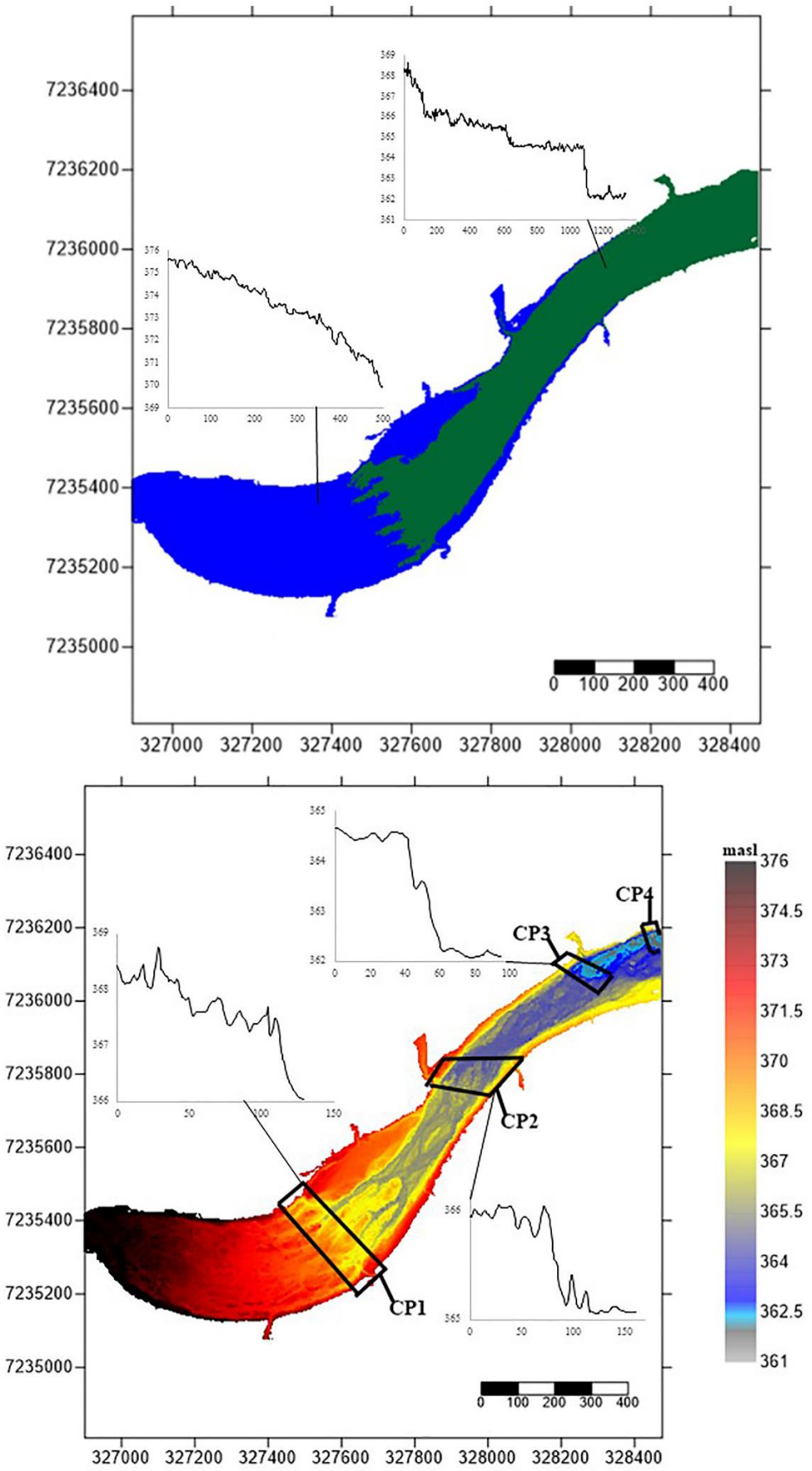

Figure 4.4. Top: Slope settings found at the Anastomosing channel (blue) and pool-rapid (green); Bottom image consists of a Digital Terrain model (DTM) displaying each control point (CP#) and their gradient settings, with gradient plots consisting of an X and Y axis respectively comprised of 'chainage (m)' and 'elevation (masl)'.

Extracted at selected regions of site one, cross-sections enable an additional view of topographic conditions presented by the digital terrain model. Overall, 14 cross-sections were extracted from the reach, with four lifted from the anastomosing channel and 10 taken from the pool-rapid. In addition to channel bed cross-sections, extractions of water surface elevations placed on top of each specific cross-section took place. Water surface cross-sections are useful as they also provide complimentary point of view to two-dimensional simulations of such, giving an account of inundation rates to topographical features within the channel.

Cross-sectional extractions also exhibit changes in area at each specific section during an individual discharge scenario, with the possibility of observing differences found in cross-sectional area between anastomosing and pool-rapids as well as individual channel units. Cross-sectional area was calculated by the following the equation:

$$\boldsymbol{CSA = Wd}$$

Cross-sectional area or ‘CSA’ is a product of ‘W’ (total width) and depth presented as ‘d.’ The figure for depth used within the formula was the maximum value modelled within the specific cross section, as maximum value for width was implemented within the formula. Completion of cross-sectional area calculations then enabled one to estimate discharge through the following:

$$\boldsymbol{Q = CSAv}$$

The formula can be broken down to Q indicating calculated discharge, whilst ‘v’ highlighted mean velocity used in cross-sectional area calculations (CSA). Table 4.2 displayed each derived discharge scenario.

Table 4.2. Discharge scenarios derived from the site one.

Scenario	Discharge (m^3s^{-1})
Q_1	29
Q_2	111
Q_3	358
Q_4	564
Q_5	605
Q_6	786
Q_7	1406
Q_8	2289
Q_9	2870
Q_{10}	3545
Q_{11}	4080
Q_{12}	5085

Topographic cross-sections appeared to differ in accordance to each given channel type, with those extracted from the bedrock anastomosing channel (cross-sections A – D) comprised of multiple islands, each positioned at alternate elevations as seen in figure 4.5. As discharge increased so did the number of islands and bar that became submerged, as differential elevations caused some islands to continue to break water surface during specific discharges. In the case of this thesis, analysis of water surface extractions occurred at five of the twelve estimated discharge scenarios, to allow for clear representation on cross-sections found in figure 4.4. Additionally, the five selected discharge estimations exhibit considerably

significant increases in cross-sectional area as opposed to more progressive rises with all twelve scenarios, which would overcrowd each cross-section.

At cross-sections following control point one, channel topography became less frequented with islands as the channel became much wider and typical of a pool-rapid. However, immediately downstream of control point one (E – I), islands persisted across the channel with particularly emphasis on a large lateral bar that dominated the region. Submergence of this bar during Q_{12} caused cross-sectional area of the channel to increase considerably in comparison to areas found within the anastomosing channel. Once downstream of cross-section I, islands did not dominate the channel at each given extraction (J – M), although a large lateral bar once again dominated channel topography at cross-section N.

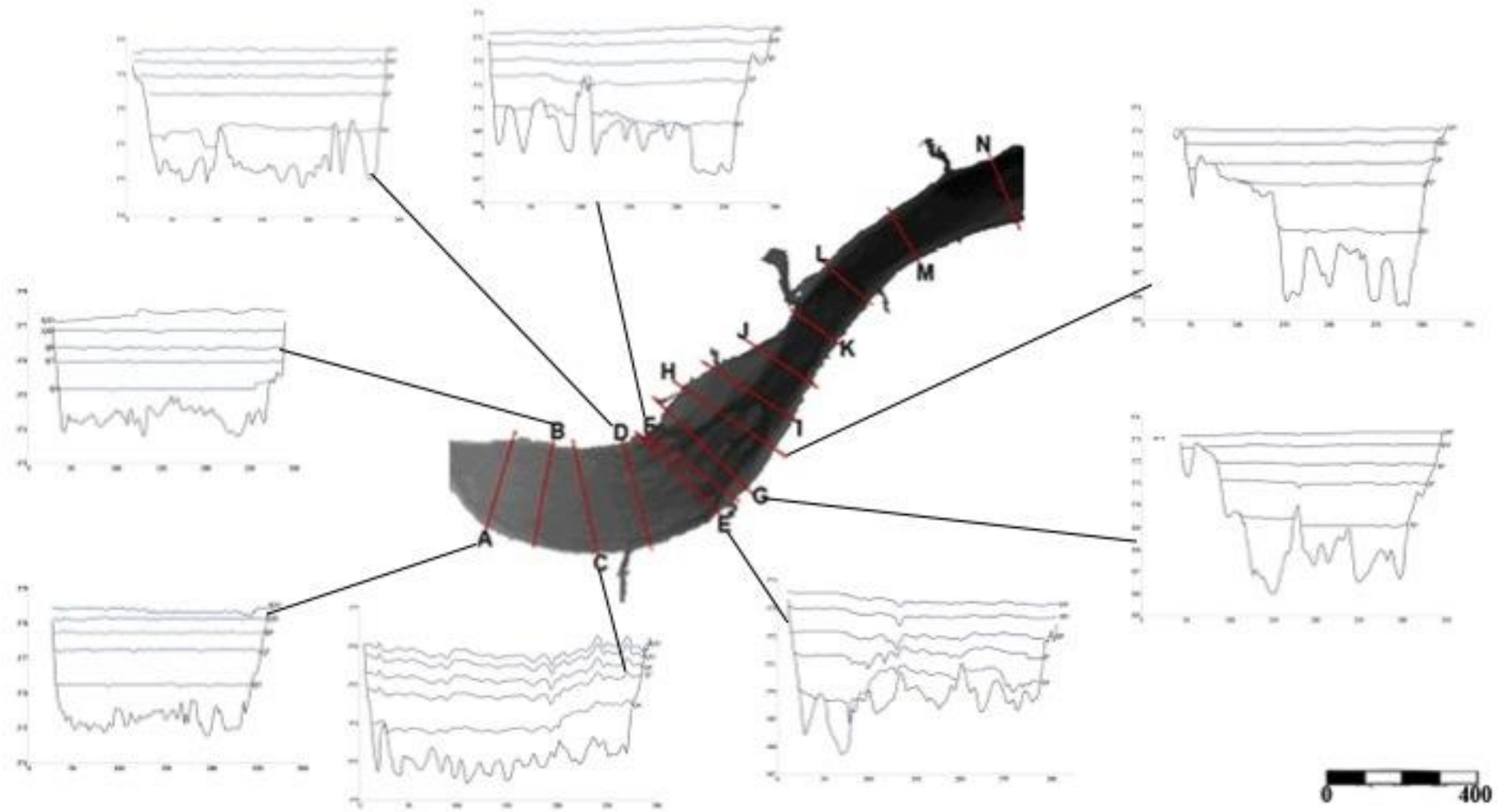

Figure 4.5. Cross-section schematic, highlighting location of each extracted cross-section taken from the DTM, which is accompanied by one-dimensional models of sections A to N accompanied by water surface elevations for specific discharge scenarios (Q_4, Q_7, Q_9, Q_{11}, Q_{12}); X and Y axis represented as chainage (m) and elevation (masl) respectively.

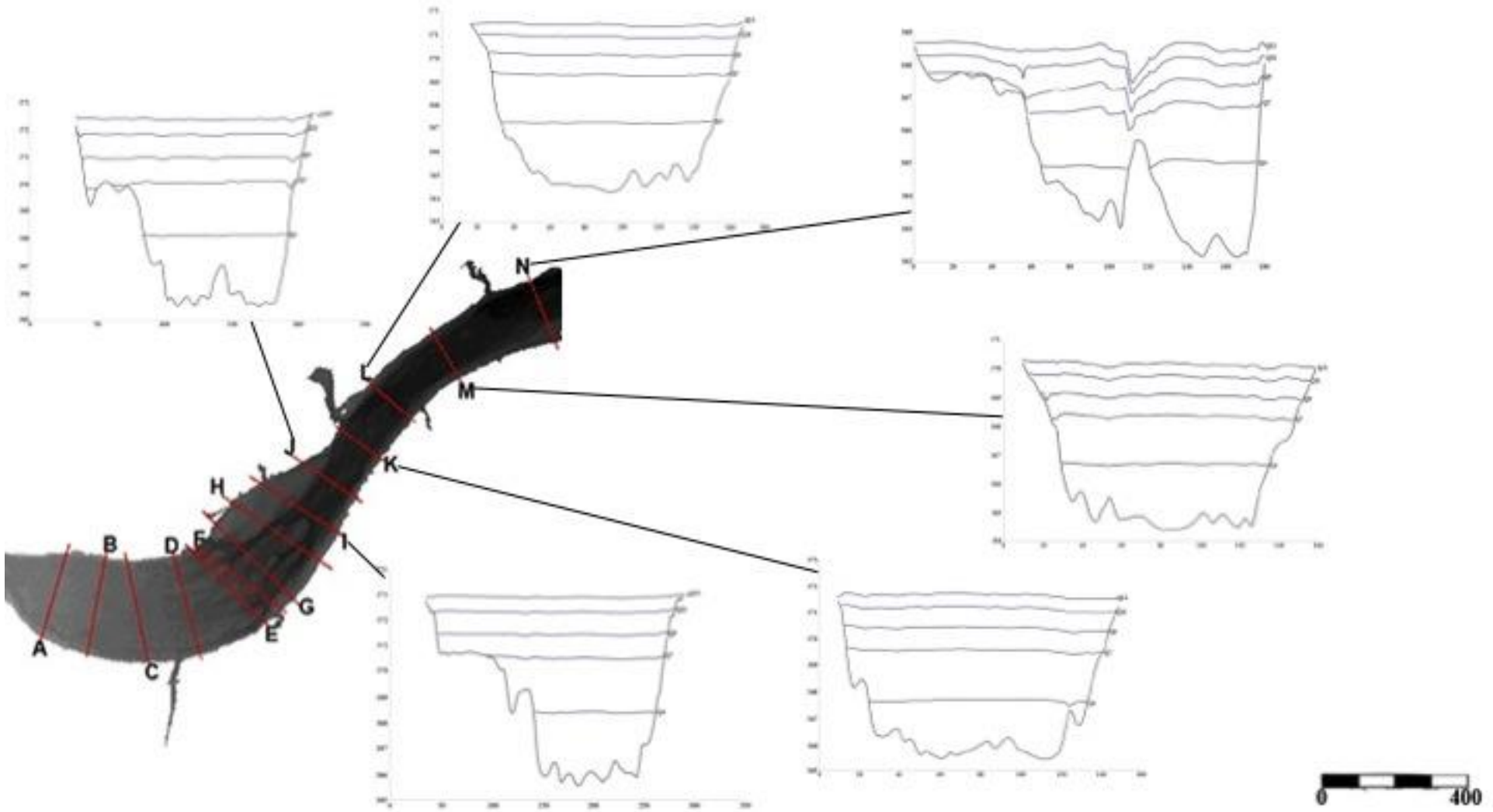

Figure 4.5 (continued). Cross-section schematic, highlighting location of each extracted cross-section taken from the DTM, which is accompanied by one-dimensional models of sections A to N accompanied by water surface elevations for specific discharge scenarios (Q_4, Q_7, Q_9, Q_{11}, Q_{12}); X and Y axis represented as chainage (m) and elevation (masl) respectively.

4.3. Morphological change analysis

As part of objective one, scrutiny of historic aerial photographs took place to highlight obvious changes in channel form. Images before and after both Cyclones Dando and Eline allow interpretations to be made of effected sedimentary features and vegetation patches within each study reach. Analysis of erosion and deposition within both sites particularly in site one, aided in linkage establishment with changes to hydraulics found at each river simulation model, in addition to how changes to vegetation also affected hydraulics and vice versa.

Overall, images originated from four sources with those found before Cyclone Eline taken via aerial Lidar by Aerial Photogrammetry Company; Fotogramensura, whilst images taken before and after Cyclone Dando came from both DigitalGlobe and CNES/Astrium. DigitalGlobe is a privatised distributor of high-resolution photographs of the Earth, implementing satellite and aerial imagery for a variety of purposes including research, civil matters and military intelligence (Digitalglobe, 2015), whilst Astrium solely gained high-resolution imagery through their SPOT 5 to SPOT 7 satellites (Airbus Defence and Space, 2015). Imagery capture of the River Sabie took place within Austral winter months, associated with South Africa's dry season. Implementation of a longer time series took place at site two, involving both cyclone's Eline and Dando. Imagery that immediately followed cyclone Dando at site two did not employ those archived by DigitalGlobe. Instead, aerially derived high-resolution images collected through a NERC grant gave a clear indication to morphological change. Collection of these images involved an aerial LiDAR scan covering a 150km reach of the River Sabie found at Kruger National Park during May 2012 (Entwistle *et al.,* 2014; Heritage *et* al., 2014).

4.4. Hydraulic analysis

Observations of flow hydraulics during a high-magnitude flood took place through two-dimensional flood inundation models within the River Sabie's macrochannel. Two-dimensional flood models provide a highly useful tool for flood management (Lamb *et al.*, 2009), as they provide precise simulations of flooding extent within a river catchment (Yu and Lane, 2009). For this current thesis, research regarding two-dimensional simulations employed a raster-based flood inundation model known as JFLOW (Bradbrook *et al.*, 2005).

Two-dimensional JFLOW models use a discretised form of diffusive wave equations, directly simulating outline boundaries of a given flood (Bradbrook *et al.,* 2005). Classed as a simple GIS tool, JFLOW is a product of consulting group 'JBA Ltd' (Dow and Saillofest, 2008), and designed for observations of overland floods (Bradbrook, 2006). Applied in a variety of different aspects, common uses for JFLOW models include studies on flood depth, velocity and extent (Bradbrook, 2006; Dow and Saillofest, 2008). Two-dimensional JFlow allow users to observe additional routes taken by a river during increased discharge via high-resolution topographic data (Yu and Lane, 2006). As JFLOW model formation is inherently mass conservative compared to alternative reproductions (Hunter *et al.* 2008), it is a fast and cost effective method for estimating channel response to floods (Dow and Saillofest, 2008).

Analysis of JFLOW models took place with geographical information systems software, Surfer 11, which is an authoritative grid based mapping program, designed to produce contour and grid maps efficiently through interpolating XYZ data (Golden Software, 2014). Hydraulic variables employed during the study include channel velocity, depth, water surface elevations, bed shear stress and Froude numbers.

Two-dimensional JFLOW models originally produced simulations involving depth, water level and velocity for the primary study site at the River Sabie, as well as a digital terrain model (DTM) of most of the channel. Through pre-existing JFLOW model aspects development of further simulations that exhibit bed shear stress and Froude also took place, for example, the following equation produced a bed shear stress model:

$$\boldsymbol{\tau_{bed}} = \frac{\mathbf{PgV^2n^2}}{\sqrt[3]{\boldsymbol{y}}}$$

From the above formula, variable representation consists of; 'P' representing water density, 'g' equating to gravity, 'V' exhibiting velocity and 'n' signifying sediment density, whilst 'y' is depth. Models of Froude numbers within the channel represent a unidimensional value of energy within the channel and critical measurements of fluid (Merritt and Wohl, 2002), with the following formula can develop such Froude number models:

$$\boldsymbol{Fr} = \frac{\boldsymbol{V}}{\sqrt{\boldsymbol{gD}}}$$

Were 'V' is velocity, 'g' signifies gravitational acceleration and 'd' represents flow depth. By subdividing periods of Froude that are between the values of 0 and 1, where flow is subcritical and gravitational forces are dominant, biotopes can be differentiated (Heritage *et al.*, 2010).

4.5. JFLOW model assessment

To validate the peak discharge modelled through JFLOW river simulation models, comparisons were made in regards to such models and actual flood inundation recorded at the Sabie River. To measure actual floodwater extent, extractions of differential GPS (dGPS) points at remnant strandlines along the Sabie River took place following cyclone Dando. Once collected, observations of distance found between them and the extent of water surface simulated through two-dimensional JFLOW occurred through plan view and longitudinal profiles. If there is distance between water surface extent and strandpoint data, error percentages involving the differences in modelled discharge and actual discharge occur before being compared to the remainder of the specific cross-section.

Digital GPS point's representative of actual water surface elevations during the flood within River Sabie (figure 4.6 and 4.7), appeared to be relatively close to water surface extremities displayed within two-dimensional JFLOW models (figure 4.6). Additionally, long profiles of each modelled site at River Sabie closely correlate with actual recordings of elevations (or strandpoints) (figure 4.7). However, errors found in both JFLOW models and field samples taken at each site exist because strandline data and model projections do not contact one another within the modelled water surface threshold.

Greatest precision was present within River Sabie at site 10, where strandlines and water surface charts almost overlay one another. In relation to distance between strandlines and the modelled channel at site 10, greatest detachments between them was 14.53 m, with an overall error between modelled and actual discharge of 2.09%. In contrast, site 8 within River Sabie revealed a much weaker correlation, with most adjacent of strandpoints located 9.52 m from

the projected water surface. Whilst site 8's most distant strandpoint was 49 m from simulations, giving site 8 an error of 7.55%.

Overall, the two-dimensional JFLOW models used on the River Sabie was of high precision, consisting of an overall error between modelled 5000 m^3s^{-1} and strandpoints indicative of actual discharge levels of just 5.09%. As other selected sites consisted of relatively low errors between modelled discharge and actual discharge of just 7.05% and 3.69% respectively.

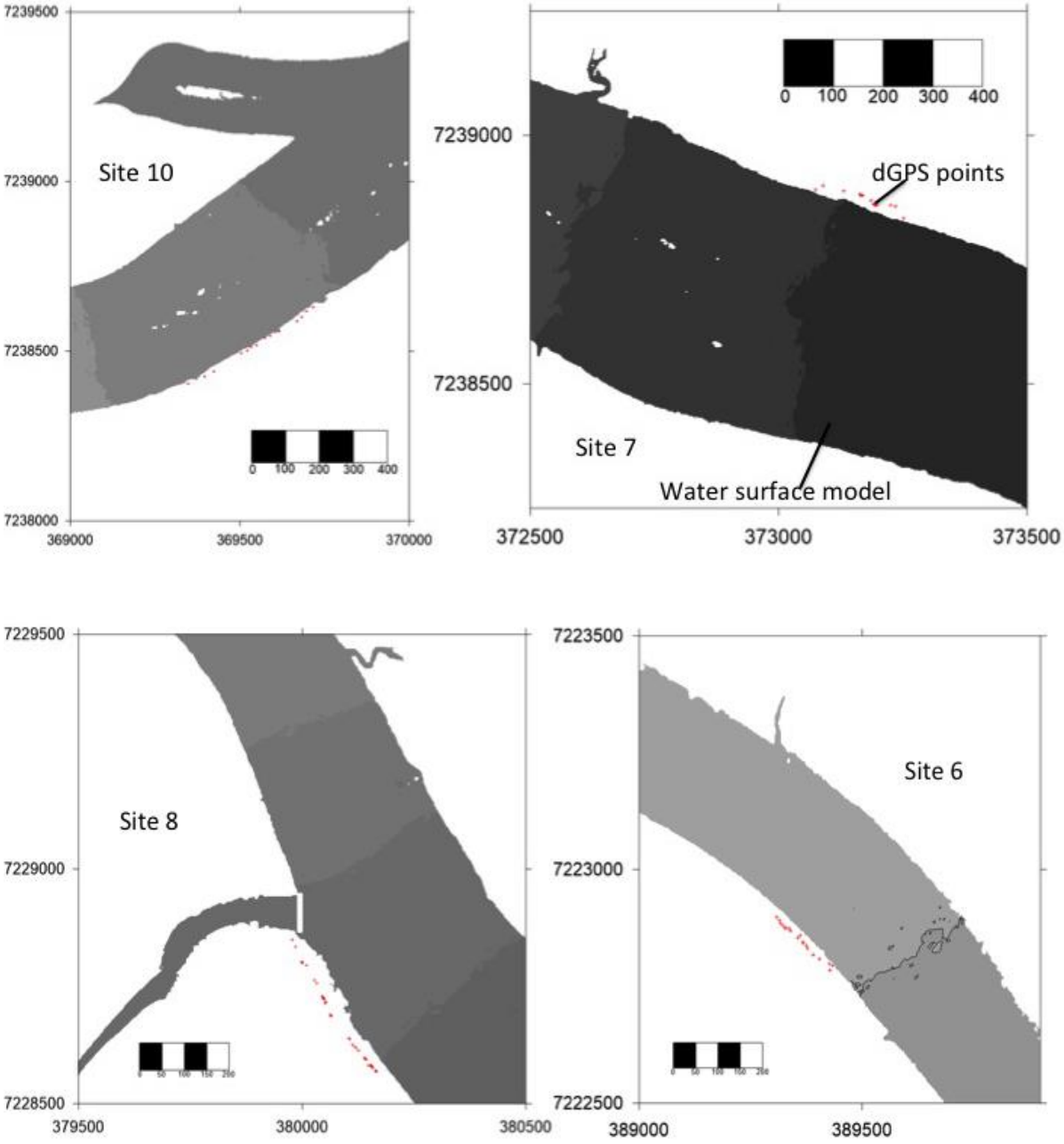

Figure 4.6. River Sabie validation sites with water surface from 5000m^3s^{-1}, sites ordered in accordance to its position downstream, starting at Site 10 and followed downstream by site 7, site 8 and site 6.

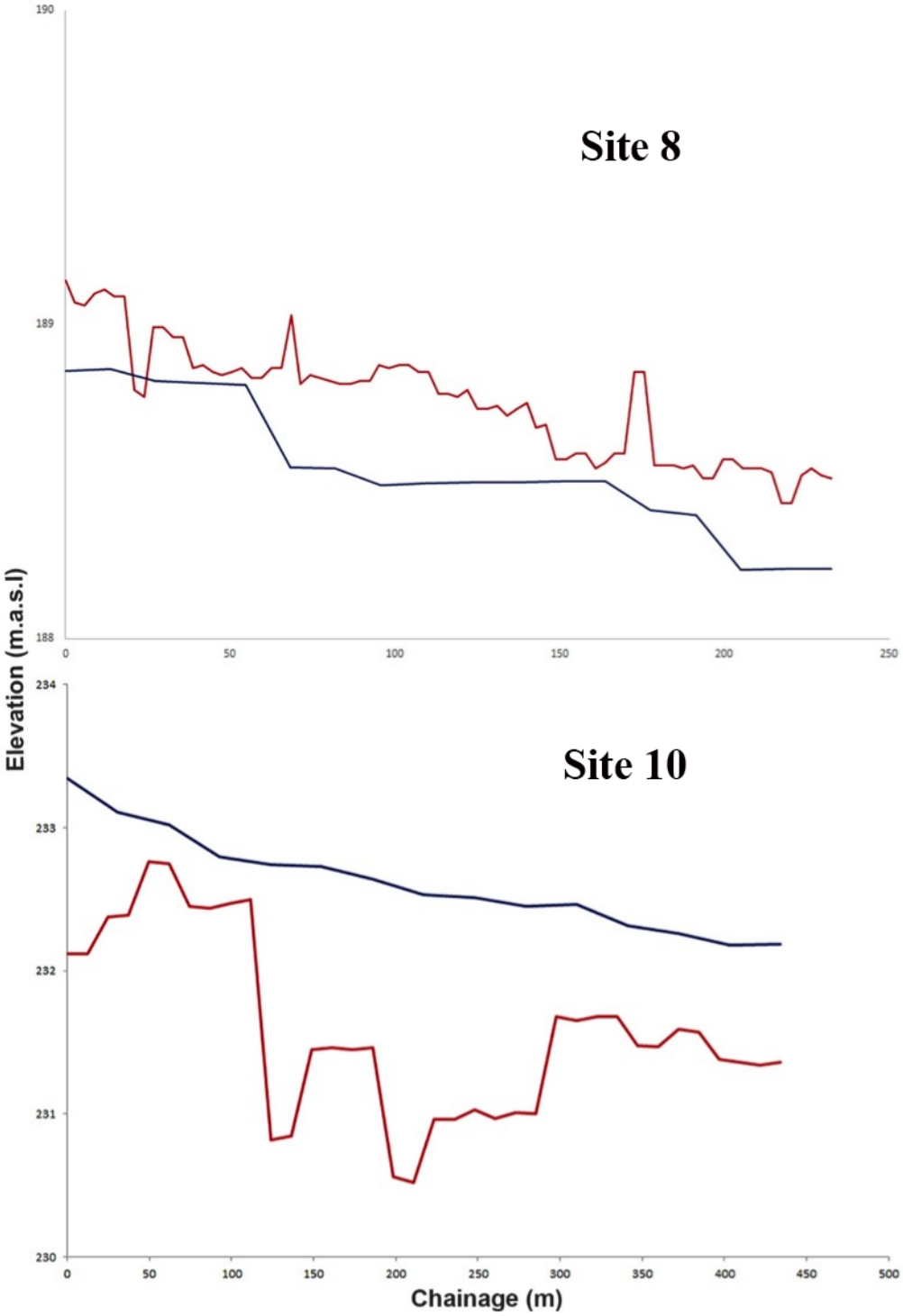

Figure 4.7. One-dimensional long profiles of selected validation sites at River Sabie; red: dGPS points; blue: plots extracted from the water's edge of the two-dimensional water surface model.

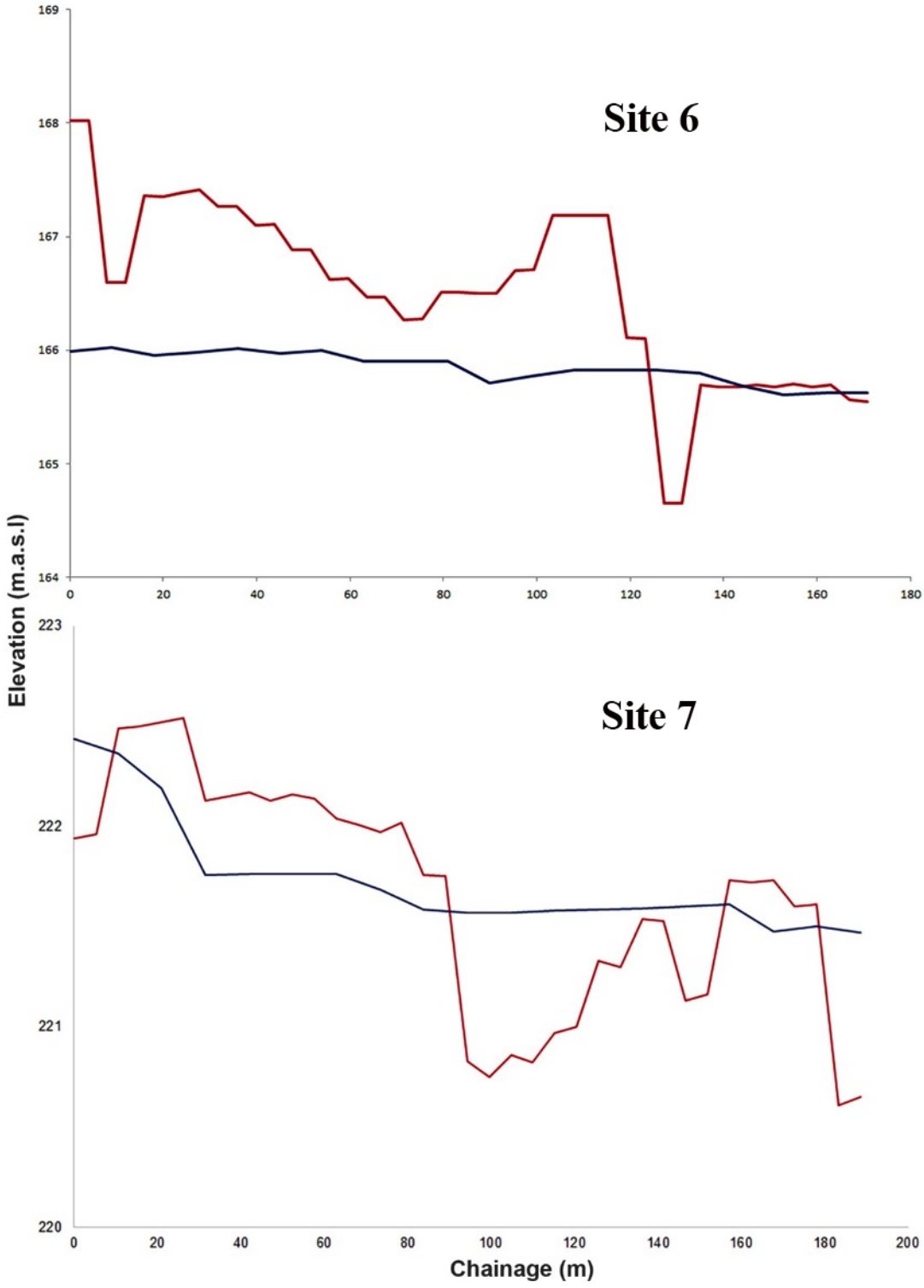

Figure 4.7 (continued). One-dimensional long profiles of selected validation sites at River Sabie; red: dGPS points; blue: plots extracted from the water's edge of the two-dimensional water surface model.

River Olifants is a neighbouring channel located centrally in Kruger National Park, consisting of similar lithology and structural settings to the River Sabie. Although Olifants remained outside of the main focus of this research, it was modelled and validated in the same way as the River Sabie but at considerably higher discharge (10000 m^3s^{-1}) Therefore, the Olifants River was ideal for further validation of simulated discharge within two-dimensional JFLOW models.

Figure 4.8 and figure 4.9 displayed both validated two-dimensional plots of selected sites at the Olifants River (figure 4.8) in addition to their one-dimensional counterparts (figure 4.9). Overall, precision improved to findings at the River Sabie, with strandpoints much closer to modelled water surfaces. Longitudinal profiles of dGPS sites at the River Olifants represented further improvements to correlation with JFLOW compared to those found at the River Sabie.

Errors found between discharge that was modelled and estimated through dGPS strandpoint at the Olifants River were similar albeit lower than sites found at the River Sabie, with the highest error found at site 1 (6.18%). Each ascending site at the River Olifants that succeeded site 1 numerically contained a much higher degree of precision with errors consisting of: 6.05% and 2.10% respectively. Finally, site 5 ends such a trend of improving precision as a slight increase in error occurred (4.32%), however such errors are still relatively minor compared to sites 1 and 2. Therefore, JFLOW models developed for observing hydraulics was not only considerably precise at the River Olifants, which consists of an overall error between modelled discharge strandpoints of 4.66% but also at the River Sabie.

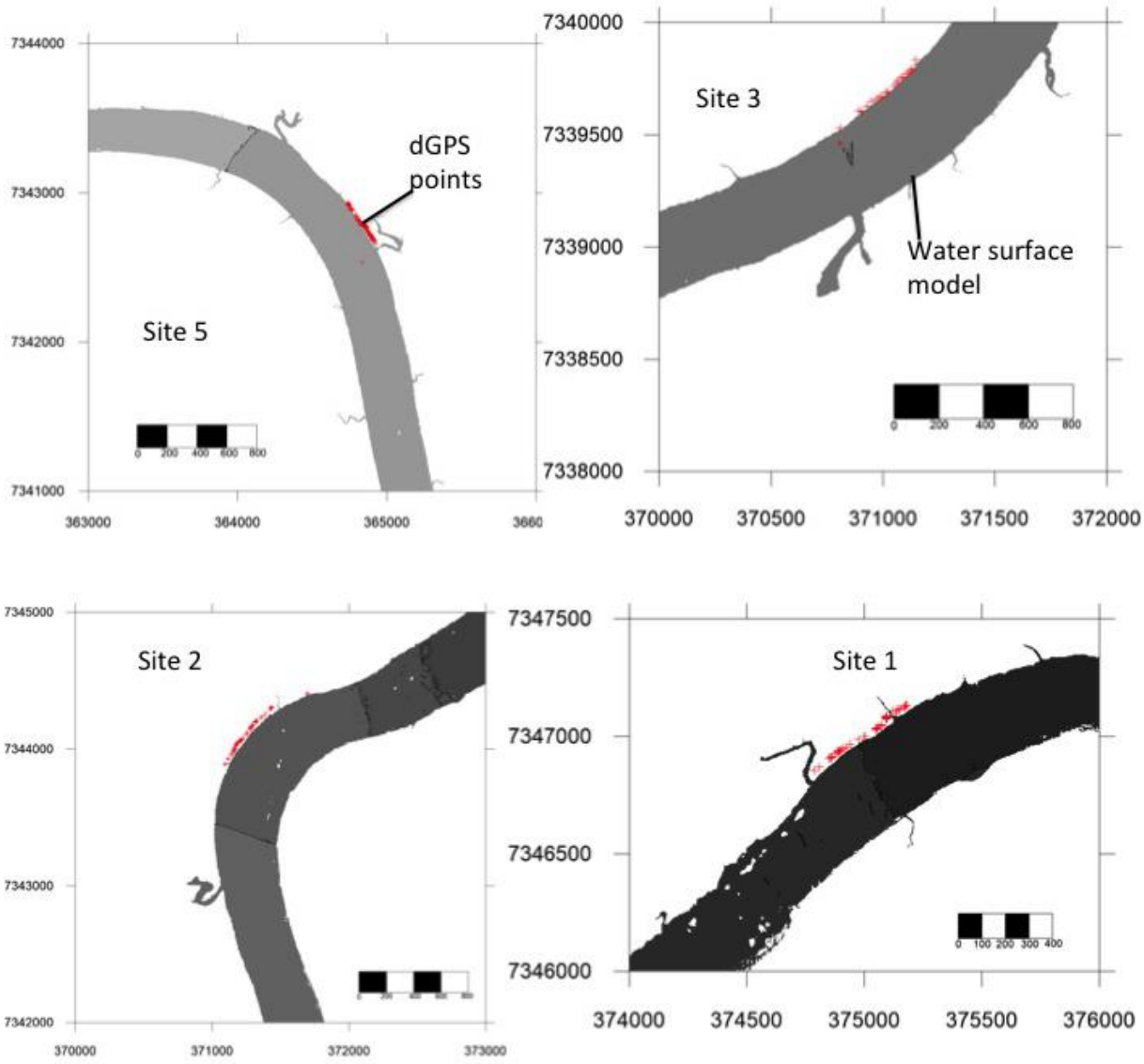

Figure 4.8. Model validation at selected sites in Olifants River, Kruger National park, ascendingdownstream; site 5, site 3, site 2 and site 1 water surface plots with strandline dGPS points (red).

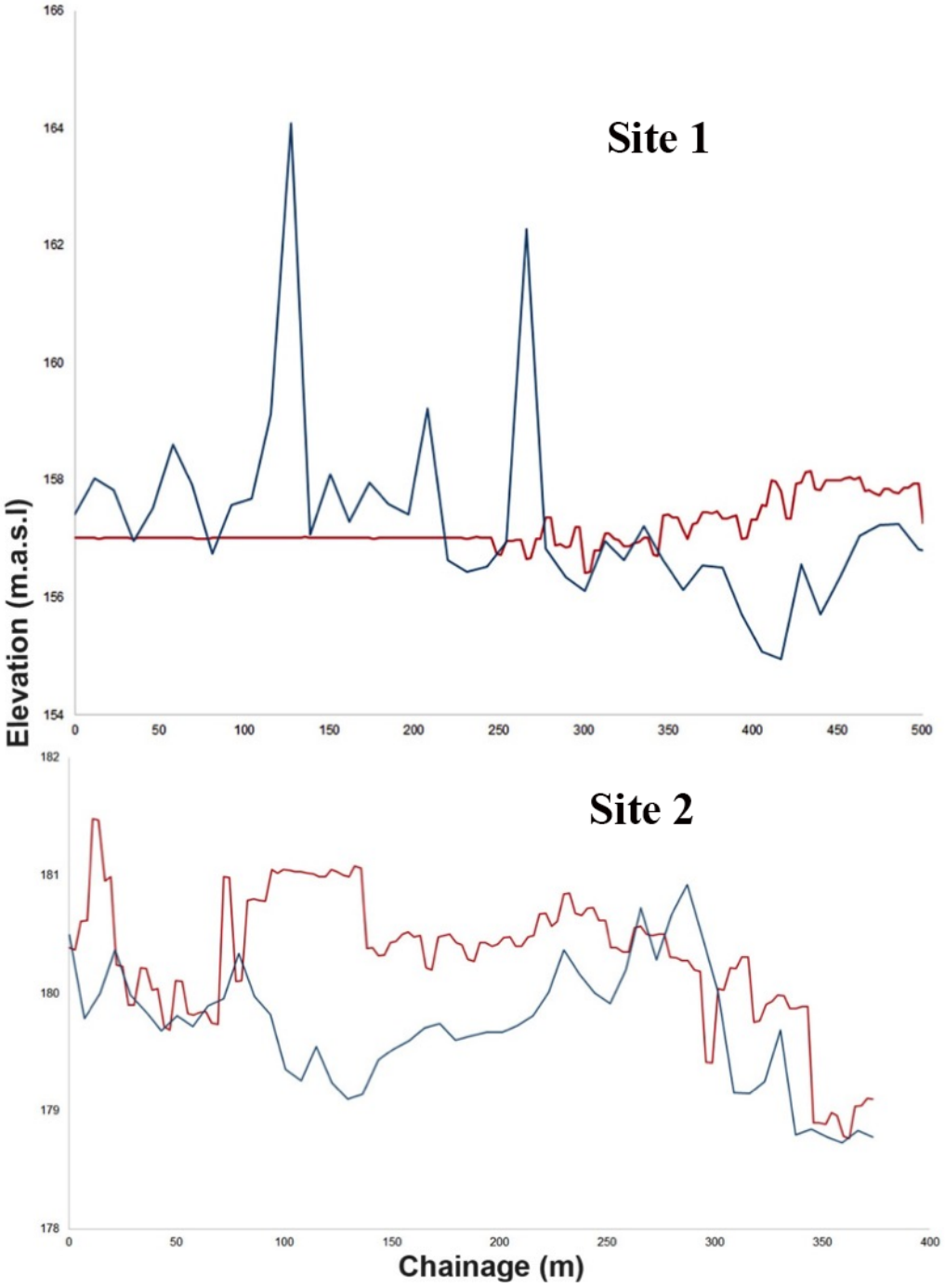

Figure 4.9. Longitudinal profiles of each site used in model validation at the Olifants River, Kruger National park; Water surface model boundary: Blue; dGPS strandpoints: Red.

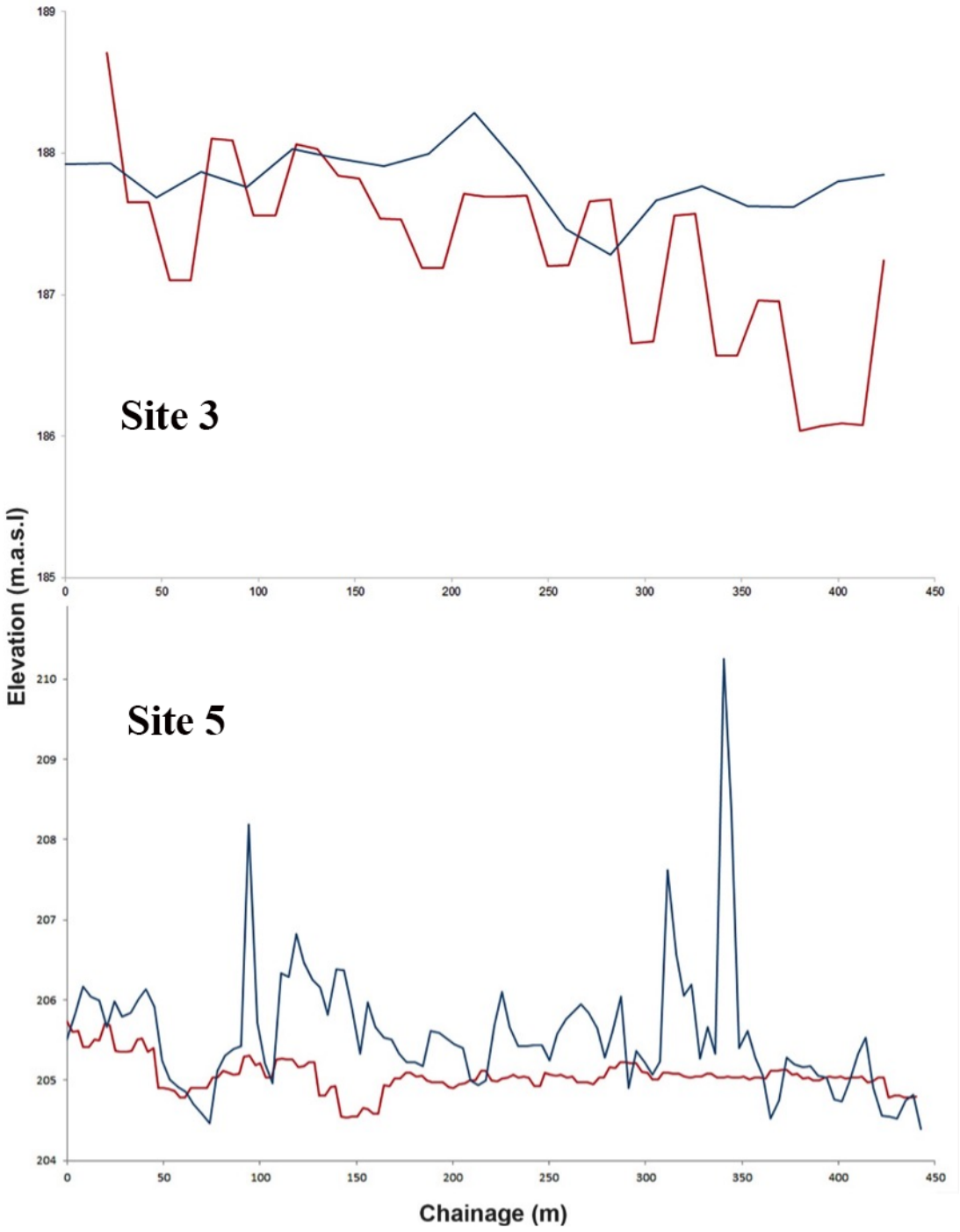

Figure 4.9 (Continued). Longitudinal profiles of each site used in model validation at the Olifants River, Kruger National park; Water surface model boundary: Blue; dGPS strandpoints: Red.

5. Results

Results produced through hydraulic control and geomorphic change analysis following high-magnitude flood events within the Sabie River are displayed throughout this chapter, comprised of alternative sections and sub-sections depending on the method of analysis and variable involved. With this in mind, section 5.1 describes changes to geomorphology in relation to erosion and deposition within two study sites, with site one comprised of an anastomosing channel and pool-rapid, whilst site two solely consisted of the latter. Following on from section 5.1, hydraulic controls through two-dimensional JFLOW models were narrated within section 5.2, with bed shear stress and velocity found in sub-section 5.2.1, water surface and cross-sectional areas in sub-section 5.2.2, and biotope variations within 5.2.3.

5.1. Geomorphic modifications

The anastomosing channel at site one overall displayed minor cases of erosion, however relatively significant quantities of soft sediment were removed at its upstream boundary (figure 5.1, top), with erosion at successive regions of the channel being progressively reduced further downstream (figure 5.1, bottom). Following the anastomosing channel boundary, erosion affected channel form through the enlargement of channel pathways as softer sediments found on top of bedrock core-bars were stripped. Erosion also destroyed occasional bedrock core bars adjacent the anastomosing channel's upstream boundary as well as a medial bar associated with a single-thread channel found upstream (figure 5.1, top), with both contributing to an enlarged channel pathway (as seen in figure 5.1, top). Further downstream from the anastomosing channel boundary, erosion persisted but at considerably reduced rate, with erosion of soft sediments only being of significance at bedrock-core bars lacking in riparian vegetation (figure 5.1, bottom). Deposition in years following cyclone

Dando occurred at a minimal rate, with more obvious occurrences of such deposition located at the anastomosing channel's upstream boundary were an alluvial lateral bar began to develop (Figure 5.1, top; October 2014 and May 2015).

The pool-rapid channel within site one experienced a mixed response to the high-magnitude flood produced by cyclone Dando, with a combination of uncohesive soft sediment removal and sedimentation. This alternative response to flooding was dependant on each specific channel unit, as concentrations of deposition occurred at the first pool following the pool-rapid boundary at control point one, where sedimentation occurred mostly on pre-existing islands and bars, whilst also developing fresh alluvial features (see figure 5.2 – 5.3, top image). Erosion occurred downstream of the first pool near to and downstream of control point two where soft sediment situated on in-channel islands and lateral bars was exposed to the full force of flow from the flood (as seen in figure 5.3). A larger rapid located furthest downstream within the channel displayed no clear changes following cyclone Dando's flood, as no obvious signs of deposition or sediment removal occurred (figure 5.4). However, even though changes to channel form did not occur at the rapids, erosion occurred at a large lateral bar adjacent to them, resulting in a small stream cutting across it. In years following on from cyclone Dando, recovery of lost sediment appeared to occur through gradual aggradation throughout the channel, whilst riparian vegetation also appeared to recolonise geomorphic features such as bars and islands.

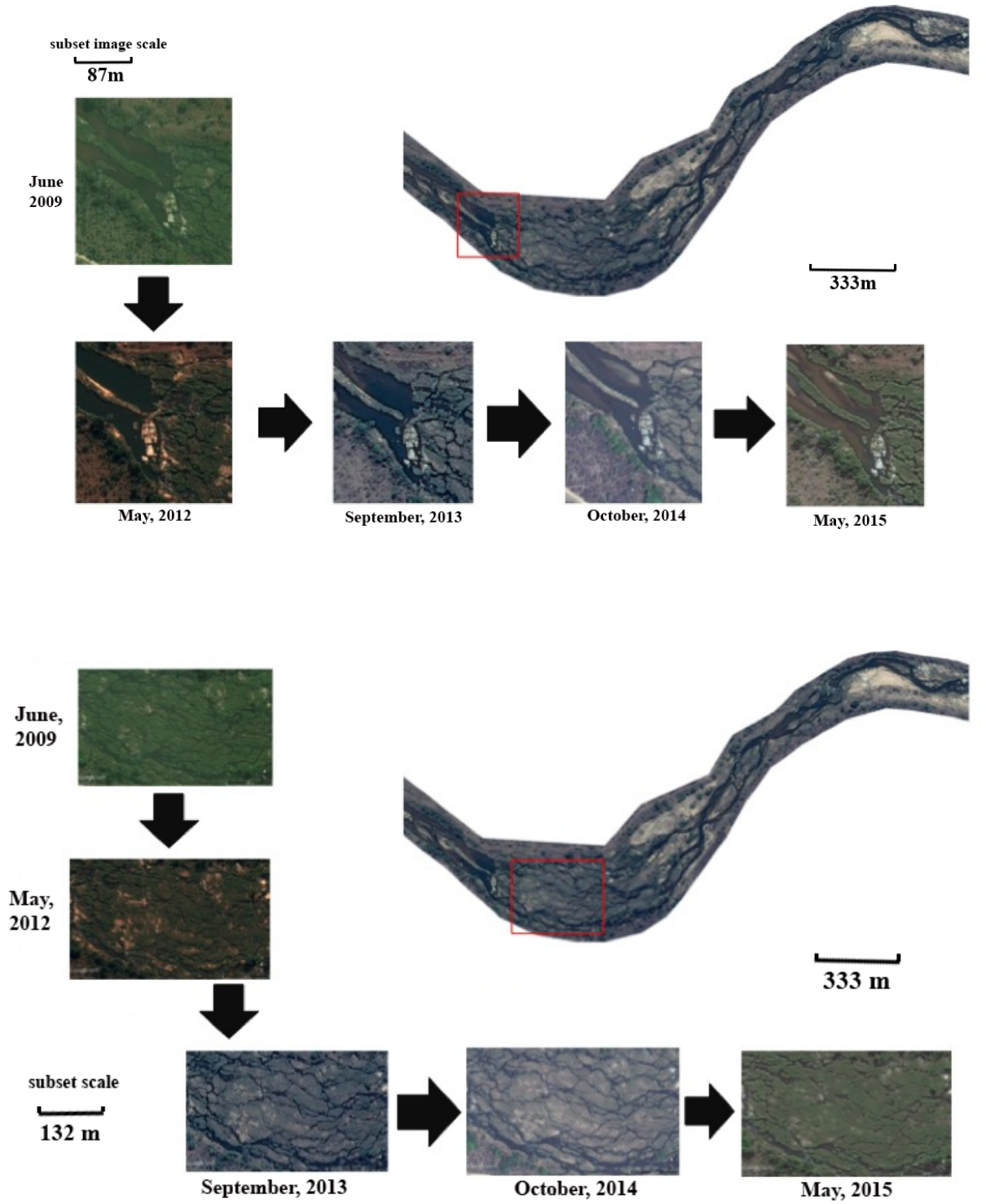

Figure 5.1. Bedrock anastomosing channel schematic time series with area of interest highlighted by red box (intial region (top); main body of channel (bottom), whilst changes there plotted from top left to bottom right, the whole reach is located at within the top right (DigitalGlobe, 2015).

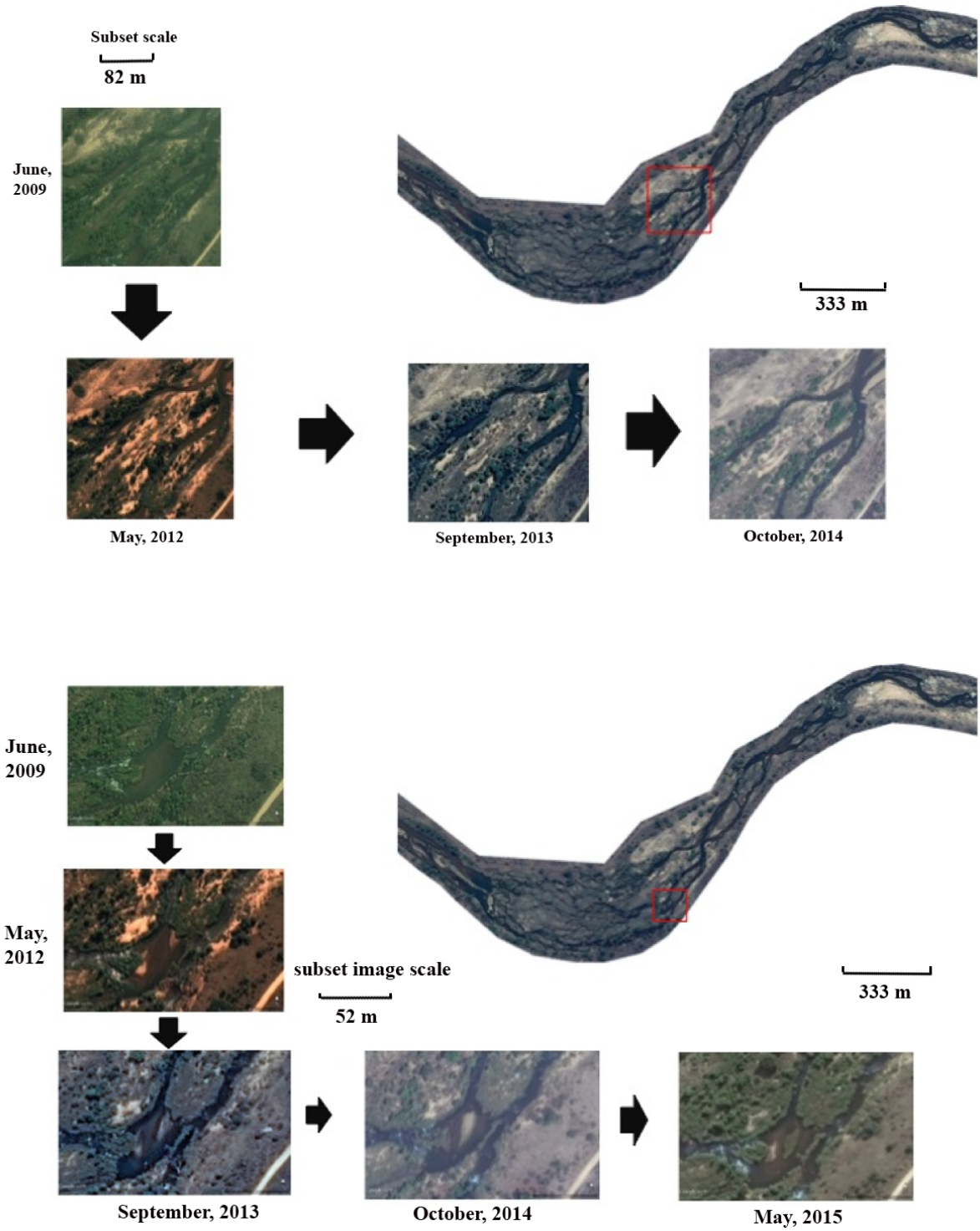

Figure 5.2. Pool-rapid channel schematic time series, with AOI highlighted by red box with changes positioned from top left to bottom right, whilst whole reach found on the to right Top right (DigitalGlobe, 2015).

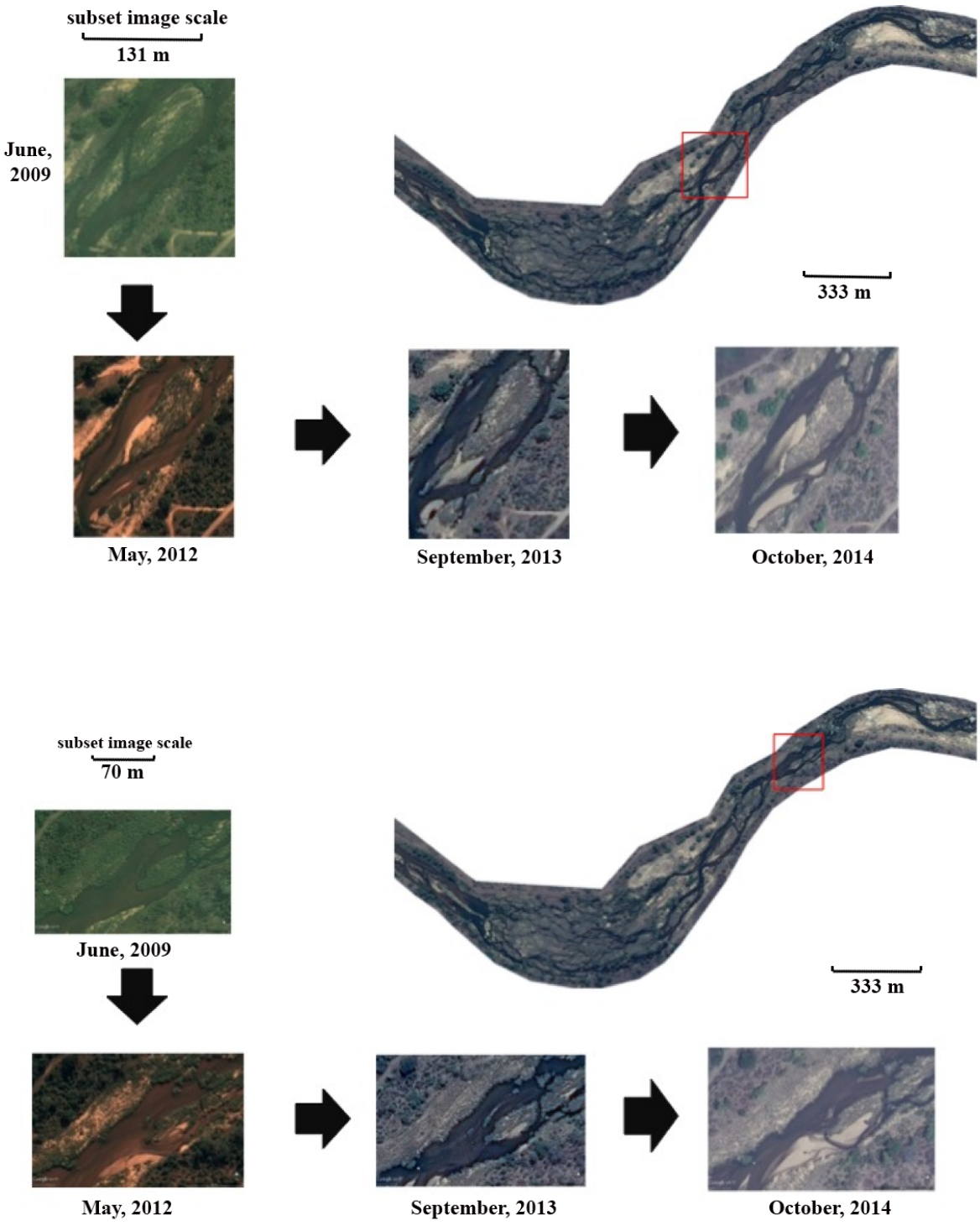

Figure 5.3. Pool-rapid schematic with AOI highlighted by red box with times series images positioned from top left to bottom right, whilst whole reach is situated at the top right (DigitalGlobe, 2015).

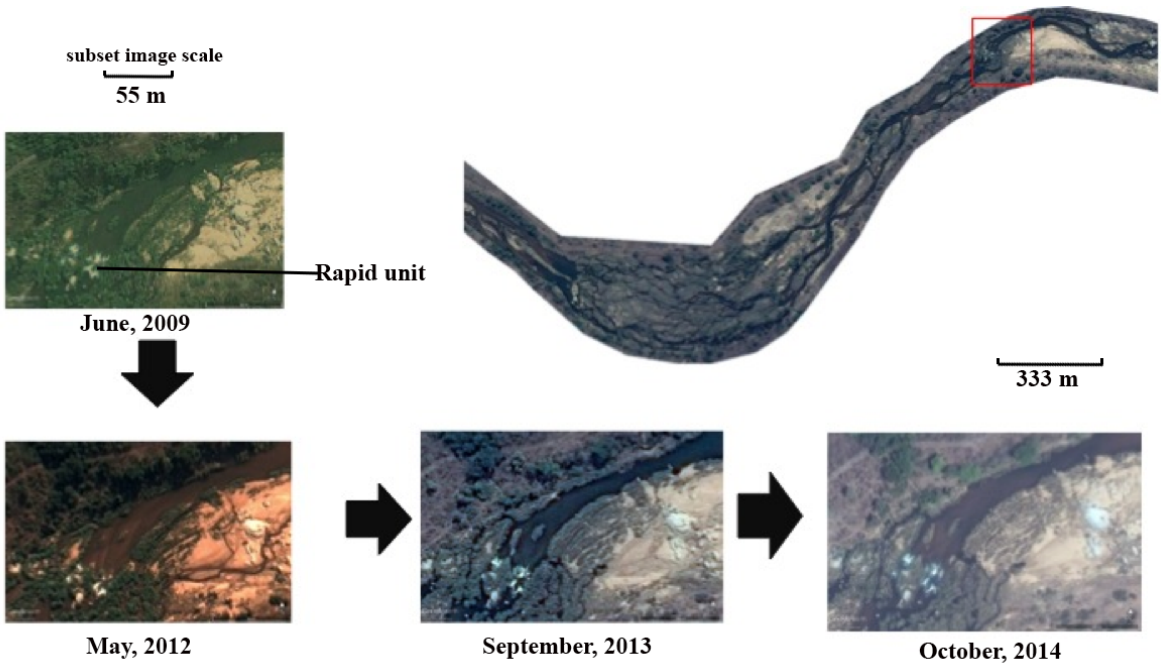

Figure 5.4. Geomorphic change following cyclone Dando,at a rapid unit highlighted by red box positioned from top left to bottom right, whilst whole reach is situated at the top right (DigitalGlobe, 2015).

At site two interruption to prolonged aggradation occurred through stripping of soft uncohesive sediments following a cyclone Elines accompanied flood event. Such flooding also caused high levels of sediment removal that lead to reduced alluvial and large bedrock core bars on either side of the channel (Figure 5.5). Between each cyclone event and after 2012's cyclone Dando, sedimentation rapidly enabled alluvial features to recover through aggradation as seen upstream at the primary study site.

Cyclical modifications of the pool-rapid towards both cyclone-driven flood events are more apparent further downstream (figure 5.6), with extensive stripping of soft sediments evident following cyclone Eline. Again, destruction of sedimentary features has increased the presence of active channels throughout adjacent to the pool-rapid succession, although stripped sediment did occur at as large a scale following cyclone Dando, as sedimentation appears to persist following it. Whilst, Rapid units presented at site two were almost untouched by peak flows in 2012, with no visible occurrences of erosion and minimal

deposition. Following cyclone Dando, elevated rates of deposition occurred throughout site two that allowed previously devastated alluvial and vegetated areas to recover.

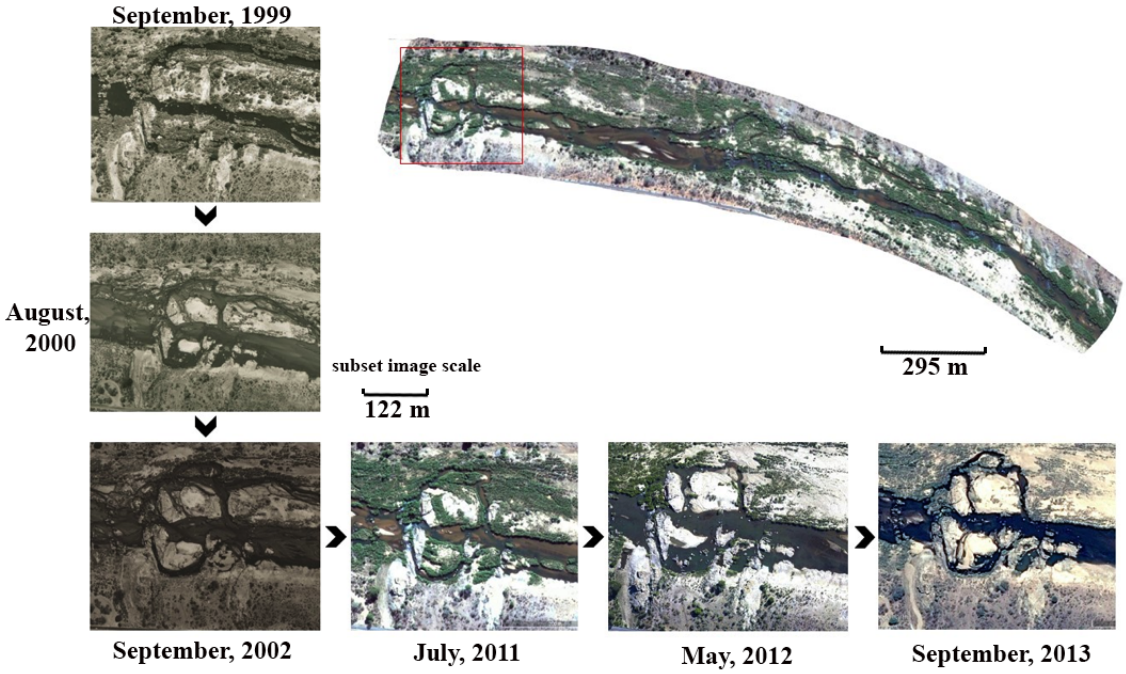

Figure 5.5. The upstream channel boundary of Site two (highlighted by red box), with time series changes displayed from top left to bottom right, whilst the whole reach is located on the top right (Fotogramensura, 1999; Fotogramensura, 2000; Fotogramensura, 2002; CNES/Astrium, 2011; JBA Consulting Ltd., 2012; DigitalGlobe, 2013).

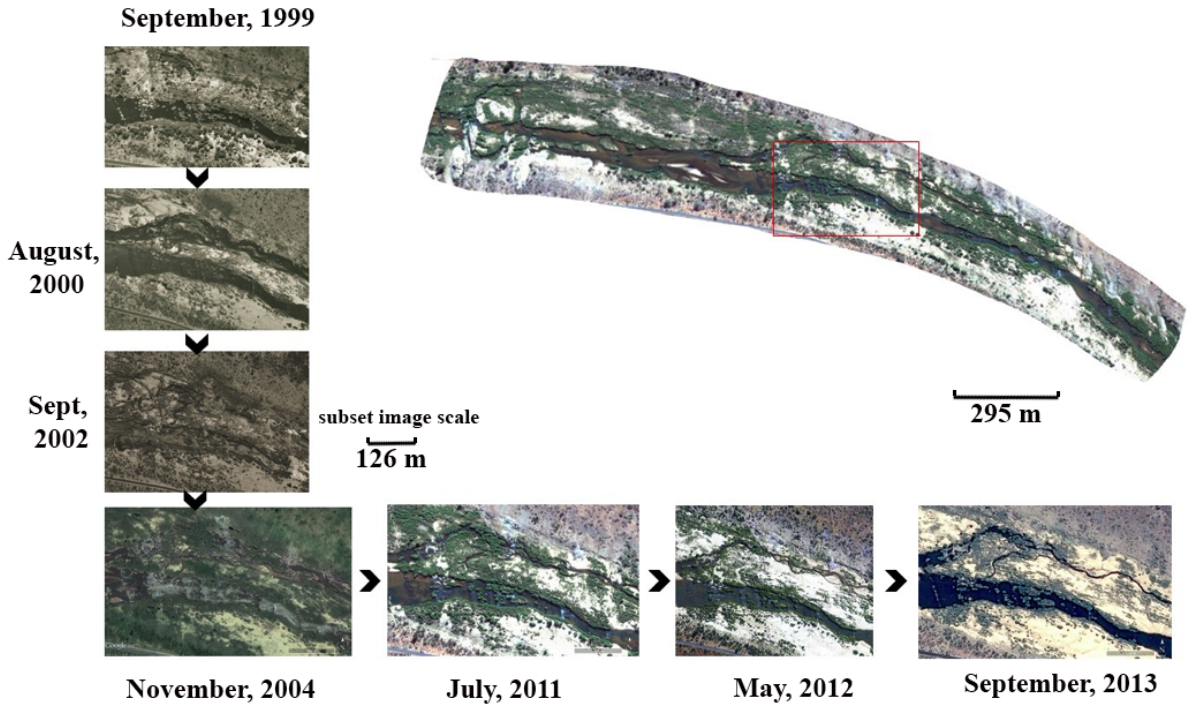

Figure 5.6. Pool-rapid sequence at site two, highlighted by red box with scaled with time series geomorphic changes situated from top left to bottom right, whilst overall image positioned in the top right (Fotogramensura, 1999; Fotogramensura, 2000; Fotogramensura, 2002; CNES/Astrium, 2004; CNES/Astrium, 2011; JBA Consulting Ltd., 2012; DigitalGlobe, 2013).

5.2. In-channel hydraulics

This section is split-up dependant on each variable and whether they correlate with one another. The split resulted in section 5.2.1 describing velocity and bed shear stress models in relation to each discharge scenario, whilst water surface elevation narratives occurred separately in section 5.2.2. Finally, section 5.2.3 involved hydraulic biotope variations via Froude number calculations.

5.2.1. Velocity and bed shear stress variations

Increases in discharge have an almost equally significant effect on bed shear stress and velocity within the reach, as significantly positive R^2 value found between bed shear stress

and velocity (figure 5.7), albeit differences between them involved a greater intensity of mean velocity than bed shear stress with each ascending discharge. Despite some contrasts found between each variable, a close relationship enabled one to collectively observe their retort to an extreme flood event.

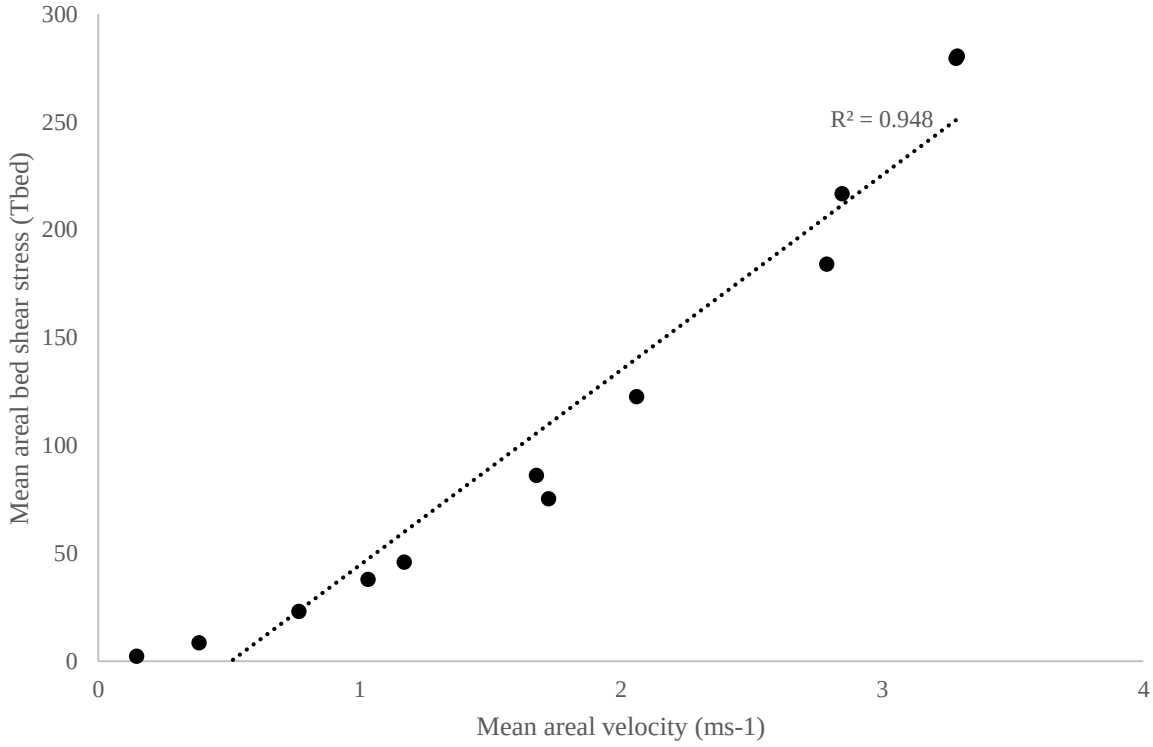

Figure 5.7. Mean areal velocity against bed shear stress for each progressive discharge scenario from Q_1 to Q_{12} for the whole reach.

The anastomosing channel consisted of a tortuous wetted perimeter made up of an assorted array of bed shear stress (>80 Nm^{-2}) and velocity (>1.5 ms^{-1}) during Q_1, however as discharge increased towards Q_6, the complex channel network transformed into a single channel unit. Alterations in the active channel template at the anastomosing channel produced sharp rises in both bed shear stress and velocity, which by Q_6 saw values range between 1 – 4 ms^{-1} and 80 – 150 Nm^{-2} respectively. At extreme discharge (Q_7 – Q_{12}), the anastomosing channel displayed considerable highs in velocity (~>6 ms^{-1}-8 ms^{-1}) and bed shear stress (~>600 Nm^{-2}-1000 Nm^{-2}), with most notable peaks in them found at the anastomosing channel boundary found

upstream. Such highs in both variables progressively reduced in overall value further downstream, with occurrences of relative highs found sparingly across the macrochannel before reaching the pool-rapid boundary at control point one.

The pool-rapid channel displayed a typical distribution of high and low values in velocity and bed shear stress dependent on control point locations, which contrasted considerably to variable distribution found at the anastomosing channel. High values in both bed shear stress and velocity occurred at rapid units as opposed to lower levels mostly transpiring within pool habitats, as peaks became increasingly larger in area throughout each discharge scenario. In addition to increases in velocity and bed shear stress, changes to pool-rapid channel physiology became increasingly apparent at each control point, as inundation of sedimentary features further amplified active channel geometry. However, to fully appreciate such diverse changes throughout the pool-rapid channel, individual accounts of changes in velocity and bed shear stress at each identified control point must occur.

Control point one exhibited a dramatic transformation from a diverse assortment of relative highs and lows into comparatively monotonous hydraulics coherent with relatively reduced velocity (>3.5 ms^{-1}) (figure 5.8) and bed shear stress (>133 Nm^{-2}) (figure 5.9). Progressive reductions in bed shear stress and velocity were combined with a gradual increase in channel width immediately downstream of control point one, submerging lateral bars and small islands in the process. However, reduced values in bed shear stress and velocity found at the pool following control point one were no different to hydraulics immediately downstream of each rapid unit during increased discharge. Such enlarged geometric characteristics following control point one not only reduced bed shear stress and velocity there but also neighbouring rapid units at increased discharge. This is evident at control point two, which became

subsumed by upstream hydraulics causing it to consist of a less distinct velocity and bed shear stress template during increased discharge scenarios. However, despite control point two being overwhelmed by hydraulics found upstream, distinct peaks in velocity and bed shear stress that were lost by Q_7 returned at Q_{12}.

The highest values in velocity and bed shear stress occurred at control points three and four, with peaks during extreme discharge (Q_{12}) ranging between ~6 – 7.5 ms^{-1} and ~500 – 800 Nm^{-2} respectively. During Q_1, control point three's influence on hydraulics was presented as perpendicular band of comparatively greater values in bed shear stress (80 – 150 Nm^{-2}) and velocity (0.75 – 3.5 ms^{-1}). However, as discharge scenarios increased to those represented in Q_7 – Q_{12}, values in velocity and bed shear stress found at the pool immediately downstream of control point three increased in area, once again displaying a distinct boundary between highs and lows in both variables. Confinement of highs in velocity and bed shear stress found at Q_{12} concentrated flow down the channel's centre, however the position of these highs evidently expanded upstream differing considerably to conditions present during low flows.

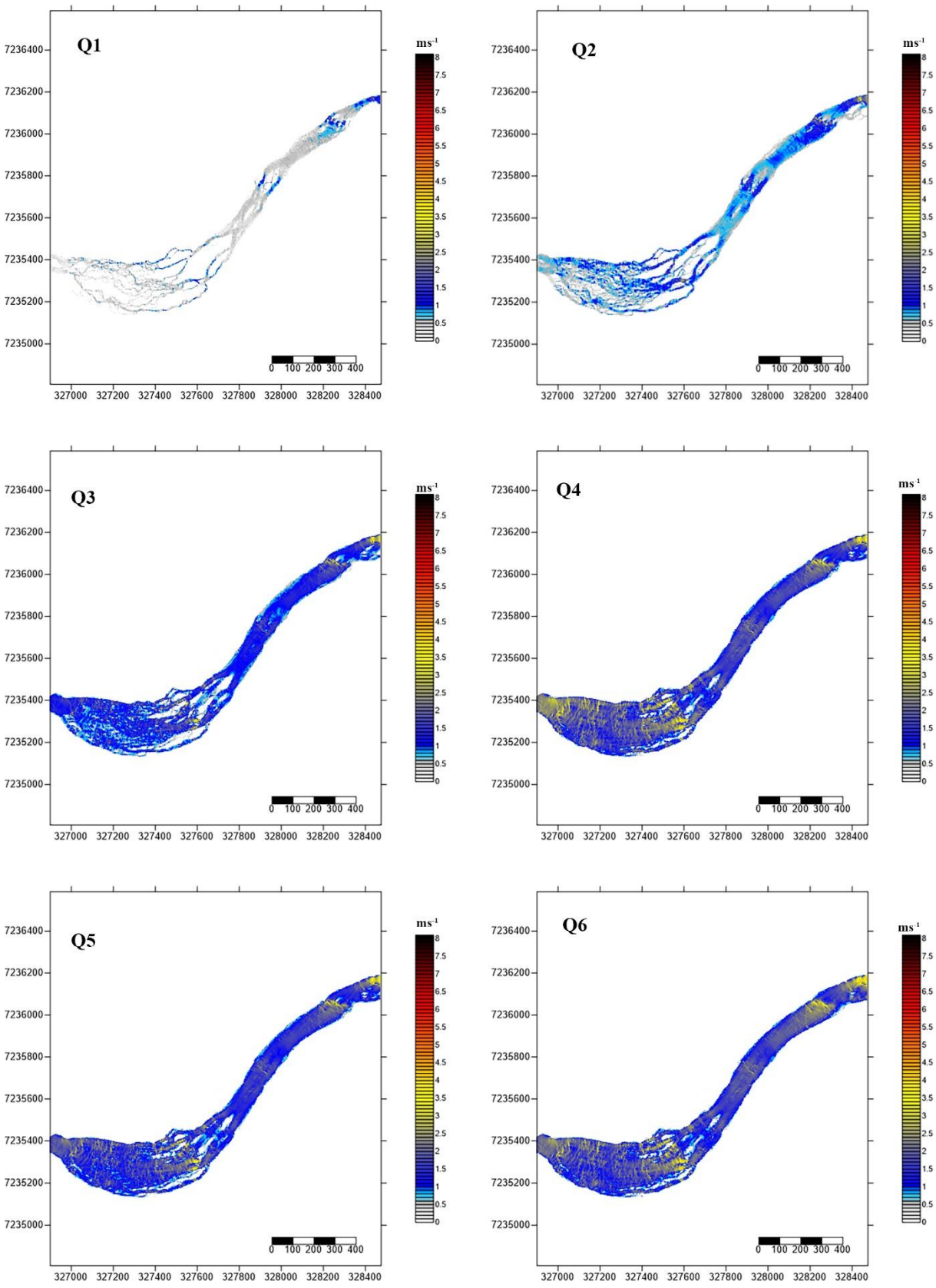

Figure 5.8. Two-dimensional velocity models of study reach ordered in accordance with ascending discharge scenarios (Q1-Q12); velocity ranged between 0-8 ms^{-1} whilst flow travelled from left to right.

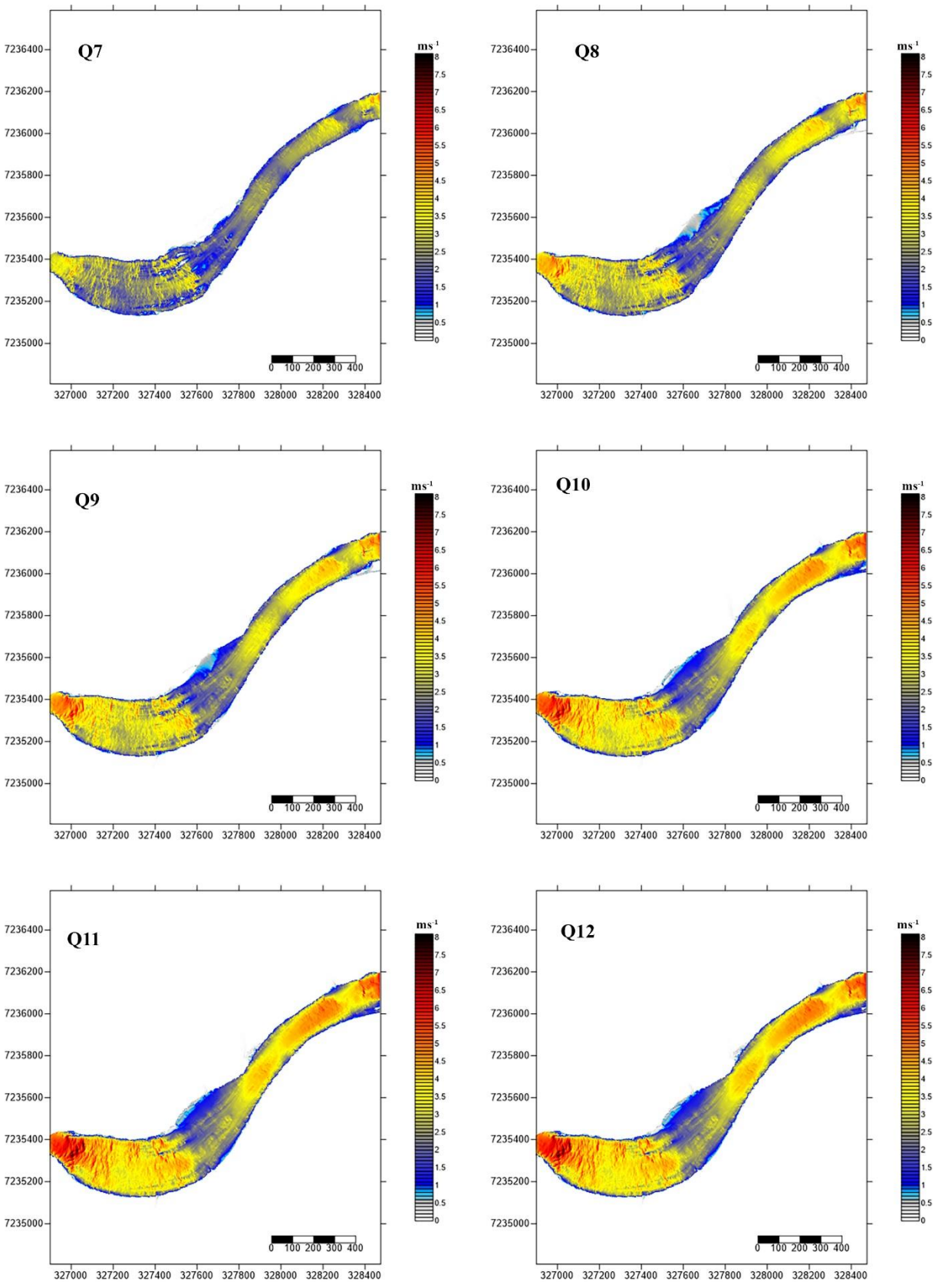

Figure 5.8 (continued). Two-dimensional velocity models of study reach ordered in accordance with ascending discharge scenarios (Q1-Q12); velocity ranged between 0-8 ms^{-1} whilst flow travelled from left to right.

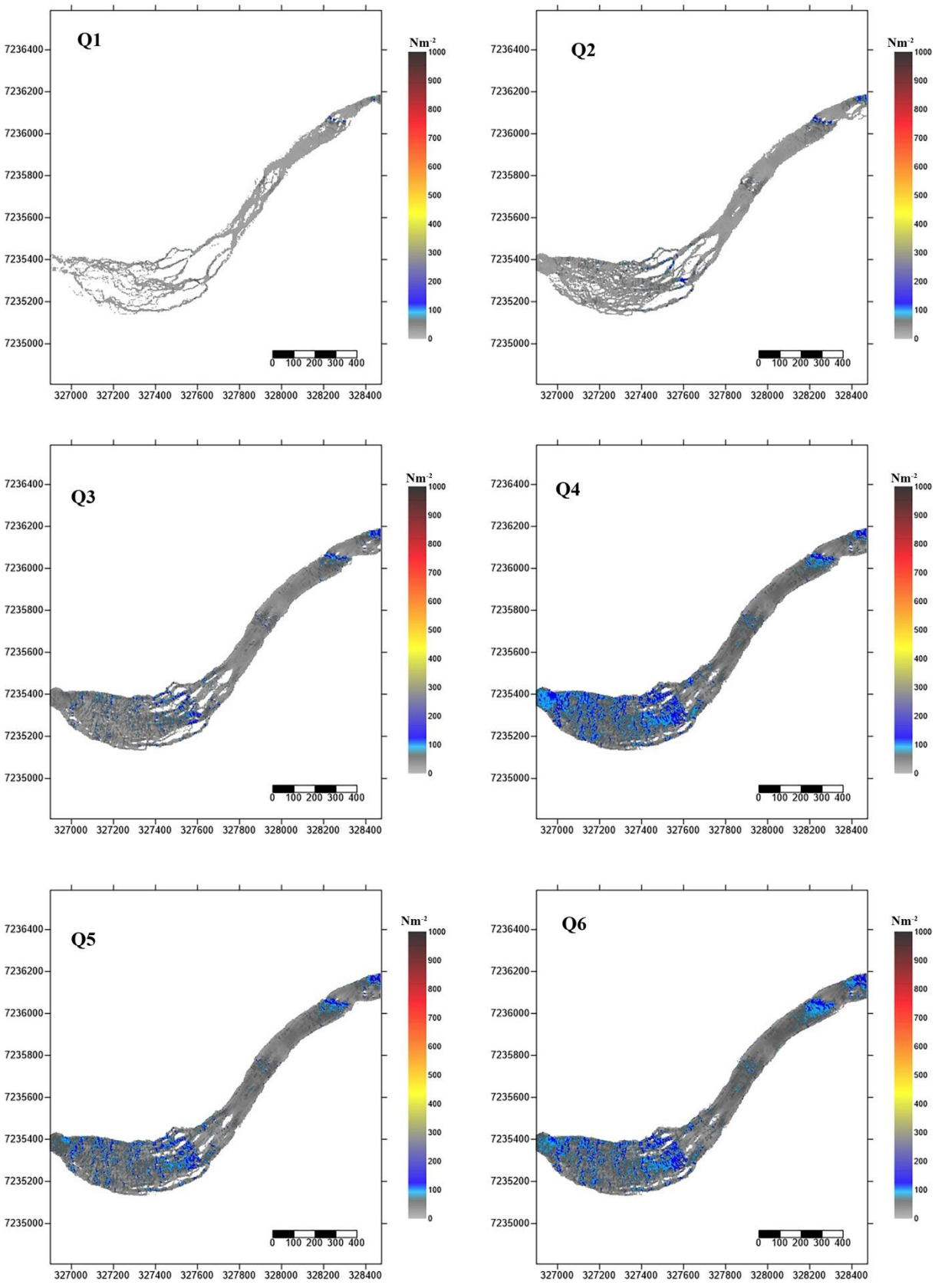

Figure 5.9. Two-dimensional Bed shear stress models of study reach ordered in accordance with ascending discharge scenarios (Q1-Q12); water surface ranged between 0-1000 Nm^{-2}, whilst flow travelled from left to right.

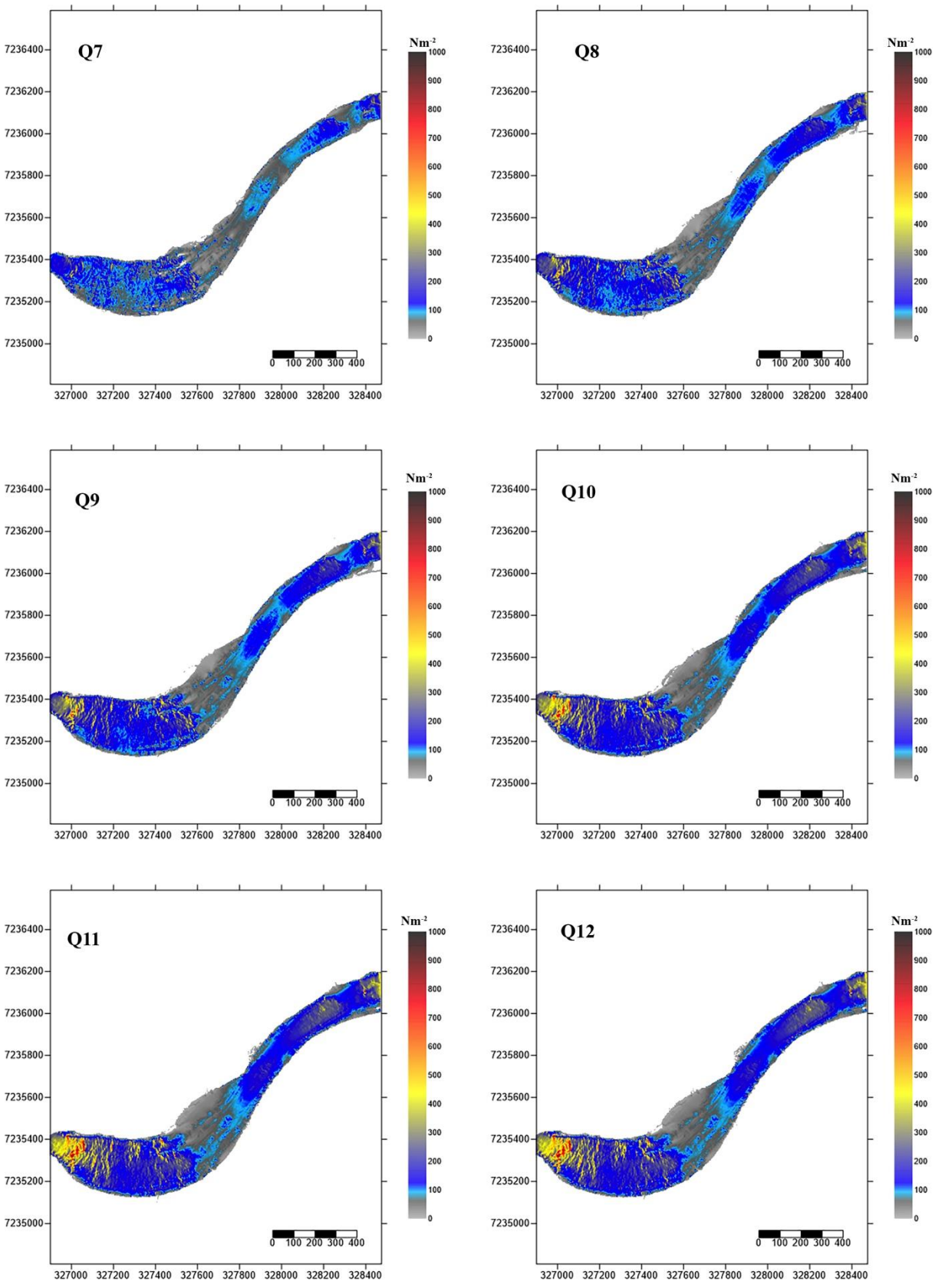

Figure 5.9 (continued). Two-dimensional Bed shear stress models of study reach ordered in accordance with ascending discharge scenarios (Q1-Q12); water surface ranged between 0-1000 Nm^{-2}, whilst flow travelled from left to right.

5.2.2. Water surface

Correlations between water surface elevations and velocity were positive (figure 5.10), however R^2 values did not attain the same strength found between bed shear stress and mean water surface elevations (figure 5.11; top). Despite R^2 values found between water surface and both bed shear stress, and velocity being not as strong as anticipated, water depth (the by-product of water surface and the DTM) consisted of a comparatively more significant relationship with each variable (Bed shear stress: figure 5.12; Velocity: 5.11, bottom).

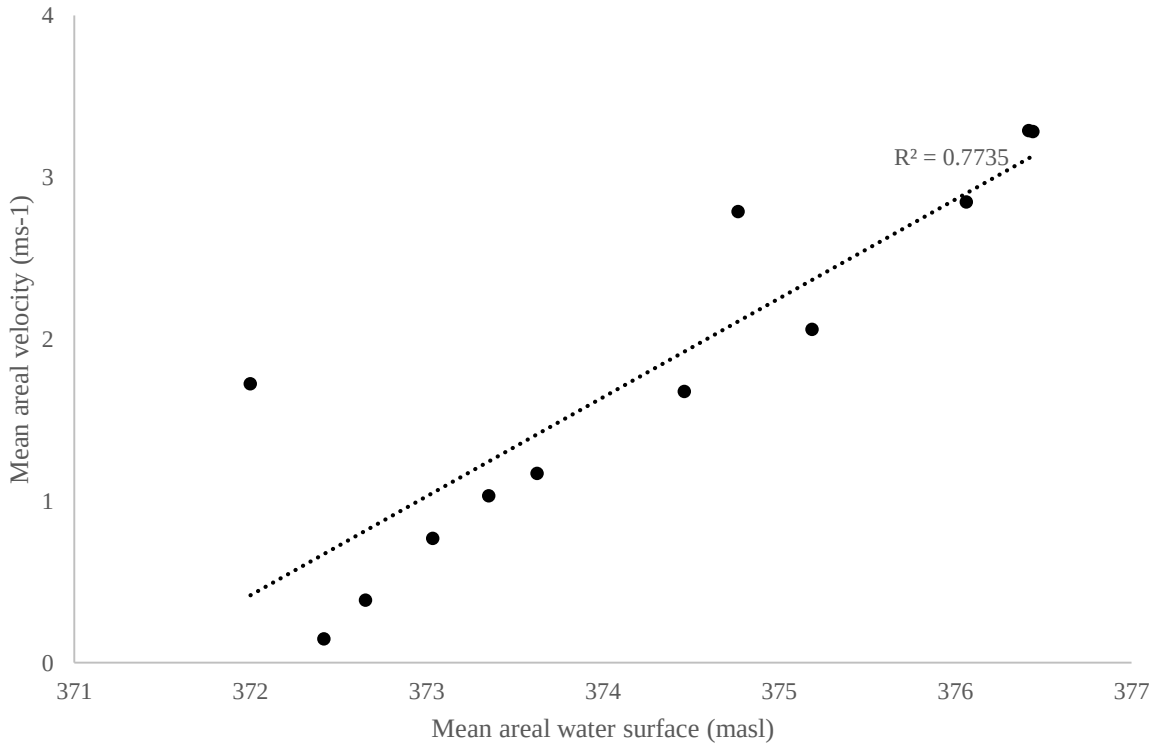

Figure 5.10. Mean areal water surface elevations (masl) against mean areal velocity (ms^{-1}).

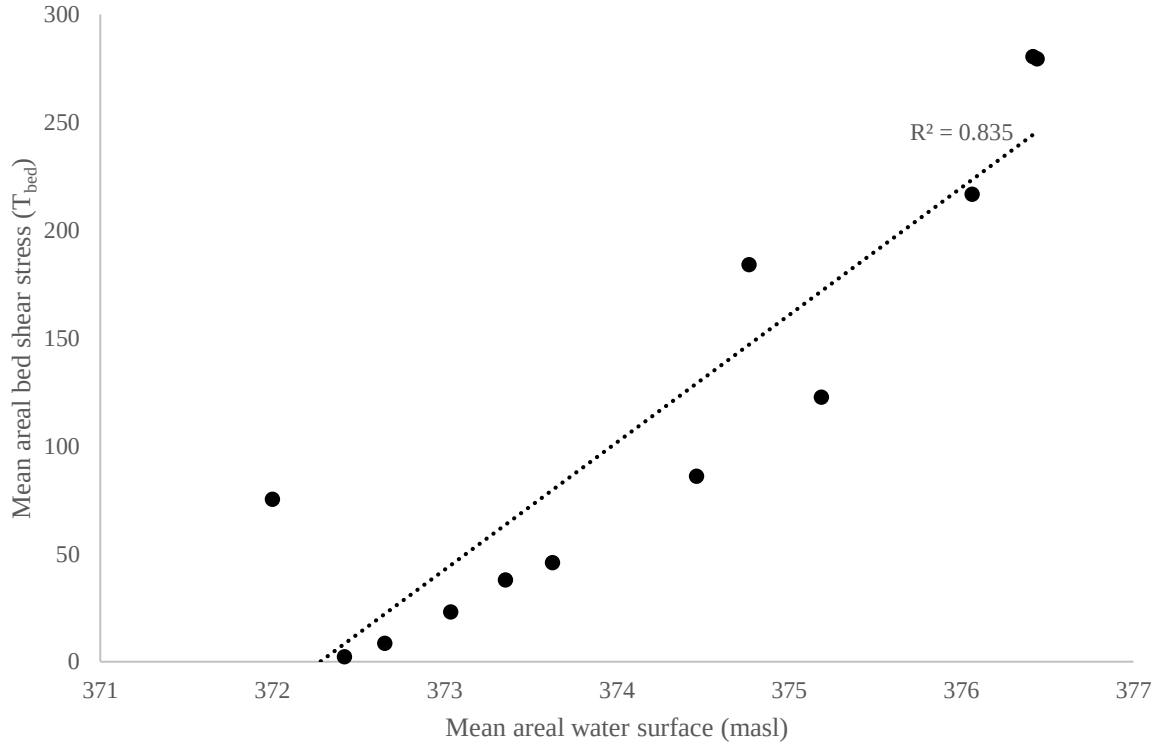

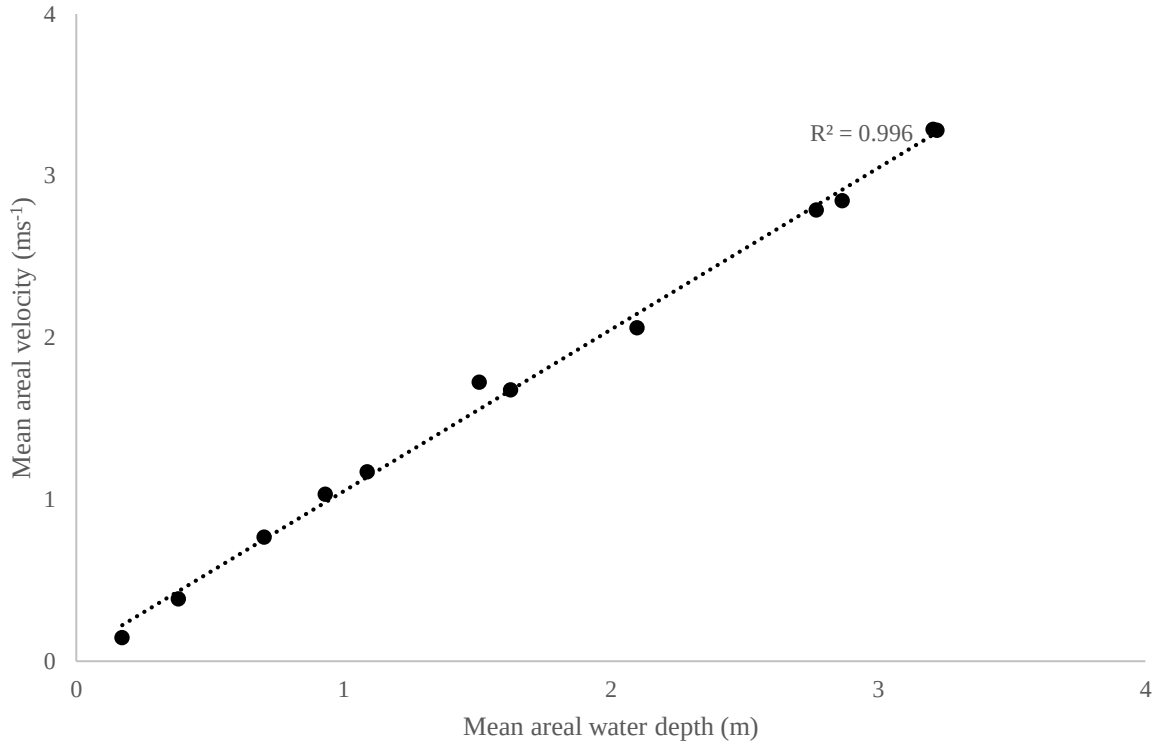

Figure 5.11. Top: Mean areal water surface elevation (masl) against mean areal bed shear stress (Nm^{-2}); bottom: Mean areal water depth (m) against mean areal velocity (ms^{-1}).

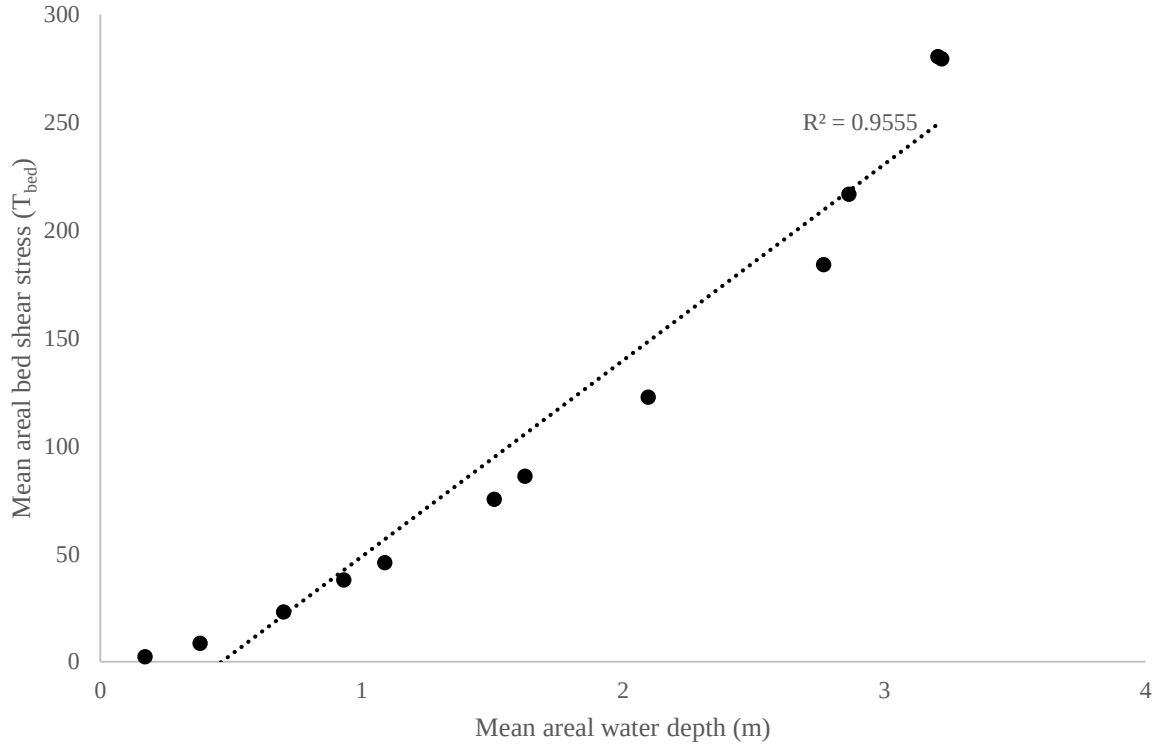

Figure 5.12. Mean areal water depth (m) against mean areal bed shear stress (Nm^{-2}).

Overall, water surface elevations within the reach increased with each discharge scenario; with the most significant rises in elevation following control point one. Water surface elevations displayed at the pinnacle of control point one (~373 masl) appeared to spread as far downstream as control point two from Q_8 to Q_{12} (figure 5.13). At extreme discharge, water surface elevations reduced at a slower rate of 4 m between control points two and three; nevertheless, more abrupt reductions in stage occurred between control points three and four, made more significant by the short distance between them.

General analysis of the anastomosing channel displayed a continual water surface increase across the reach, however the bedrock-anastomosing channel's wetted perimeter appeared somewhat altered to bed shear stress and velocity models as channel singularity within the former was mostly present at lower discharge scenarios. As discharge ascended towards extreme levels, water surface models displayed an almost completely inundated anastomosing

channel, as exposed topographical units large to remain visible at reduced discharge scenarios became submerged.

Similar to velocity and bed shear stress projections, the pool-rapid attained a diverse water surface template dictated by each control point where water surface elevations experienced an abrupt reduction (figure 5.13). Q_1 water surface elevations was consistent with the highest levels of variability, as stage reduced considerably at each control point, particularly at control point one where water levels reduced by 6 m. However, each control point during low flow displayed a boundary between relative highs and lows in water surface elevations, which continually became less distinct as discharge increased.

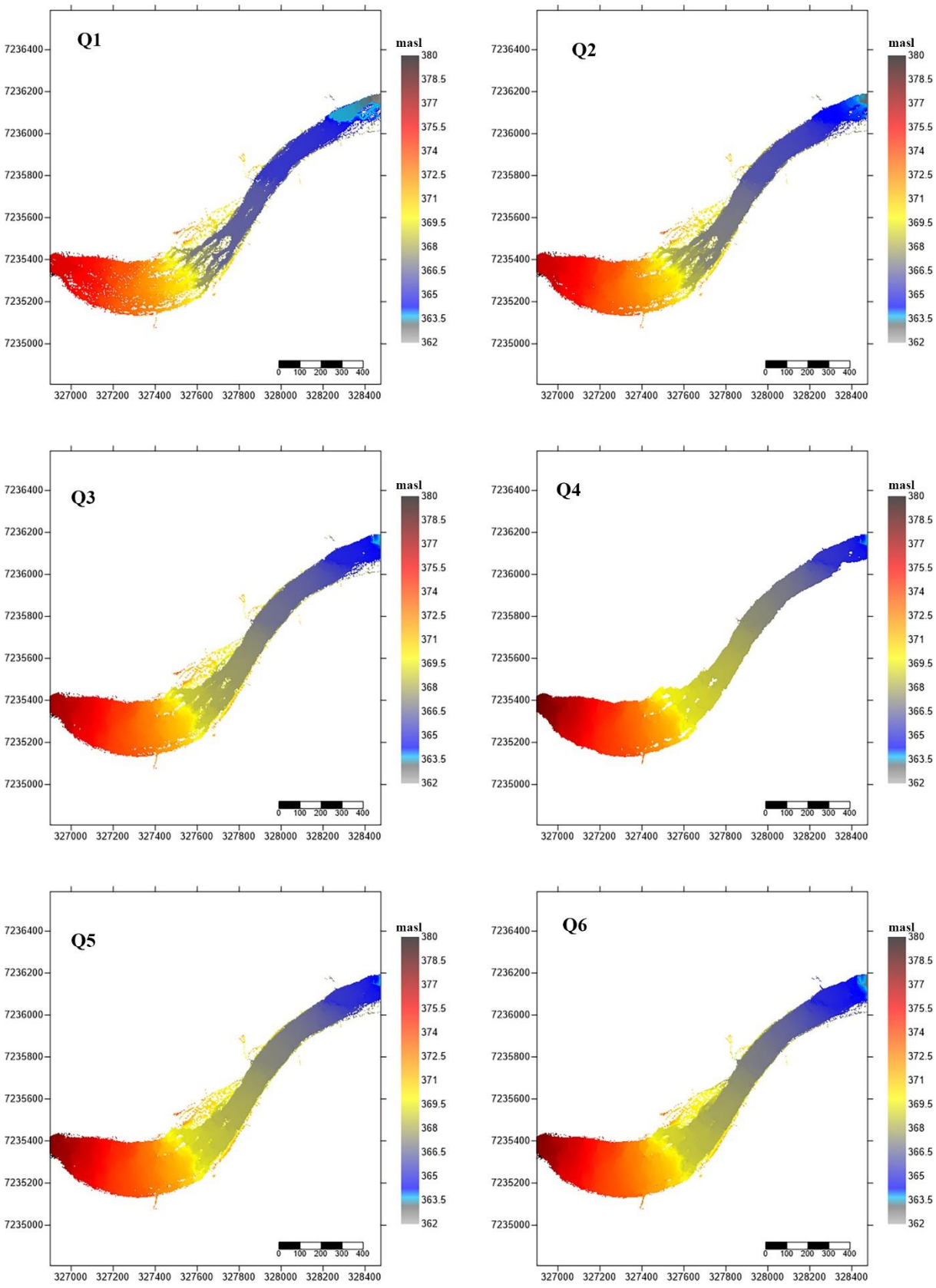

Figure 5.13. Two-dimensional water surface models of study reach ordered in accordance with ascending discharge scenarios (Q1-Q12); water surfaces are between 362-381 masl, Flow travelled from left to right.

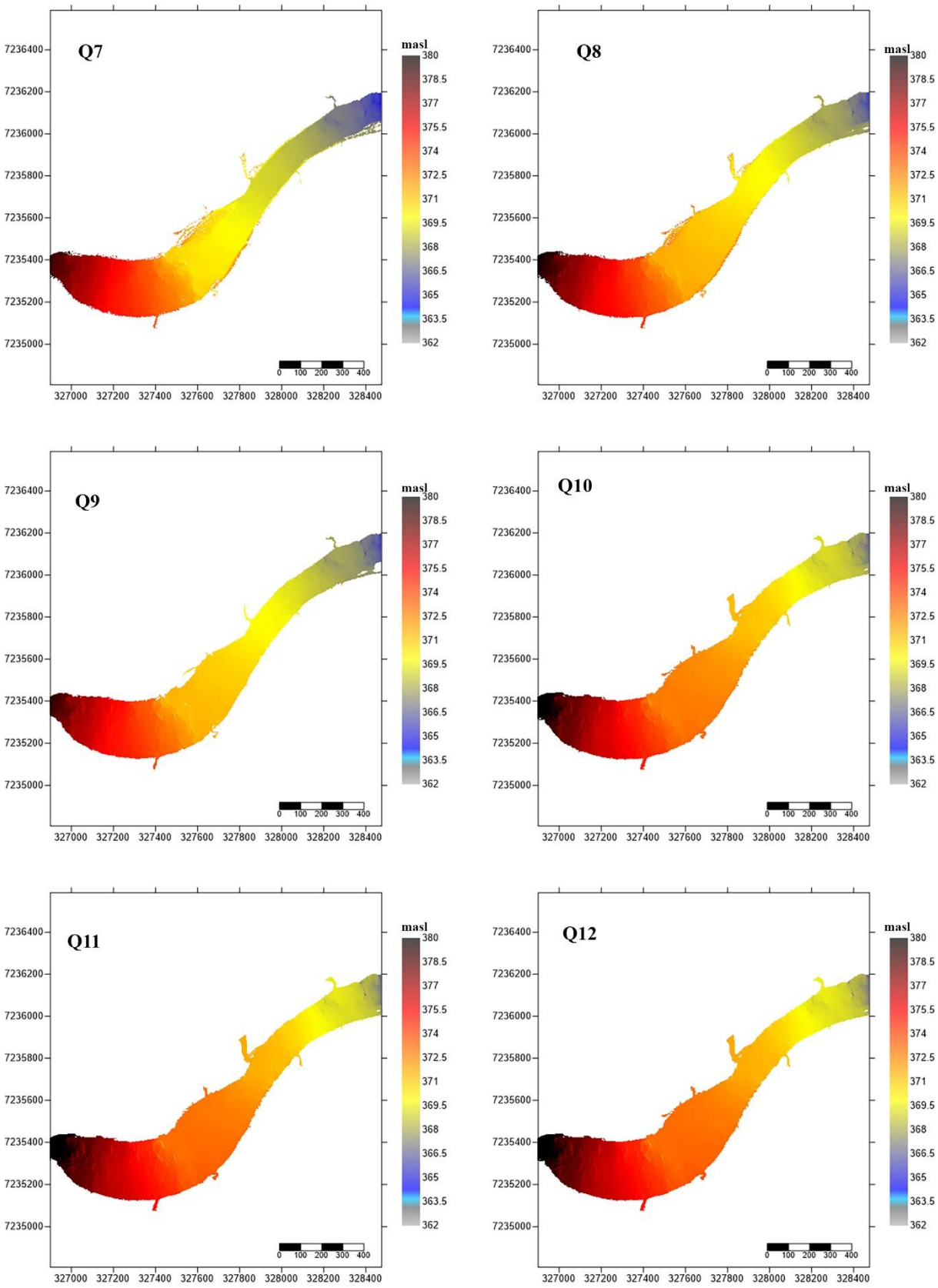

Figure 5.13 (continued). Two-dimensional water surface models of study reach ordered in accordance with ascending discharge scenarios (Q1-Q12); water surfaces are between 362-381 masl, flow travelled from left to right.

Table 5.1 displays cross-sectional areas of selected discharge scenarios throughout the anastomosing channel, which exhibit rapid and significant increases in area. Each subsequent cross-section exhibits comparatively larger rises in cross-sectional area at each increased discharge scenario. Particular growth in cross-sectional area was evident at cross-section C, which does not follow the trend of having a larger cross-sectional area during Q_4, however increased discharge at Q_{12} displayed a much greater area than those found upstream. Each cross-section found throughout the anastomosing channel displayed a significant difference between what was evident during Q_4 in comparison to findings made during Q_{12} as all four areas surge by over 500 m^2.

Pool-rapid cross-sectional area is considerably more varied than the progressive increases present at each subsequent anastomosing cross-section, as abrupt increases and reductions found throughout the pool-rapid (table 5.2 and 5.3). Initial regions of the pool-rapid including its channel boundary (Cross-section E – J) are consistent with considerably high levels of cross-sectional area, which in most discharge scenarios is much larger than any recorded at the anastomosing channel, with some cases (cross-section G) being more than double that of the largest anastomosing cross-section (D). Such abrupt alterations in cross-sectional area are highlighted within two-dimensional representations of velocity, with areas of relatively slower velocity producing much larger wetted areas of the channel throughout the pool-rapid channel. Further downstream at cross-sections K to N, diversity occurs in cross-sectional area as it rises and declines at each selected discharge scenario dependant on its position within the channel, with particular emphasis at cross-sections containing large alluvial features such as 'N', which increases in area by ~>700 m^2.

Table 5.1. Cross-sectional area (m^2) of sections A to D (anastomosing).

Cross-section A

Scenario	Width (m)	Average depth (m)	Area (m^2)
Q_4	213.97	1.64	350.91
Q_7	227.53	2.49	566.55
Q_9	230.67	2.93	675.86
Q_{11}	235.88	3.34	787.84
Q_{12}	238.14	3.61	859.69

Cross-section B

Scenario	Width (m)	Average depth (m)	Area (m^2)
Q_4	238.16	1.61	383.44
Q_7	259.53	2.45	635.85
Q_9	266.52	2.77	738.26
Q_{11}	266.66	3.15	839.98
Q_{12}	266.74	3.34	890.91

Cross-section C

Scenario	Width (m)	Average depth (m)	Area (m^2)
Q_4	245.56	1.53	375.71
Q_7	274.21	2.33	638.91
Q_9	277.28	2.76	765.29
Q_{11}	284.44	3.17	901.67
Q_{12}	287.51	3.44	989.03

Cross-section D

Scenario	Width (m)	Average depth (m)	Area (m^2)
Q_4	250.28	1.66	415.46
Q_7	256.48	2.64	677.11
Q_9	275.08	3.10	852.75
Q_{11}	274.07	3.54	970.21
Q_{12}	278.20	3.81	1059.94

Table 5.2. Cross-sectional areas (m^2) at each of the selected discharge scenarios for cross-section analysis at the pool-rapid.

Cross-section E

Scenario	Width (m)	Average depth (m)	Area (m^2)
Q_4	263.21	1.93	508
Q_7	270.09	3.56	961.52
Q_9	287.91	4.39	1263.92
Q_{11}	292.14	5.22	1524.97
Q_{12}	293.85	5.77	1695.51

Cross-section F

Scenario	Width (m)	Average depth (m)	Area (m^2)
Q_4	248.2	2.14	531.15
Q_7	263.1	3.96	1041.88
Q_9	283.29	4.82	1365.46
Q_{11}	287.92	5.66	1629.63
Q_{12}	292.44	6.22	1818.98

Cross-section G

Scenario	Width (m)	Average depth (m)	Area (m^2)
Q_4	190.12	3.42	650.21
Q_7	234.8	5.08	1192.78
Q_9	249.42	5.92	1476.57
Q_{11}	295.31	6.71	1981.53
Q_{12}	331.16	7.23	2394.29

Cross-section H

Scenario	Width (m)	Average depth (m)	Area (m^2)
Q_4	150.12	3.13	469.88
Q_7	201.68	5.18	1044.7
Q_9	234.07	6.08	1423.15
Q_{11}	268.24	6.93	1858.9
Q_{12}	292.25	7.5	2191.88

Cross-section I

Scenario	Width (m)	Average depth (m)	Area (m^2)
Q_4	117.29	2.84	333.1
Q_7	174.52	4.94	862.13
Q_9	225.15	5.87	1321.63
Q_{11}	234.66	6.74	1581.61
Q_{12}	257.69	7.31	1883.71

Cross-section J

Scenario	Width (m)	Average depth (m)	Area (m^2)
Q_4	106.76	2.64	281.85
Q_7	155.79	4.61	718.19
Q_9	163.06	5.5	896.83
Q_{11}	170.28	6.34	1079.58
Q_{12}	182.33	6.89	1256.25

Table 5.3. Cross-sectional area (m^2) statistics with each selected discharge scenario at distal segment of pool-rapid.

Cross-section K

Scenario	Width (m)	Average depth (m)	Area (m^2)
Q_4	107.50	2.25	241.88
Q_7	125.34	4.14	518.91
Q_9	130.56	4.98	650.19
Q_{11}	135.60	5.75	779.70
Q_{12}	139.47	6.25	871.69

Cross-section L

Scenario	Width (m)	Average depth (m)	Area (m^2)
Q_4	116.92	2.94	343.74
Q_7	131.39	4.98	654.32
Q_9	134.66	5.84	786.41
Q_{11}	143.90	6.61	951.18
Q_{12}	151.83	7.12	1081.03

Cross-section M

Scenario	Width (m)	Average depth (m)	Area (m^2)
Q_4	104.92	2.31	242.37
Q_7	122.43	4.01	490.94
Q_9	132.46	4.15	549.71
Q_{11}	142.23	5.38	765.20
Q_{12}	149.00	5.81	865.69

Cross-section N

Scenario	Width (m)	Average depth (m)	Area (m^2)
Q_4	107.11	2.84	304.19
Q_7	115.30	4.46	514.24
Q_9	167.71	5.15	863.71
Q_{11}	174.41	5.79	1009.83
Q_{12}	176.26	6.23	1098.10

5.2.3. Hydraulic biotopes

Biotopes showed remarkable diversity throughout the reach (figure 5.18) although such assortment was dependant on channel type, as initial observations of the anastomosing channel presented a highly assorted template consistent with each biotope. As discharge increased, these biotopes became increasingly monogamous in their diversity yet comprised of high-energy (i.e. rapids and chutes), such rapids began to progressively dominate the anastomosing channel (minus the sharp increase seen in Q5), replacing much lower energy biotopes in the process. At extreme discharge, more energetic in-channel chutes spread throughout the anastomosing channel from the anastomosing channel boundary, interchanging with rapids further downstream.

The pool-rapid exhibited a more structured yet non-uniform biotope template, where lower energy biotopes (pools, boils, riffles) dominated the channel accompanied by small interruptions of higher Froude numbers characterised as rapids and chutes found at each control point during lower flow. During low flow scenario, biotope templates leading up to each rapid unit frequently consisted of a specific order commonly structured as boil-riffle-run-rapid. This biotope template altered significantly in addition to area coverage of high-energy biotopes as discharge ascended towards extreme levels ($>Q_{12}$), with biotopes comprised of lower Froude numbers (<0.245 *Fr*) were lost, replaced by runs and rapids.

Contrasts in biotope diversity between the anastomosing and pool-rapid channel was clear following control point one, as the multi-formed passages transformed into a singular unit. Runs quickly dominated the initial pool-rapid segment by Q_3 and replaced its varied template found there, however riffles persisted by surrounding the large lateral bar found there.

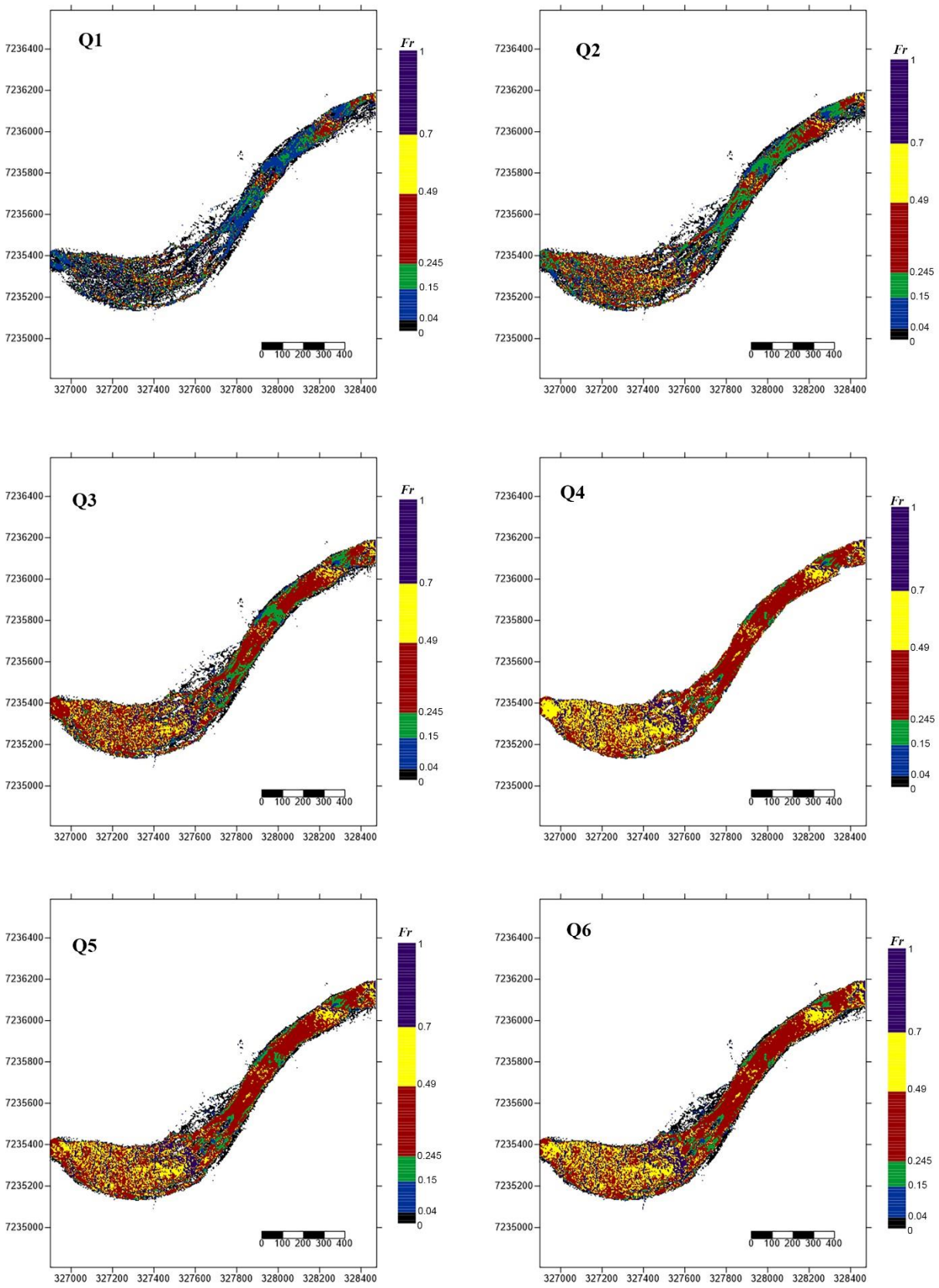

Figure 5.14. Two-dimensional Froude number models of study reach ordered in accordance with ascending discharge scenarios (Q1-Q6); Hydraulic biotopes are calculated via Froude number categories between Fr No. 0 and 1; black: pool; Blue: boil; Green: riffle; Red: run/glide; yellow: rapid and purple: Chute, flow travelled from left to right.

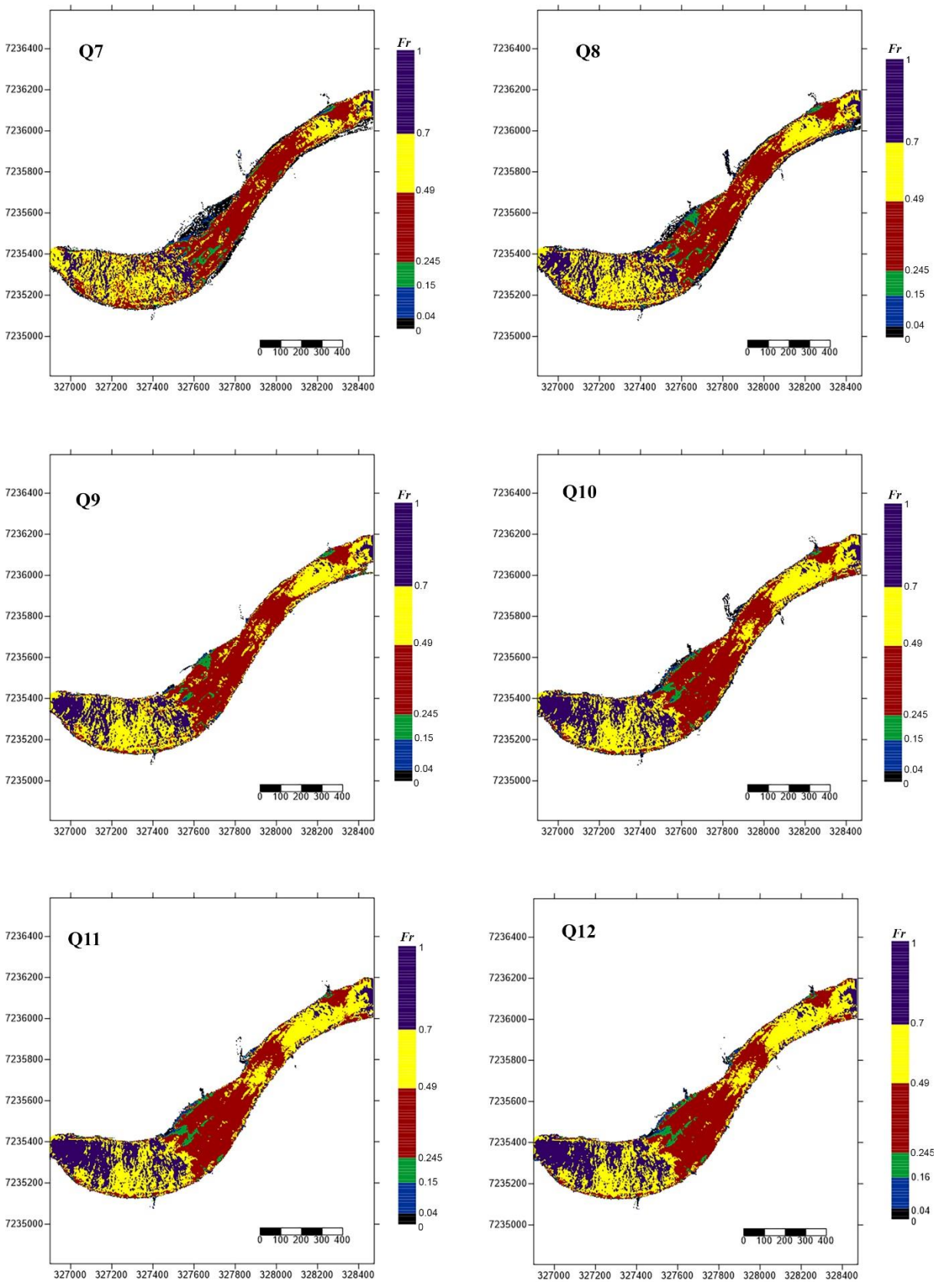

Figure 5.14 (continued). Two-dimensional Froude number models of study reach ordered in accordance with ascending discharge scenarios (Q7-Q12); Hydraulic biotopes are calculated via Froude number categories between Fr No. 0 and 1; black: pool; Blue: boil; Green: riffle; Red: run/glide; yellow: rapid and purple: Chute, flow travelled from left to right.

Area percentages of biotopes are found throughout each discharge in figure 5.15, which displayed contrasting patterns in the dominance of specific biotopes. Area percentages within the anastomosing channel (figure 5.15; top) differ considerably to those found within the pool-rapid, as the former displayed an increasing dominance of high-energy biotopes at each ascending discharge scenario. Initially, biotopes typical of lower Froude numbers dominated such as pools during 29 m^3s^{-1} whilst runs replaced them as discharge increased. Once discharge reached 564 m^3s^{-1}, rapids replaced runs temporarily as the most commonly placed biotope, however, despite their interchanging appearance on two-dimensional simulations, high-energy chutes replaced rapids as the dominant biotope during extreme discharge.

The pool-rapid (figure 5.15, bottom) was completely dominated by low energy biotopes throughout each discharge scenario, again initially dominated by pools but are then overwhelmed by runs following 358 m^3s^{-1}. Rapids do have some increase area as discharge ascended towards extreme discharge as seen in the two-dimensional models, which highlighted them as the second most dominant biotope. However, rapids only took up half of the area percentages that runs occupied during extreme discharge, which during 5085 m^3s^{-1}, was over 50% of the channel.

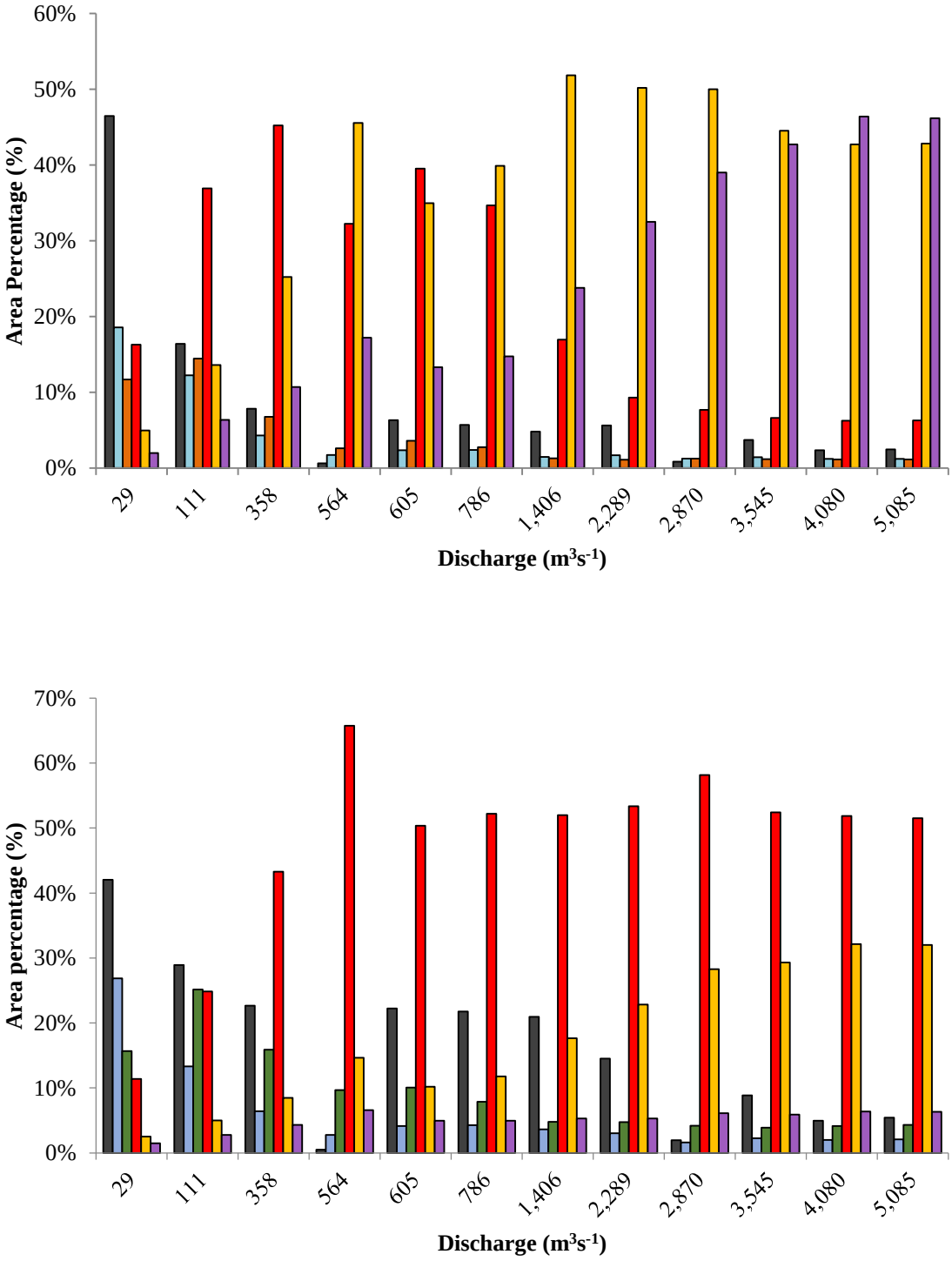

Figure 5.15. Area percentages of the bedrock-anastomosing channel (top) and pool-rapid channel (bottom) at each subsequent discharge scenario with each biotope highlighted by differing colours; Dark green: pools; cyan: boils; orange: riffles; red: runs/glide; yellow: rapids; purple: chutes.

6. Discussion

Referring back to section 1.3, specific objectives set out to scrutinise the influence that longitudinal bed gradients and geometry of the active channel has on hydraulic templates within both a pool-rapid and an anastomosing channel. Control points that represented individual rapid units, as well as conditions found at the anastomosing channel displayed a significant influence on velocity, bed shear stress and Froude numbers (see figure 6.1). Schmidt *et al*. (2001) and Petr (1970) also found that hydraulic variables such those documented within this thesis increased considerably over rapid units as discharge ascended. However, Vieira (2015) suggested that each rapid unit displayed differential controls on hydraulics dependant on their individual slope and geometric settings, highlighting the need to individually assess each control point and its influence on channel hydraulics, in addition to discuss any alternative influences found at them including alluvial bedforms and external inputs such as tributaries.

In addition to hydraulic influences this thesis set out to analyse geomorphic response to flooding, therefore an additional section (6.2) will interpret linkages between hydraulics found at the reach and its geomorphic template following cyclone Dando. With interpretations of the links between hydraulics and geomorphology at the anastomosing and pool-rapid, a conceptual model displaying geomorphic change during rising discharge was developed. This discussion will also attempt to describe possible links between the reach at site one and changes found in site two.

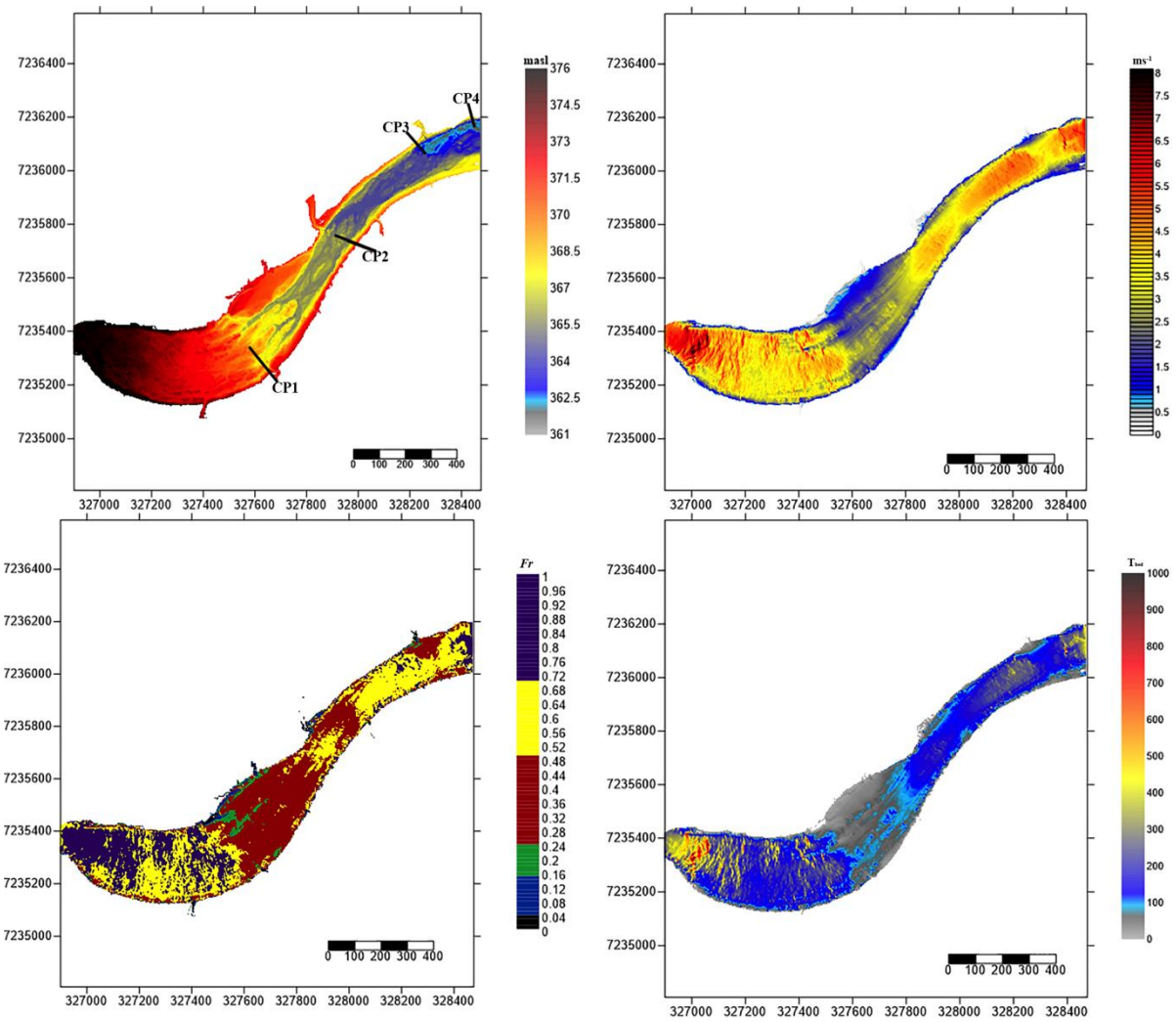

Figure 6.1. Hydraulic template of the reach, a) DTM and control point locations, b) Velocity, c), Froude numbers, d) bed shear stress, flow travelled from left to right.

6.1. Hydraulic influences

The overall reach at site one included a bedrock-anastomosing channel, which contrasted to the neighbouring pool-rapid in relation to its hydraulic response following a high-magnitude flood. During low flow, the anastomosing channel consisted of a highly sinuous channel with a large wetted perimeter comprised of narrow pathways found within bedrock fissures (Heritage *et* al., 2004; Burroughs *et* al., 2004). Where pathway activation was dependent on their size and the given flow regime, as two-dimensional JFLOW models displayed how lesser channel braids only became active during increased discharge. Ultimately at extreme discharge following Q_7, the bedrock-anastomosing channel's physiology went through a

remarkable transformation as the tortuous wetted perimeter during low flow resembled conditions more typical of a single-thread channel (Van Niekerk *et al*., 1999).

Slope conditions found at the bedrock-anastomosing channel was continuously steep, similar to slope conditions found at individual rapid units, therefore, during extreme discharge it displayed continuous highs in velocity and bed shear stress (Kale *et al*., 1996; Burrough *et al*., 2009). The highest of such values occurred at the upstream boundary of the anastomosing channel, which during maximum discharge was comprised of a comparatively reduced width to depth ratio than elsewhere in the channel (Baker and Kale, 1998). As flow began it's descent through the completely inundated anastomosing network, flow diffusion occurred because of wider channel settings (Entwistle *et al*., 2014), therefore, relatively higher velocities became sparsely located, as such velocities became isolated to shallower segments. This assorted template in regards to velocity, bed shear stress and Froude numbers within the anastomosing channel was indicative of diverse topographic settings where each bedrock core bar consisted of differential elevations. However, despite changes in channel geometry and differential submergence rates of topographic features causing an assorted hydraulic template; velocity and bed shear stress remained consistently high due to slope conditions at the bedrock anastomosing channel, which maintained higher energy availability during peak flow as waters found there remained shallow (Heritage *et al*., 2001).

Similar to the bedrock-anastomosing channel, initial regions of the pool-rapid downstream of control point one during low to intermediate flow is comprised of a multi-channel network. These passageways flow around low-lying islands made up of sandy sediments and dense riparian vegetation (predominantly prior to cyclone Eline), in addition to a large lateral bar at northern bank of the macrochannel. As discharge increased, consolidation of distributary

channels found immediately downstream of control point one submerged such low-lying islands and the large lateral bar, causing the active to behave. Therefore, channel geometry altered as the now freshly developed pool consisted of an increased width to depth ratio, which indirectly reduced velocity and bed shear stress through rises in flow resistance (Yen, 2002).

With a widened channel during increased flow regimes, flow resistance occurred due to the submergence of alluvial features, causing a significant reduction in velocity, bed shear stress and Froude numbers (figure 6.1). Examples of this are found through large lateral bars presented downstream of both control point one and three, which correlated with lower velocity and bed shear stress values. As stated by Heritage *et* al. (2004), who discussed how grain roughness influenced lower velocity and bed shear stress values at the lateral bar following control point one and at a smaller cluster of alluvial features found at its across the channel (figure 6.1, b and c). Most notable findings involved bed shear stresses following control point one, which had been considerably influenced by such alluvial features consistent of sand deposits, with Q_{12} distributions being much less than velocity readings in the same segment of channel (see figure 6.1, c). Similar findings regarding sandy bar presence were made by Ferguson *et al*. (1989), who suggested that sedimentary features comprised of sand have an overwhelmingly negative influence on bed shear stress because of grain roughness.

During extreme discharge however, grain and bed resistance associated with in-channel islands reduced as water depth reached its maximum, as Heritage *et al*. (2004) described that such resistance aspects decline as discharge surpassed a threshold of intermediate regimes through findings made at low gradient regions of the Sabie River. However, as seen throughout figure 6.1, resistance remained as sudden reductions in velocity, bed shear stress

and Froude numbers occurred following control point one, which was marked by a distinct boundary between relative highs and lows of each variable. During extreme discharge, flow resistance that derived from distinct channel geometries and cross-sectional areas found between the channel unit following control point and its adjacent anastomosing channel located upstream, replaced flow resistance that previously occurred through alluvial topographic units during lesser discharge.

However, relatively higher levels of velocity and bed shear stress remained within the centre of the active channel following control point one (figure 6.2, b and c), as discussed by Knighton (1998), hydraulic variables such as velocity and bed shear stress naturally rise at the centre of the active channel. Despite increased levels of velocity and bed shear stress, they both remained essentially lower than conditions found at the anastomosing channel and further downstream, which Knighton (1998) also stated that naturally higher velocities found down the centre of flow cannot increase extensively if width-to-depth ratios are of such a magnitude.

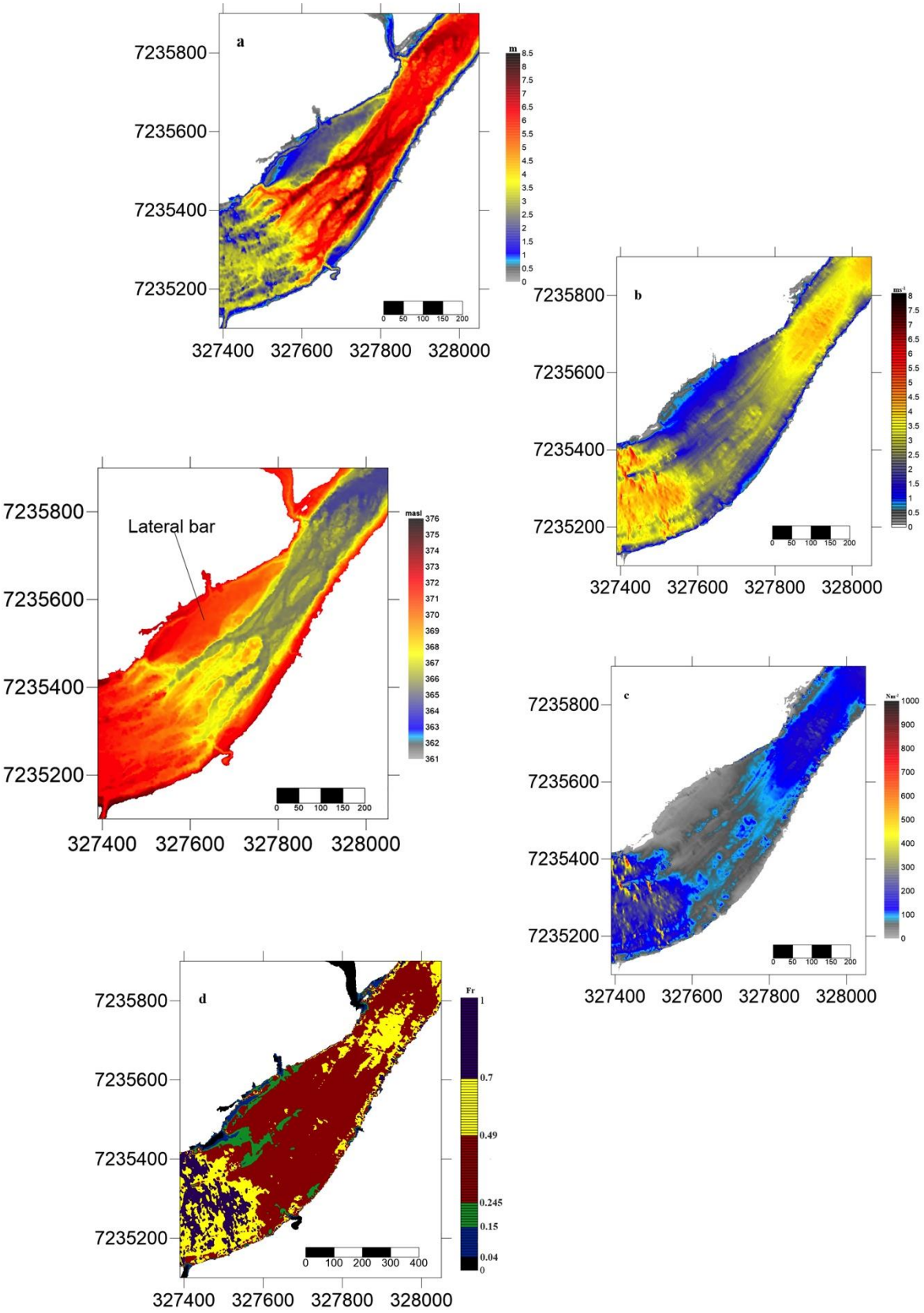

Figure 6.2. DTM (left) displaying control point one and two, compared with water depth (a), velocity (b), bed shear stress (c) and Froude numbers (d) during Q_{12}, Flow travelled from left to right.

At extreme discharge, as grain resistance from most of the topographic features following control point one became drowned out, lower values in velocity, bed shear stress and Froude persisted as a product of energy diffusion caused by distinct geometric settings found before and after the control point. Such distinction between velocity and bed shear stress during extreme discharge is comparable to high-gradient step-pool channels, which Heritage *et al*. (2004) made similar comparisons discussing how the Sabie River resembled such high-mountainous channel types during extreme discharge through its resistance characteristics. When observing step-pool channels, their abrupt changes in velocity and bed shear stress occurred through spill resistance that dissipated energy via wake-generated turbulence (Wohl and Thompson, 2000; Wilcock *et al*., 2006), which is more than likely to have occurred following each control point at the Sabie River despite it consisting of a less pronounced water surface gradient. Froude numbers provided a gateway to such a hypothesis, particularly at control point one during extreme discharge, which displayed an abrupt transformation from energetic chutes and rapids to biotopes typical of less energetic deeper waters (i.e. runs) (Shoffner and Royall, 2008). This sudden transformation would be caused by a hydraulic jump, that are seen throughout step-pool channels as a result of spill resistance, causing an abrupt change in energy availability, which can be seen in Froude number models in figure 6.1.

Through one-dimensional analysis, the reach displays a diverse topographic profile, with sharp reductions in bed elevation at each control point (figure 6.3 and 6.4). Water depth profiles highlight how waters became progressively shallower the closer to a knickpoint, where flow constrictions continually increased velocity towards and on top of each control point. Velocity, bed shear stress and Froude only reduced following the initial sharp increase in gradient, which links to each given control point, with variations in velocity displayed in figure 6.4. Correlating with the position of each control point and where velocity, bed shear

stress and Froude instantly declined was a small but sharp jump in water surface elevations. These small and sudden increases water surface found above control points during extreme discharge are also presented in two-dimensional models, however they are somewhat lost within its vast array of micro-scale alterations. Such dramatic changes in velocity, combined with sudden and short-lived water surface elevations (hydraulic jump) can be seen clearly through one-dimensional analysis as seen in figure 6.2 and 6.3. Thus leading to increased clarification of wake-generated energy dissipation associated with hydraulic jumps found more commonly at step-pool channels as the cause of distinct hydraulics following each control point, particularly downstream of control point one.

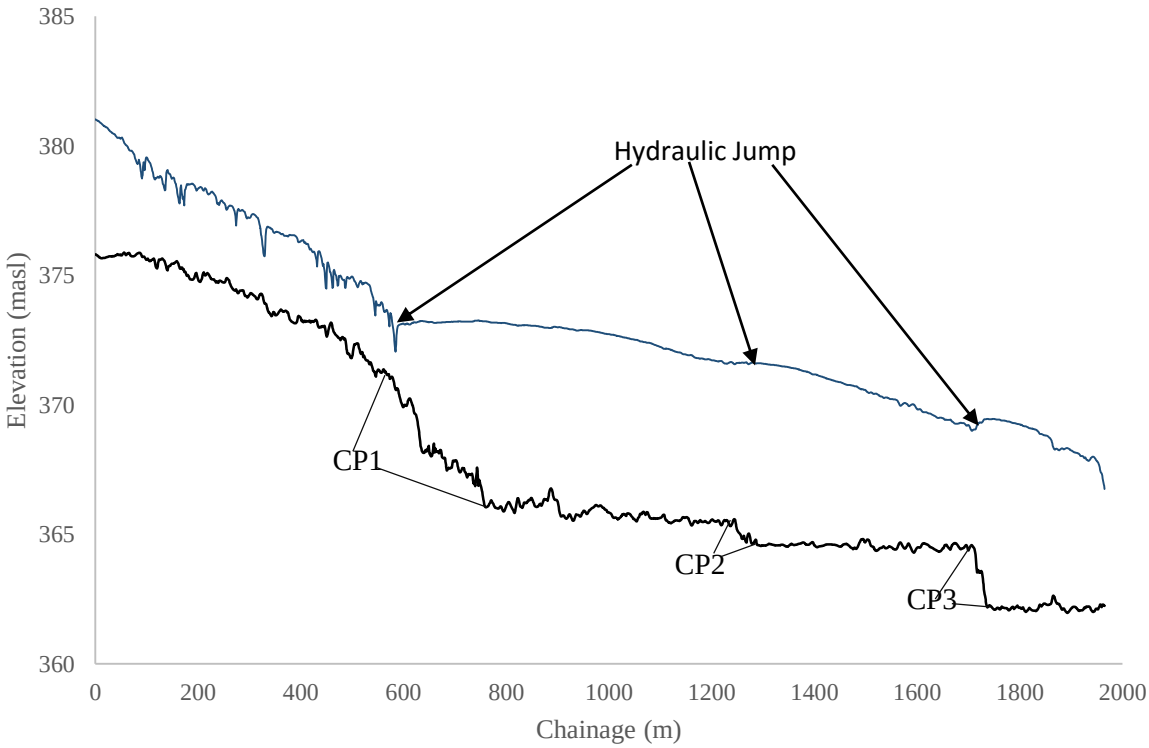

Figure 6.3. Bed (black) and Water surface elevations (blue) long profiles consistent with highlighted hydraulic jumps found at the initiation of each control point (CP#).

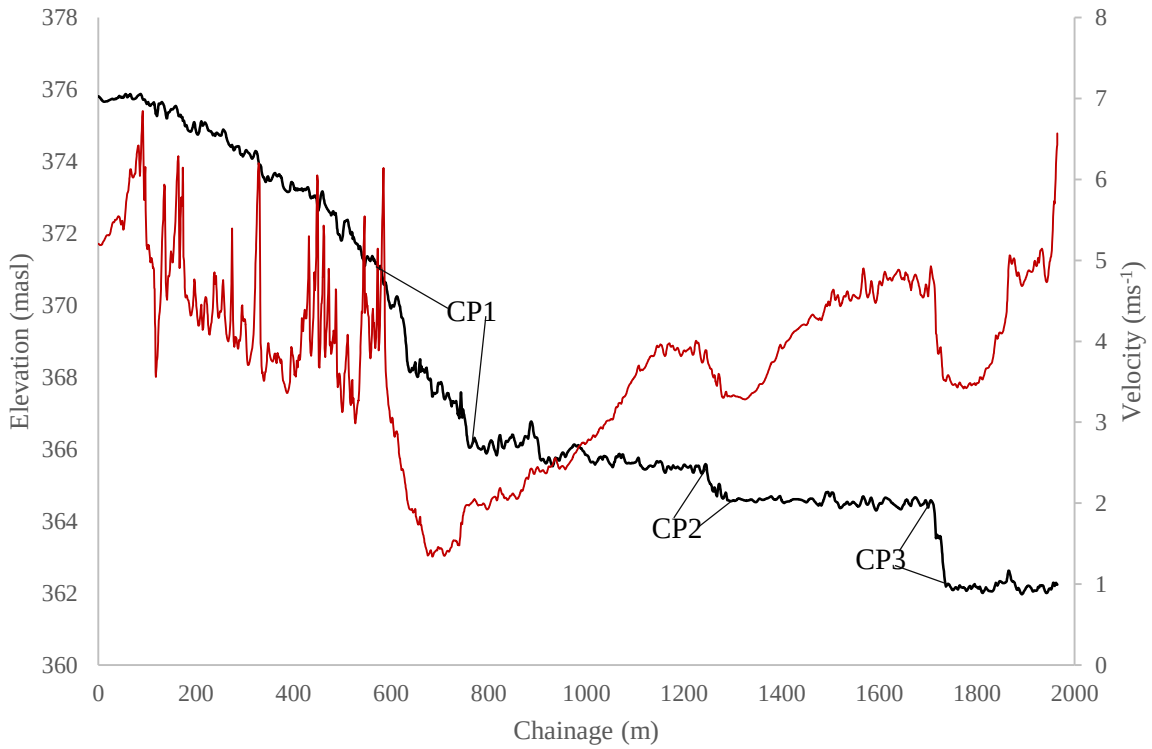

Figure 6.4. Bed (black) and velocity (red) long profiles associated with hydraulic jumps found at the initiation of each control point (CP#) during figure 6.2.

Arguments against wake turbulence and the behaviour of an inundated pool-rapid were expressed by Zimmermann and Church (2001), and D'Agostino and Michelini (2015), who both argued how rises in water surface elevations during increased discharge submerged each rib thus reducing flow resistance. Wilcox *et al*. (2006) also argued how contrary resistance aspects influenced flow through flume based research to model resistance derived from spill, grain and (large woody) debris, with all these aspects displaying a negative relationship with discharge. However, arguments relating to the relinquishment of step control do not take into account knickpoint spacing, as Whittaker (1987) discussed the inverse relationship found between pool size and general channel gradient within stepped channels. Such a negative relationship found by Whittaker (1987) is favourable within the currently analysed pool-rapid channel at the Sabie River, which does not consist of a profoundly high overall gradient thus comprised of elongated pools. Wohl and Wilcox (2006) also explained how the flume used in their research was smooth and straight, which is considerably different to conditions presented at the Sabie River's pool-rapid channel. Therefore, flume experimentation

performed by Wohl and Wilcox (2006) was unable to exhibit how changing geometry, channel curvature and bank roughness affected resistance characteristics in a naturally stepped channel during a flood. Whereas other observations involved changes found in step-pool channels located at much higher gradients compared to the pool-rapid channel analysed at the Sabie River (Zimmermann and church, 2001; Wohl and Thompson, 2000; D'Agostino and Michelini, 2015).

Downstream of the initial pool-rapid segment that followed control point one, higher velocity and bed shear stress values increased due to flow convergence in relation to channel constriction leading up to control point two. Throughout most discharge scenarios presented at the reach, flow conditions overwhelmed control point two, although, minor increases in velocity and bed shear stress became apparent at the very top of control point two's knickpoint during Q_{12}. A multitude of factors were involved in hydraulics presented at the second control point during a high-magnitude flood event, with a major aspect involving the location of each rapid unit in relation to the overall macrochannel. These rapid units were centrally located within the macrochannel before joining at the pool during Q_1. At increased discharge, backwaters situated at the larger pool downstream of control point one became confined forcing it down the channel, thus overwhelming its associated rapids with increased flow (Graf, 1980; Zimmermann and Church, 2001). Despite control point two's reduced overall influence, there remained distinct highs in velocity and bed shear stress situated on top its rapid units during Q_{12} as water depths were considerably less than adjacent regions of the channel. However, raised figures in velocity and bed shear stress are spatially minor before eventually dissipating because of neighbouring tributary inputs and topographic changes prompting increased water depths.

Leading up to the third control point, influences on velocity arise from comparatively reduced water depth during extreme discharge (figure 6.5a and c), which is also visible the closer to the control point four. In addition to progressive reductions in water depth leading up to control points three and four, channel constriction associated with a relatively large lateral bar adjacent to the channel unit between control points three and four also produced increased velocity, bed shear stress and Froude numbers found there (Rhoads and Kenworthy, 1995). Hydraulics associated with conditions leading up to control points three and four are reflected by Wang *et al*. (2009), who described how such hydraulics are similar to conditions found at a riffle, where increased velocity is a product of bed-generated turbulence. However, distinct alterations in the hydraulic variables were found at control point three, which marginally differs to factors controlling hydraulics at control point one and two during extreme discharge.

Photographic evidence of control point three indicated the presence of a large sandy bar, laterally positioned on the macrochannel's southern bank, which is also visible within the DTM (figure 6.3, left). Previously cited for its influence on raised velocity through constriction, this lateral bar also has a contrasting influence over hydraulics on top of and following control point three. Once discharge scenarios reached $Q_{11,}$ increased water surface elevations almost completely submerged the lateral bar, as also seen in one-dimensional cross-sections of the region in section 5.2.2. The lateral bar's locality in relation to the rapid units as well as its relatively high elevation produced significantly deeper waters at some of its adjacent rapid units. Increased channel geometry due to inundation of the lateral bar adjacent to the rapids together with grain resistance provided by it caused a relative reduction in velocity and bed shear stress at neighbouring rapid units (figure 6.5 b and c).

Neighbouring the rapid units found at control point three is a tributary; DTM observations exhibit a reduction in elevation potentially associated with introductory flow from its confluence (figure 6.3, left). This tributary influenced hydraulics found downstream of the rapids at control point three as seen in figure 6.5, where reduced velocity and bed shear stress characteristics adjacent to its confluence occurred due to lateral flow input diffusing energy availability by barricading relative highs in velocity, bed shear stress and Froude (Rhoads and Kenworthy, 1995).

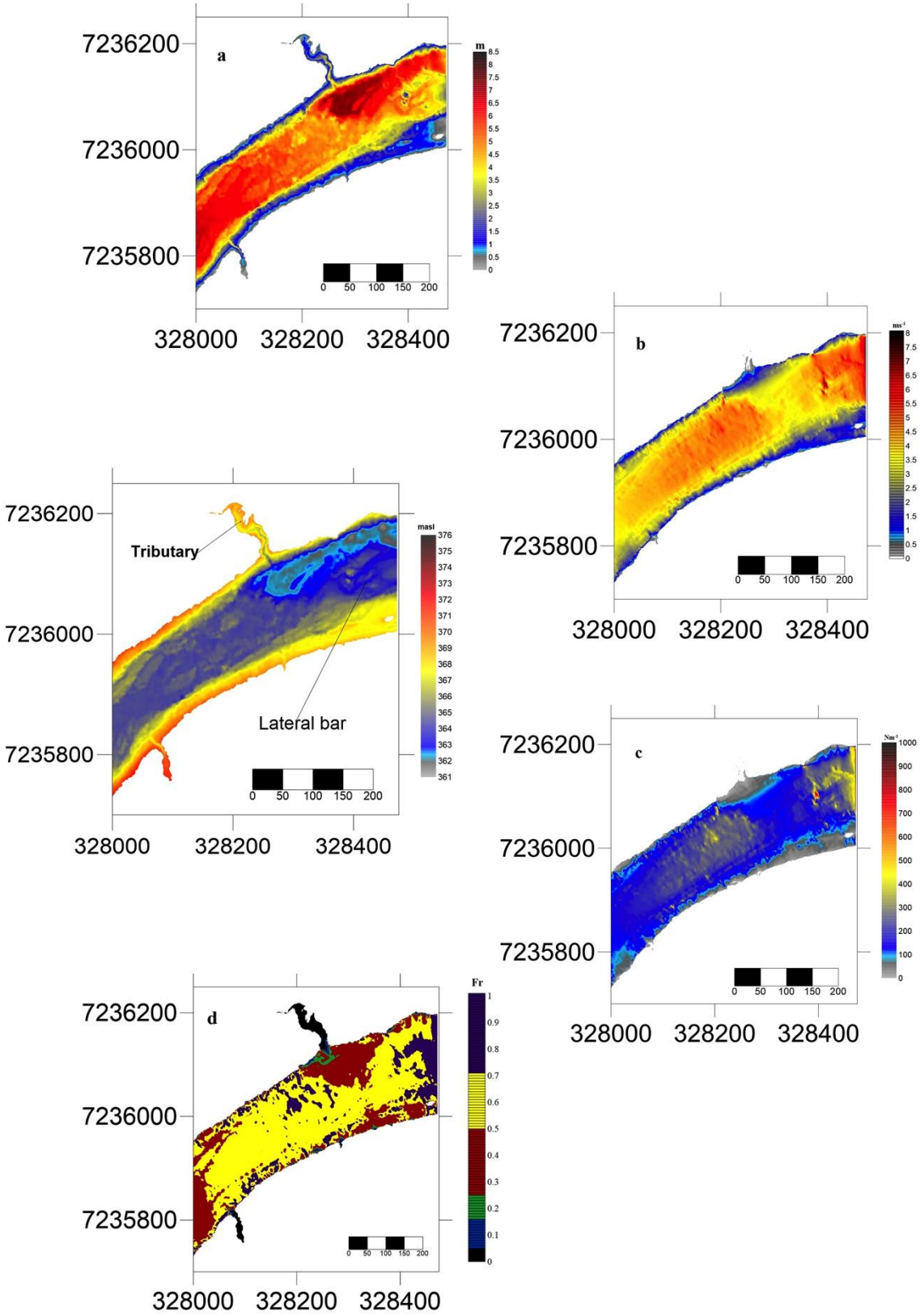

Figure 6.5. DTM (left) displaying control point three and four, compared with water depth (a), velocity (b), bed shear stress (c) and Froude numbers (d) during Q_{12}, flow travelled from left to right.

6.2. Hydraulic and geomorphic linkages

Active channel geometry played a crucial role in geomorphic response to high-magnitude flood events made noticeable in both anastomosing and pool-rapid channels. Significant levels of bed shear stress and velocity occurred at the anastomosing channel particularly at narrower segments found at both of its channel boundaries, particularly during extreme discharge at the upstream boundary, where considerable destruction of bedrock core bars and soft sediment features occurred. Bedrock-core bar and soft sediment destruction produced widened channel pathways as flood-intolerant vegetation was removed therefore exposing such morphologic units to hydraulics found there (Van Coller *et al.,* 2000; Nardi and Rinaldi, 2015).

Overall, the anastomosing channel remained relatively stable, correlating with Parsons *et al*. (2006), who found that structural controls from underlying lithology prevented major alterations to bedrock-anastomosing form following a flood. Such stability was also related to the presence of riparian vegetation, which was evident throughout time series aerial imagery. The influence vegetation had on stability within the anastomosing channel were demonstrated by Heritage *et al*. (1999), vegetation remained densely populated following Cyclone Dando as the flood had an insignificant effect on it. Whilst Van Niekerk *et al*. (1999) suggested how such densely colonised vegetation provided bedrock core-bars with stability, as robust riparian species at the Sabie River's bedrock anastomosing channels are themselves dependent on inundation from high flow events in order to flourish. Through aerial photography, alluvium deposits found on top of bedrock-core bars are associated with the presence of vegetation, whilst those that lack such coverage were stripped by extreme flows as demonstrated within the conceptual model regarding sediment removal during a flood event (figure 6.6.). Findings of flood resilient plant species comes into conflict with Rountree

et al. (2000), who identified that flood impacts on vegetation at a bedrock-anastomosing channel within the Sabie River are substantial, which was characteristic of large scale destruction produced following cyclone Eline, however such destruction to plant communities was not as considerable following cyclone Dando.

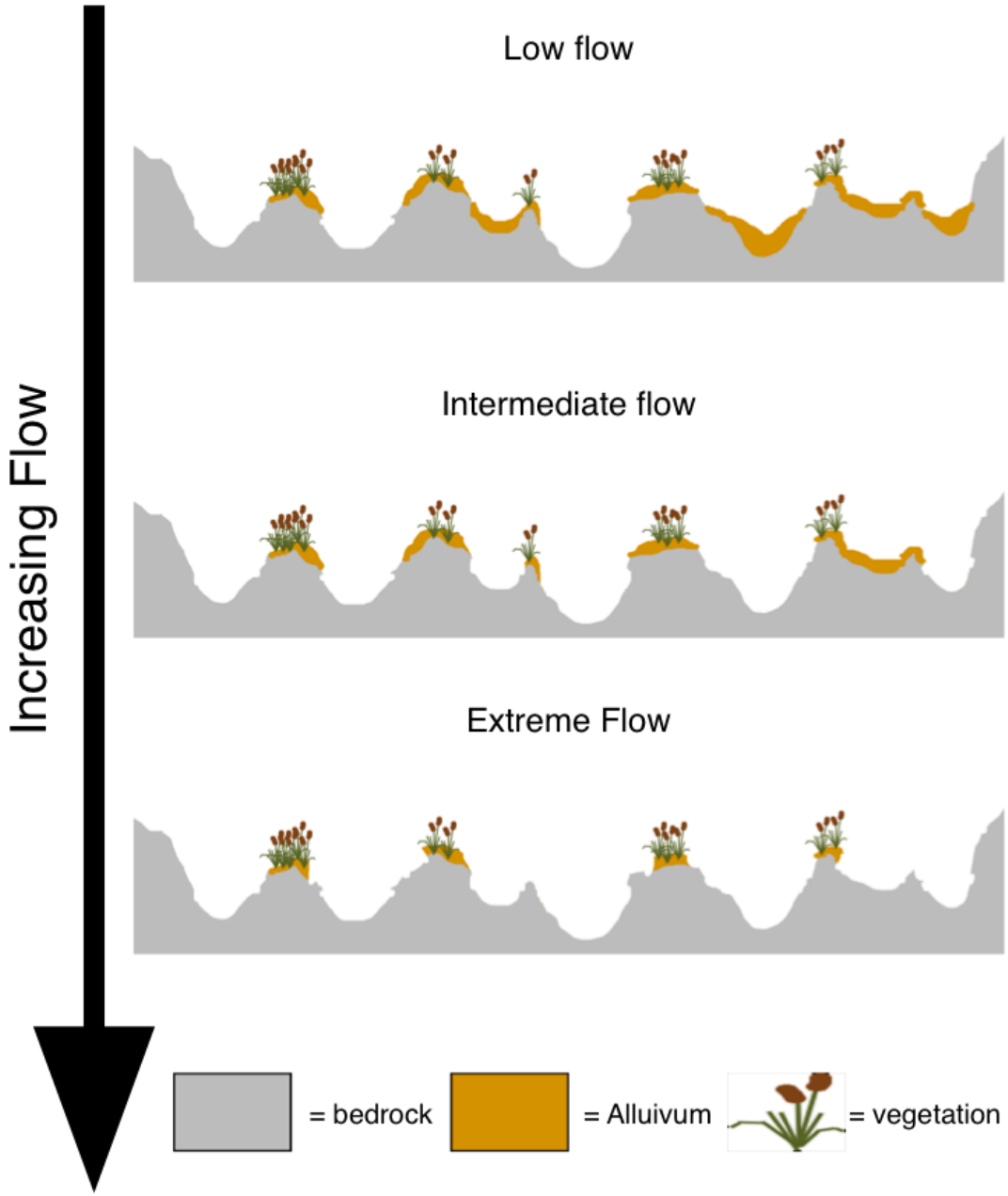

Figure 6.6. Conceptual model displaying the geomorphic response of an anastomosing channel to progressive flow regimes found during a high-magnitude flood, which displays increased removal of unstable sediment that lacks the protection of riparian vegetation during a flood, however with extreme flows, vegetation that is exposed or intolerant of such flows is also removed.

Despite the anastomosing channels overall stability, soft sediment removal continued at specific bedrock core-bars, which also experienced extensive vegetation removal due to flooding intolerance of specific species found there (Van Coller *et al.,* 2000). Vegetation and sediment removal further reflected spatial distributions of velocity, Froude and bed shear stress models at extreme discharge scenarios, which were also diverse. In spite of minor cases of sediment removal, roughness characteristics of the anastomosing channel altered with flow resistance characteristics associated with inundated yet stable riparian vegetation (Van Niekerk *et al*., 1999). Thus, in addition to a wider and singular active channel resulting in energy diffusion at extreme flow, vegetation also influenced velocity and bed shear stress values within the bedrock-anastomosing channel.

The extreme flood event following cyclone Dando did not cause any major transformation to the pool-rapid channel, as no sign of a switch favourable to an alluvial single-thread or braided channel occurred through excessive deposition or erosion, as seen following cyclone Eline by Rountree *et al*. (2001). Deposition did occur however at areas of the pool-rapid consistent with lesser gradient conditions (i.e., pools), focused on lateral bars and embankments, most notably following control point one.

The considerably larger pool habitat produced during extreme discharge found immediately downstream of control point one provided a multitude of reasons as to why such changes in bed shear stress and velocity took place. Considerably lower values in bed shear stress, velocity and Froude numbers provided a platform to potential areas of geomorphic change following the first control point. Sand induced flow resistance in addition to the significant increases in cross-sectional area following control point one produced a severe reduction in bed shear stress, which caused sediment transportation to reach a threshold were entrained

sediment was at full capacity (Ferguson *et* al., 1989; Heritage, Birkhead *et al*., 1999), therefore leading to deposition. Aerial photography of the pool-rapid downstream of control point one also provided further correlation to JFLOW models at extreme flow regarding bed shear stress as no obvious signs of erosion was present but deposition occurred throughout, modifying pre-existing alluvial features and creating fresh topographic units.

Deposition downstream of control point one as well as other regions of the pool-rapid could have additionally occurred at the lowering limb of the flood hydrograph because of reduced stream power, as stated by Leopold (1969) and Van Niekerk *et al*. (1999). Unfortunately, both JFLOW models and time series aerial photography could not determine specifically when deposition occurred despite strong links with relatively low bed shear stress at increased discharge scenarios. Observations of how deposition affected the pool-rapid channel occurred through modifications of already present alluvial features or through compensation of previously stripped areas of soft sediment as seen in site two following cyclone Dando (Entwistle *et al*., 2014). Due to deposition on larger islands and bars, stability of alluvial features within the pool-rapid remained intact following cyclone Dando at site one (Heritage *et al*., 2004).

Most notable physical changes within the pool-rapid occurred through vegetation removal, particularly following control point one. Within the widened active channel between control point's one and two, vegetation inundated by a progressively higher water line could no longer tolerate powerful flows present during extreme discharge (Webb *et al*., 2006). Similar to the anastomosing channel, vegetation removal found throughout the pool-rapid appeared to be selective, potentially dependent on a specific species' tolerance to high flows (Van Coller *et al*., 2000). However, in contrast to the bedrock-anastomosing channel, riparian tree removal

occurred in considerable quantities at the pool-rapid, particularly towards control point two, which corresponded with Rountree *et al.* (2001). Therefore, vegetative success within the Sabie River is determined by a combination of factors including, channel type, physical settings (i.e., gradient, macrochannel geometry and geomorphic features) and individual plant species.

Stripping of sediments found at the reach appeared to be minimal, which contrasted to geomorphic response found by Parsons *et al*. (2005) and Heritage *et al*. (2001) following cyclone Eline, which displayed significant devastation to alluvial bedforms through uncoheive sediment removal. Destruction of sedimentary features following cyclone Eline was also demonstrated at site two's pool-rapid channel as bars and islands where stripped, with cases of distributary channels flowing through the aftermath, although considerable levels of deposition occurred following cyclone Dando. However, the region of site one that lead towards control points three and four, displayed signs of erosive processes, particularly at exposed bars such as the large lateral bar adjacent to control point four, which consisted of a small channel flowing through it, following cyclone Dando. Erosion within this area of the channel could be a result of the dynamic flow conditions presented within it, as flow is pushed towards the bar by tributary inputs as demonstrated in figure 6.8. Despite overall minor setbacks in sediment accumulation, stripping of soft sediment islands occurred following cyclone Dando, particularly to unprotected sediments located at both pool-rapid sites that lacked in vegetation coverage (Tooth, 2000). Pool-rapids found throughout River Sabie following cyclone Dando experienced a distinct response to aggradation that occurred in subsequent years from cyclone Eline, where evidence of both erosion and deposition was evident throughout both pool-rapid sites (Heritage *et al*., 2014).

Stripping of the sedimentary units mostly appeared at regions exposed to the full force of flow within the pool-rapid, which correlated to JFLOW simulations at extreme discharge. Sediment stripping appeared to occur following control point one where the macrochannel became constricted, as agreed by Stark's (2006) landscape evolution model, which highlighted how modification of channel morphology is dependent on several factors including hydraulics, erosion, sediment transport and, channel geometry. As the channel narrows leading up to control point two, stream power and energy availability increased (Ferguson and Brierley, 1999), leaving finer sediments located at in-channel islands exposed to erosion (Baker, 1984). Despite the loss in sediment, aerial imagery of subsequent years from 2012 provided evidence to consistent aggradation, which replenished lost sediment at effected islands and bars coupled with rapid vegetation recovery. Such colonisation of rapid outcrops and alluvial features by vegetation was common throughout both sites in years following Cyclone Dando.

Rapid units that make up each control point found within site one's reach did not show any signs of change, as Leopold (1969) and Graf (1979) described rapids as areas consistent of a minimal response to floods due to their fixed topographies. Despite recorded loose sediment removal following cyclone Eline (Heritage, Charlton *et al*., 2001; Parsons *et al*., 2005), the rapid units appeared to have attained significant levels of stability, whilst no deposition of loose sediments occurred therefore they maintained a robust bedrock dominated structure. As discussed by Tooth (2000), the lack of sinuosity at a channel with increased gradients, caused a rise in bedload transport and bed shear stress thus, making deposition on rapid units within both reaches at extreme flood events highly improbable.

7. Conclusion

This thesis has analysed and demonstrated controls present within an anastomosing and pool-rapid channel during a high-magnitude flood event. Through two-dimensional JFLOW, one-dimensional analysis, and time series aerial photography comprised of two alternative pool-rapid reaches, this thesis offered great insight into a multitude of differential controls on hydraulics and its subsequent geomorphology at a pool-rapid found within the Sabie River. These controls include longitudinal topography, channel geometry, channel bedforms and tributary confluences, in addition to how these controls differ as a flood achieves maximum discharge, which are all detailed within this chapter, throughout each section. With final considerations on limitations found within this method of research and how it could be expand the knowledge gap regarding pool-rapid channels within the Sabie River.

7.1. Two-dimensional river simulation model appraisal

Section 4.5 demonstrated how discharge estimations for two-dimensional JFLOW models compared to field derived dGPS points, which are representative of the maximum extent of floodwater within the Sabie River. Validation of peak discharge estimations took place through overlay of dGPS points onto their corresponding two-dimensional hydraulic models found at selected sites along the River Sabie, where model precision is displayed by the distance between modelled water surface and the marked dGPS points. If there was distance between dGPS points and water surface simulations, an error percentage calculation took place to identify the extent of missing water surface.

River simulation models at the Sabie River displayed considerable precision, however errors between simulated peak discharge and actual floodwater extent was present at each site. Such

distance between modelled discharge and actual dGPS plots was minor, consisting of a significantly small error percentage of ~5%. In addition to model validation at the Sabie River, Such appraisal of peak discharge simulations also occurred at the Olifants River as it experienced greater maximum discharge (~10000 m^3s^{-1}). As validation of river simulation models consisted of increased precision with an error percentage, found between modelled and actual peak discharge of 4.66%. Despite such errors found between the simulated and actual discharge at both channels, the model was suitable for observations of realistic flow regimes within the Sabie River, due to consisting of only marginal imprecision.

7.2. Geomorphic response to high-magnitude flooding

Pool-rapids at the Sabie River displayed a varied response to high-magnitude flood events, with individual response dependant on the given reach and flood. As seen through time series aerial photography, each pool-rapid consisted of a markedly different physiology; therefore, there was no collective response by both pool-rapids following a flood event comprised of extreme discharge (Heritage *et al*., 2014; Vieira, 2015). Analysis of geomorphic modifications to extreme discharge occurred through time series aerial photography, which highlighted areas of obvious change within two pool-rapid channels.

Site one, which was the most scrutinised of pool-rapid sites, displayed a mixed response to high-magnitude flooding, although both sites experienced erosion and deposition, site one consisted of significant occurrences in deposition particularly following its upstream boundary. At the initial region of site one's pool-rapid, deposition was evident throughout, as small in-channel islands consisted of freshly deposited sediment, whilst newly developed alluvial bedforms emerged from the channels water surface, which developed further as years progressed. This evidence of deposition reflected two-dimensional JFLOW models that

demonstrated the significant reduction in bed shear stress during extreme discharge compared to adjacent regions of the channel, therefore enabling deposition to occur as sediment entrainment reduced significantly (Ferguson *et al*., 1989; Heritage *et al*., 1999).

Erosional processes later replaced considerable deposition initially found at the pool-rapid, with notable occurrences demonstrated at islands located at regions of flow constriction, therefore increasing bed shear stress and the potential for sediment removal (Stark, 2006). Exposure of bars consistent with an irregular geometry during extreme flow also displayed signs of erosion, particularly within the narrower region of site one's pool-rapid, where bars and small islands reduced in size following cyclone Dando.

Rapid units found along the reach at site one demonstrated no significant response to floodwaters produced by cyclone Dando. As each rapid unit retained pre-flood characteristics, with no evidence of deposition or erosion present at each unit, thus escaping the effects of floodwater during extreme discharge. This was a similar case for rapid units found at site two's reach, where rapid units situated within close proximity of one another did not show any signs of change.

Overall, site two displayed a relatively distinct response to flooding compared to site one, with the former site also displaying a contrasted retort to individual cyclone-driven flood events. Following cyclone Eline, site two displayed significant occurrences of deposition through the destruction of alluvial features along the macrochannel's banks, as some cases of erosion exposed bedrock outcrops found at its upstream channel boundary. Erosion also occurred further downstream, where the channel widened and originally consisted of a large lateral bar adjacent to a sequence of pools and rapids. This lateral bar, which once displayed a

single unit became exposed to significant erosive processes during the 2000 flood event, and split the bar as distributary channels later flowed from the more commonly observed active channel. Albeit evidence of erosion was less prominent following cyclone Dando as the whole channel displayed considerable cases of deposition, with examples including increased cohesion of lateral bars.

7.3. Hydraulic response to high-magnitude flooding

Accompanying a diverse geomorphic response to high-magnitude flood events, pool-rapids displayed a varied hydraulic template because of extreme discharges associated with such floods (Yen, 2002). Analysis of these dynamic hydraulics occurred through two-dimensional JFLOW models, which simulated changes in hydraulic settings through twelve discharge scenarios. Simulations of such involved pre-prepared velocity, water surface and water depth models (however, the latter was not a part of the thesis's results), with additional models developed that displayed bed shear stress, Froude numbers and a digital terrain model (DTM).

The reach used for hydraulic analysis was site one, which displayed a distinct hydraulic template during extreme discharge, with each identified rapid comprised of varied hydraulics dependant on its physical settings, therefore analysis focused on each control point individually. Initial analysis however took place at the bedrock-anastomosing channel adjacent to the pool-rapid, which located upstream of it displayed markedly distinct hydraulics compared to the former channel.

Initially the bedrock-anastomosing channel displayed considerable highs in velocity, bed shear stress and Froude numbers, which progressively dissipated further downstream. Energy

dissipation remained relatively assorted however, because of its dependency to topographic features and individual channel elevations (Heritage *et al*., 2001). Despite such assortment in energy availability, velocity, bed shear stress and Froude numbers remained generally high throughout the anastomosing channel. Such changes in elevation found at each channel, caused them to have alternative depths, which altered each hydraulic variable as shallower regions of the channel associated with inundated bedrock-core bars produced much greater levels of each. Overall, the significant high levels of each variable progressively reduced further downstream, although general levels of velocity, bed shear stress and Froude remained considerably higher than elsewhere in the reach.

Control point one displayed a marker between simulated highs in velocity, bed shear stress and Froude numbers found at the anastomosing channel and considerably lower levels of such within the initial region of the pool-rapid channel. Control point one was the reach's first and largest knickpoint, which spanned across the macrochannel's widest section and acted as a boundary between each channel type. During extreme discharge, increased levels of velocity, bed shear stress and Froude occurred immediately upstream of control point one, however at the point where channel type changes, so did its hydraulics. This change resulted in contrasting velocity, bed shear stress and Froude, with considerably lower levels of each present, as rapids and chutes found throughout the anastomosing channel now became a run.

Further downstream of the pool-rapid channel towards control point two, channel constriction produced increased levels of velocity, bed shear stress and Froude. Increased discharge produced velocity and bed shear stress values that commonly spread throughout the remainder of the pool-rapid channel, as the rapid unit found a control point two became overwhelmed by hydraulics immediately upstream of it. However as discharge scenarios achieved extreme

levels, the hydraulic template of control point two displayed an increased influence on hydraulics as velocity and bed shear stress increased further on top of its rapid unit as water surface gradients became more continuous, however such highs in each variable was minor.

Upstream of control points three and four displayed hydraulics typical of those found more commonly on top of a riffle (Wang *et al*., 2009), with reduced depths coherent with a progressive rises in velocity and bed shear stress, although the latter reached its peak levels further upstream than velocity, albeit velocity. Similar to control point one, control point three demonstrated a distinct boundary between relative highs and lows in velocity and bed shear stress, caused by the presence of a sharp gradient there and the combined influence of an adjacent tributary mouth and almost completely inundated lateral bar (Rhoads and Kenworthy, 1995; Wilcock *et al*., 2006).

7.4. Longitudinal and geometric influence on hydraulics

This thesis also analysed hydraulic influences caused by channel physiology, which included its longitudinal gradient and geometric settings. Similar to hydraulic analysis, scrutiny of longitudinal and geometric settings found at the Sabie River consisted of two-dimensional JFLOW models, but further scrutiny took place through one-dimensional analysis. The addition of one-dimensional analysis helped to supplement two-dimensional models, as presentation of the latter occurred in plan view, intricate changes to topography and water surface could be difficult to identify.

Throughout the reach, longitudinal control on local hydraulics was dependant on individual gradient settings found at the channel, for example at each control point as they consisted of

alternative slope settings (Vieira, 2015). Overall, each knickpoint appeared to lose considerable control over hydraulics as discharge increased, with steeper control points such as one and three acting as a boundary between areas of high and low velocity, bed shear stress and Froude. Control point two also displayed a reduced influence on hydraulics, however it did not consist of such distinction between the relative highs and lows in such variables but instead became almost completely subsumed by adjacent hydraulic settings.

In contrast to longitudinal settings, channel geometry consisted of considerable control on hydraulics during high-magnitude floods, as differential geometry occurred both upstream and downstream of each control point at both low flow and extreme flow. In regards to hydraulics discussed at control point one, the geometry of the active channel downstream of it caused immediate energy dissipation through wake generated turbulence (Wohl and Thompson, 2000), as width to depth ratios increased significantly compared to settings found upstream of control point one. An increase in the wetted area downstream of both control points one and three had an additional affect on hydraulics due to the inundation of adjacent lateral bars that occupied significant portions of the macrochannel, and as a result produced flow resistance due to the relatively high roughness properties of alluvium (Ferguson *et al*., 1989). Channel geometry also influenced increased velocity, bed shear stress and Froude as evident from two-dimensional simulations, which demonstrated increased levels of each variable as the macrochannel became constrained and width to depth ratios reduced considerably between both control points one and three.

7.5. Limitations and future recommendations

Despite encouraging results regarding controls on hydraulics within a pool-rapid and a neighbouring anastomosing channel, there remained limitations within the research. A

noticeable limitation was found within JFLOW models through portions of visible non-data, particularly in low flow simulations. Such non-data did not attain any numeric value, therefore did not effect calculations such as biotope area percentages, however their visibility was still a limiting factor. Fortunately when organising colour schemes to simulations regarding velocity, bed shear stress and hydraulic biotopes, non-data could be hidden due to it not consisting of any value, however this was not the case for water surface models. The issue with non-data is apparent when comparing models of velocity and water surface, as both appear to have contrasting appearances. Unfortunately as water surface elevations are continuous, with progressive reduction in water slope dependent on the underlying DTM, non-data then becomes a part of water surface elevations, therefore is unable to be hidden from view through colour scheme parameterisation.

The JFLOW model's physical boundaries also provided a limitation to the research on pool-rapids particularly at the downstream extent of site one. Not much discussion was made about control point four in the two-dimensional model, instead three control points were focussed upon as they consisted of detailed hydraulics both up and downstream. Unfortunately, model limits have to occur for processing purposes, although the X-axis did marginally cut off control point four, which prevented a more detailed discussion. Future considerations regarding such a limitation would be the development of the same two-dimensional models but within and expanded study reach, therefore displaying the entire pool-rapid.

Additional analysis based on the pool-rapids involved using one-dimensional models extracted from JFLOW river simulations and the DTM, which provided a useful insight into the intricate changes in topography along cross-sections of the channel and along the longitudinal profile of the reach. Therefore, one-dimensional analysis aided research through

complimenting two-dimensional simulations, whilst acting as an attempt to counter a lack three-dimensional analysis that was simply beyond the scope of this thesis.

Unfortunately, one-dimensional analysis consisted of limitations, with perhaps the main limiting factor being its subjectivity, as each model was dependant on the area of channel chosen by the user. In an attempt to eliminate potential user-based errors, particularly with cross-sectional analysis, frequent extractions of cross-sections occurred, with careful consideration of them being almost perpendicular; however, a cross-section that is perfectly perpendicular to the channel is significantly difficult to achieve. To counter such subjectivity and make observations objective, development of three-dimensional models could be significantly useful, as they provide an in-depth visualisation of topographic conditions that are considerably easier to observe than such intricacies found at within two-dimensional simulations.

Despite encouraging findings within aerial imagery that displayed a dynamic geomorphic retort to high-magnitude floods along the Sabie River, they remained limited by the spatial and temporal resolution of individual photographs. Despite improvements in spatial resolution within more recent photographs, backdated images of specific regions within each pool-rapid consisted the best resolution available from archives, which in some cases lacked relevant detail of channel change only visible in high-resolution imagery. In addition to spatial resolution, archive dependency produced limitations in the temporal resolution of such aerial imagery. For example, the Sabie River is ephemeral in nature therefore at certain times of the year it does not flow (winter months); as a result, potential misrepresentation of geomorphic form within River Sabie's macrochannel is likely. Mistakes linked to such limits in temporal resolution are possible through observations of the Sabie River during late winter months as

initial observations of supposed aggradation could in fact be exposed bed material during considerably low flow. To counter this, the use of more high-quality photographs taken from an increased variety of sources could distinguish changes to geomorphic form from rarely exposed channel bed material.

In relation to aerial photography, site two consisted of images of channel bedforms affected by floods following both cyclone Eline and Dando, whilst site one only consisted of imagery concerning cyclone Dando. Results displayed at site one demonstrated contrasting responses to extreme flows between both floods, however this could not be discussed as much for site one, with only reports documented in past literature offering a window into changes that occurred there following cyclone Eline. Contrasts also occurred between changes found within site one and two following cyclone Dando as both channels consisted of distinct channel physiology, which could be a potential cause for such differences. However, investigations into hydraulic variations at site two must occur in order to truly compare both hydraulic and geomorphic retort found at both channels. In addition to sites one and two, further investigation into pool-rapids found at the Sabie River must occur in an attempt to catalogue hydraulic and geomorphic controls found within each of them. Through the same methods performed within this thesis, analysis of every pool-rapid channel within the Sabie River, could single out general characteristics found within them in order to develop a conceptual model that truly represents pool-rapid channels, as current circumstances does not allow the development of such a model due to their fundamental differences.

References

Andrews, E.D., 1982. Bank stability and channel width adjustment, East Fork River, Wyoming. *Water Resources Research, 18*(4), pp.1184-1192.

Asante, K. O., Macuacua, R. D., Artan, G. A., Lietzow, R. W., & Verdin, J. P., 2007. Developing a flood monitoring system from remotely sensed data for the Limpopo basin. *Geoscience and Remote Sensing, IEEE Transactions on*, *45*(6), 1709-1714.

Ashley, G. M., Renwick, W. H., & Haag, G. H., 1988. Channel form and processes in bedrock and alluvial reaches of the Raritan River, New Jersey. *Geology*, *16*(5), 436-439.

Baker, V. R., 1984. Flood sedimentation in bedrock fluvial systems. *Sedimentology of Gravels and Conglomerates – memoir 10,* 87- 98.

Baker, V. R., & Pickup, G., 1987. Flood geomorphology of the Katherine Gorge, Northern Territory, Australia. *Geological Society of America Bulletin*, *98*(6), 635-646.

Barton, J. M., Bristow, J. W., & Venter, F. J., 1986. A summary of the Precambrian granitoid rocks of the Kruger National Park. *Koedoe*, *29*(1), 39-44.

Bisson, P.A., Nielsen, J.L., Palmason, R.A. and Grove, L.E., 1982. A system of naming habitat types in small streams, with examples of habitat utilization by salmonids during low streamflow. *Acquisition and utilization of aquatic habitat inventory information. American Fisheries Society, Western Division, Bethesda, Maryland*, pp.62-73.

Booker, D.J., Sear, D.A. and Payne, A.J., 2001. Modelling three-dimensional flow structures and patterns of boundary shear stress in a natural pool-riffle sequence. *Earth Surface Processes and Landforms*, *26*(5), pp.553-576.

Bradbrook, K., Waller, S., & Morris, D., 2005. National floodplain mapping: datasets and methods–160,000 km in 12 months. *Natural hazards*, *36*(1-2), 103-123

Bradbrook, K., 2006. JFLOW: a multiscale two‐dimensional dynamic flood model. *Water and Environment Journal*, *20*(2), 79-86.

Bretz, J. H., 1924. The Dalles type of river channel. *The Journal of Geology*, 139-149.

Burroughs, B.A., Hayes, D.B., Klomp, K.D., Hansen, J.F. and Mistak, J., 2009. Effects of Stronach dam removal on fluvial geomorphology in the Pine River, Michigan, United States. *Geomorphology*, *110*(3), pp.96-107.

Busulwa, H. S., & Bailey, R. G., 2004. Aspects of the physico‐chemical environment of the Rwenzori rivers, Uganda. *African Journal of Ecology*, *42*(s1), 87-92.

Carling, P.A., 1991. An appraisal of the velocity‐reversal hypothesis for stable pool‐riffle sequences in the River Severn, England. *Earth Surface Processes and Landforms*, *16*(1), pp.19-31.

Carling, P.A. and Wood, N., 1994. Simulation of flow over pool-riffle topography: a consideration of the velocity reversal hypothesis. *Earth Surface Processes and Landforms*, *19*(4), pp.319-332.

Chanson, H., 1996. Prediction of the transition nappe/skimming flow on a stepped channel. *Journal of Hydraulic Research*, *34*(3), pp.421-429.

Charlton, R., 2007. *Fundamentals of fluvial geomorphology*. London: Routledge.

Chikoore, H., Vermeulen, J.H. and Jury, M.R., 2015. Tropical cyclones in the Mozambique Channel: January–March 2012. *Natural Hazards*, *77*(3), pp.2081-2095.

Chin, A., 2002. The periodic nature of step-pool mountain streams. *American Journal of Science*, *302*(2), 144-167.

Church, M., 1992. Channel morphology and typology. *The rivers handbook*, *1*, pp.126-143.

Church, M., 2002. Geomorphic thresholds in riverine landscapes. *Freshwater biology*, *47*(4), 541-557.

Codd, L. E. W., 1951. Trees and shrubs of the Kruger National Park. *Trees and shrubs of the Kruger National Park.* 192pp.

Codron, J., Lee-Thorp, J. A., Sponheimer, M., Codron, D., Grant, R. C., & de Ruiter, D. J., 2006. Elephant (Loxodonta africana) diets in Kruger National Park, South Africa: spatial and landscape differences. *Journal of Mammalogy*, *87*(1), 27-34.

Coetzee, B. J., Engelbrecht, A. H., Joubert, S. C. J., & Retief, P. F., 1979. Elephant impact on Sclerocarya caffra trees in Acacia nigrescens tropical plains thornveld of the Kruger National Park. *Koedoe*, *22*(1), 39-60.

Comiti, F., Cadol, D. and Wohl, E., 2009. Flow regimes, bed morphology, and flow resistance in self‐formed step‐pool channels. *Water Resources Research*, *45*(4).

CNES/Astrium, 2011. *Satellite imagery of the Sabie River*. [photograph]{Accessed December 2015}.

Crosby, B.T. and Whipple, K.X., 2006. Knickpoint initiation and distribution within fluvial networks: 236 waterfalls in the Waipaoa River, North Island, New Zealand. *Geomorphology*, *82*(1), pp.16-38.

D'angelo, D.J., Webster, J.R., Gregory, S.V. and Meyer, J.L., 1993. Transient storage in Appalachian and Cascade mountain streams as related to hydraulic characteristics. *Journal of the North American Benthological Society*, pp.223-235.

D'Agostino, V. and Michelini, T., 2015. On kinematics and flow velocity prediction in step‐pool channels. *Water Resources Research*. 51(6), 4650-4667.

Death, R. G., & Joy, M. K., 2004. Invertebrate community structure in streams of the Manawatu–Wanganui region, New Zealand: the roles of catchment versus reach scale influences. *Freshwater Biology*, *49*(8), 982-997.

DigitalGlobe., 2015. *Google Earth images*. [Online] Available via Google Earth {Accessed 28th December 2014}.

Dow, F., & Saillofest, O., 2008. 2D modelling of sewer flooding in the urban environment. *Water and Urban Development Paradigms: Towards an Integration of Engineering, Design and Management Approaches*, 277.

Dyson, L. L., & Van Heerden, J., 2001. The heavy rainfall and floods over the northeastern interior of South Africa during February 2000. *South African Journal of Science*, *97*(3 & 4), p-80.

Eckhardt, H. C., Wilgen, B. W., & Biggs, H. C., 2000. Trends in woody vegetation cover in the Kruger National Park, South Africa, between 1940 and 1998. *African Journal of Ecology*, *38*(2), 108-115.

Entwistle, N. S., Heritage, G., Tooth, S., & Milan, D., 2014. Anastomosing reach control on hydraulics and sediment distribution on the Sabie River, South Africa. *Proceedings of the International Association of Hydrological Sciences*, (367), 215-219.

Feng, K., & Molz, F. J., 1997. A 2-D, diffusion-based, wetland flow model. *Journal of Hydrology*, *196*(1), 230-250.

Ferguson, R.I., Prestegaard, K.L. and Ashworth, P.J., 1989. Influence of sand on hydraulics and gravel transport in a braided gravel bed river. *Water Resources Research*, *25*(4), pp.635-643.

Ferguson, R.J. and Brierley, G.J., 1999. Levee morphology and sedimentology along the lower Tuross River, south‐eastern Australia. *Sedimentology*, *46*(4), pp.627-648.

Fotogramensura., 1999. *Aerial LiDAR of Sabie River.* [Photograph] {Accessed March 2015}.

Fotogramensura, 2000. *Aerial LiDAR of Sabie River.* [Photograph] {Accessed March 2015}.

Fotogramensura, 2002. *Aerial LiDAR of Sabie River.* [Photograph] {Accessed March 2015}.

Frissell, C.A., Liss, W.J., Warren, C.E. and Hurley, M.D., 1986. A hierarchical framework for stream habitat classification: viewing streams in a watershed context. *Environmental management*, *10*(2), pp.199-214.

Gardner, T.W., 1983. Experimental study of knickpoint and longitudinal profile evolution in cohesive, homogeneous material. *Geological Society of America Bulletin*, *94*(5), pp.664-672.

Graf, W.L., 1978. Fluvial adjustments to the spread of tamarisk in the Colorado Plateau region. *Geological Society of America Bulletin*, *89*(10), pp.1491-1501.

Graf, W. L., 1979. Rapids in canyon rivers. *The Journal of Geology*, 533-551.

Graf, W.L., 1980. The effect of dam closure on downstream rapids. *Water Resources Research*, *16*(1), pp.129-136.

Grant, G. E., Swanson, F. J., & Wolman, M. G., 1990. Pattern and origin of stepped-bed morphology in high-gradient streams, Western Cascades, Oregon. *Geological Society of America Bulletin*, *102*(3), 340-352.

Gonzalez, C.A., Takahashi, M. and Chanson, H., 2008. An experimental study of effects of step roughness in skimming flows on stepped chutes. *Journal of Hydraulic Research*, *46*(sup1), pp.24-35.

Gregory, K.J. and Walling, D.E., 1973. Drainage basins form and processes: a geomorphological approach. *Huddersfield, WY, United Kingdom*. 456pp.

Gupta, A., Kale, V. S., & Rajaguru, S. N., 1999. The Narmada River, India, through space and time. *Varieties of Fluvial Form. Wiley, Chichester*, 113-143.

Gutro, R., 2012a. Hurricane Season 2012: Tropical depression Dando (Southern Indian Ocean): Tropical Depression Dando flooded Mozambique. [online] Available at: <http://www.nasa.gov/mission_pages/hurricanes/archives/2012/h2012_dando.html> {accessed 24th August 2014}

Gutro, R., 2012b. NASAs TRMM Satellite sees light rainfall over Mozambique from tropical depression Dando.[online] National Aeronautical and Space Administration. Available at:

<http://www.nasa.gov/mission_pages/hurricanes/archives/2012/h2012_dando.html> {accessed 24th August 2014}

Halwas, K. L., & Church, M., 2002. Channel units in small, high gradient streams on Vancouver Island, British Columbia. *Geomorphology*, *43*(3), 243-256.

Hattingh, J. and Rust, I., 1999. Drainage evolution and morphological development of the late Cenozoic Sundays River, South Africa. *Varieties of Fluvial Form. International Association of Geomorphologists Geomorphology Publication*, *7*, pp.145-166.

Harrison, L.R. and Keller, E.A., 2007. Modeling forced pool–riffle hydraulics in a boulder-bed stream, southern California. *Geomorphology*, *83*(3), pp.232-248.

Heitmuller, F. T., Hudson, P. F., & Asquith, W. H., 2015. Lithologic and hydrologic controls of mixed alluvial–bedrock channels in flood-prone fluvial systems: Bankfull and macrochannels in the Llano River watershed, central Texas, USA. *Geomorphology*, *232*, 1-19.

Heritage, G.L., Birkhead, A.L., Broadhurst, L.J. and Harnett, B.R., 1999. The influence of flooding on the erodibility of cohesive sediments along the Sabie River, South Africa. *Fluvial Sedimentology VI, IAS Special Publication*, *28*, pp.131-146.

Heritage, G. L., Van Niekerk, A. W., & Moon, B. P., 1999. Geomorphology of the Sabie River, South Africa: an incised bedrock-influenced channel. *Varieties of Fluvial Form*, 53-79.

Heritage, G. L., Broadhurst, L. J., & Birkhead, A. L., 2001. The influence of contemporary flow regime on the geomorphology of the Sabie River, South Africa. *Geomorphology*, *38*(3), 197-211.

Heritage, G. L., Charlton, M. E., & O'Regan, S., 2001. Morphological classification of fluvial environments: An investigation of the continuum of channel types. *The Journal of Geology*, *109*(1), 21-33.

Heritage, G. L., Large, A. R. G., Moon, B. P., & Jewitt, G., 2004. Channel hydraulics and geomorphic effects of an extreme flood event on the Sabie River, South Africa. *Catena*, *58*(2), 151-181.

Heritage, G.L. and Milan, D.J., 2004. A conceptual model of the role of excess energy in the maintenance of a riffle–pool sequence. *Catena*, *58*(3), pp.235-257.

Heritage, G.L., Milan, D.J., Large, A.R. and Fuller, I.C., 2009. Influence of survey strategy and interpolation model on DEM quality. *Geomorphology*, *112*(3), pp.334-344.

Heritage, G.L., Milan, D.J. and Entwistle, N.S., 2010. Temporal change in hydraulic habitat inferred from a high resolution 2D flow modelling approach. *BHS Third International Symposium, Managing Consequences of a Changing Global Environment, Newcastle 2010,* pp. 1-6.

Heritage, G., Tooth, S., Entwistle, N. S., & Milan, D., 2014. Long-term flood controls on semi-arid river form: evidence from the Sabie and Olifants rivers, eastern South Africa. *Proceedings of the International Association of Hydrological Sciences*, *367*, 141-146.

Holmes, P. M., Richardson, D. M., Esler, K. J., Witkowski, E. T. F., & Fourie, S., 2005. A decision-making framework for restoring riparian zones degraded by invasive alien plants in South Africa: review article. *South African Journal of Science*, *101*(11 & 12), p-553.

Howard, A. D., Dietrich, W. E., & Seidl, M. A., 1994. Modeling fluvial erosion on regional to continental scales. *Journal of Geophysical research – all series*, *99*, 13-971.

Howard, A. D., 1998. Long profile development of bedrock channels: Interaction of weathering, mass wasting, bed erosion, and sediment transport. *Geophysical Monograph-American Geophysical Union*, *107*, 297-319.

Hunter, N. M., Bates, P. D., Neelz, S., Pender, G., Villanueva, I., Wright, N. G., & Mason, D., 2008. Benchmarking 2D hydraulic models for urban flood simulations. In *Proceedings of the Institution of Civil Engineers: Water Management* (Vol. 161, No. 1, pp. 13-30). Thomas Telford (ICE publishing).

Inoue, T., Izumi, N., Shimizu, Y. and Parker, G., 2014. Interaction among alluvial cover, bed roughness, and incision rate in purely bedrock and alluvial-bedrock channel. *Journal of Geophysical Research: Earth Surface*, *119*(10), pp.2123-2146.

Jansen, J.D., 2006. Flood magnitude–frequency and lithologic control on bedrock river incision in post-orogenic terrain. *Geomorphology*, *82*(1), pp.39-57.

Kale, V. S., Ely, L. L., Enzel, Y., & Baker, V. R., 1994. Geomorphic and hydrologic aspects of monsoon floods on the Narmada and Tapi Rivers in central India. *Geomorphology*, *10*(1), 157-168.

Kale, V.S., Baker, V.R. and Mishra, S., 1996. Multi-channel patterns of bedrock rivers: An example from the central Narmada basin, India. *Catena*, *26*(1), pp.85-98.

Keller, E.A., 1971. Areal sorting of bed-load material: the hypothesis of velocity reversal. *Geological Society of America Bulletin*, *82*(3), pp.753-756.

Keller, E.A., 1999. The transportation of debris by running water, by Grove Karl Gilbert. *Geological Society of America Special Papers*, *338*, pp.253-256.

Keller, E.A. and Florsheim, J.L., 1993. Velocity-reversal hypothesis: A model approach. *Earth Surface Processes and Landforms*, *18*(8), pp.733-740.

Knighton, D., 1998. *Fluvial forms and processes: a new perspective*. Routledge.

Leopold Luna, B., Wolman, M.G. and Miller, J.P., 1964. Fluvial processes in geomorphology. San Francisco: WH Freeman. 522pp.

Leopold, L.B., 1969. The rapids and the pools—Grand Canyon. *United States Geological Survey Professional Paper*, *669*, pp.131-145.

Lisle, T., 1979. A sorting mechanism for a riffle-pool sequence: summary. *Geological Society of America Bulletin*, *90*(7), pp.616-617.

Lisle, T. E., 1982. Effects of aggradation and degradation on riffle-pool morphology in natural gravel channels, northwestern California. *Water Resources Research*, *18*(6), 1643-1651.

Maner, J. L., 2010. Controls on knickpoint formation, Big South Fork River, Tennessee. *In 2010 GSA Denver Annual Meeting.*

Marchi, L., Cavalli, M., Amponsah, W., Borga, M. and Crema, S., 2015. Upper limits of flash flood stream power in Europe. *Geomorphology*.

Mason, P. J.,1984. Erosion of plunge pools downstream of dams due to the action of free-trajectory jets. In *ICE Proceedings* (Vol. 76, No. 2, pp. 523-537).

Merritt, D. M., & Wohl, E. E., 2002. Processes governing hydrochory along rivers: hydraulics, hydrology, and dispersal phenology. *Ecological Applications*, *12*(4), 1071-1087.

Meshkova, L. V., & Carling, P. A., 2012. The geomorphological characteristics of the Mekong River in northern Cambodia: A mixed bedrock–alluvial multi-channel network. *Geomorphology*, *147*, 2-17.

Milan, D.J., Heritage, G.L., Large, A.R.G. and Entwistle, N.S., 2010. Mapping hydraulic biotopes using terrestrial laser scan data of water surface properties. *Earth Surface Processes and Landforms*, *35*(8), pp.918-931.

Milan, D. J., Tooth, S., & Heritage, G. L. (2012). *Assessing geomorphic impacts on the Sabie River, South Africa, following the cyclone Dando floods January 2012, using repeat aerial LiDAR*. Unpublished poster presentation at: American Geophysics union's fall meeting December 2012.

Milan, D.J., 2013. Sediment routing hypothesis for pool-riffle maintenance. *Earth Surface Processes and Landforms*, *38*(14), pp.1623-1641.

Miller, A.J., 1994. Debris-fan constrictions and flood hydraulics in river canyons: Some implications from two-dimensional flow modelling. *Earth Surface Processes and Landforms*, *19*(8), pp.681-697.

Milner, V.S. and Gilvear, D.J., 2012. Characterization of hydraulic habitat and retention across different channel types; introducing a new field-based technique. *Hydrobiologia*, *694*(1), pp.219-233.

Montgomery, D.R., Buffington, J.M., Smith, R.D., Schmidt, K.M. and Pess, G., 1995. Pool spacing in forest channels. *Water resources research*. Vol: 31(4), pp. 1097 – 1105.

Moon, B. P., Van Niekerk, A. W., Heritage, G. L., Rogers, K. H., & James, C. S., 1997. A geomorphological approach to the ecological management of rivers in the Kruger National Park: the case of the Sabie River. *Transactions of the institute of British Geographers*, 31-48.

Moon, B.P. and Heritage, G.L., 2001. The contemporary geomorphology of the Letaba River in the Kruger National Park. *Koedoe*, *44*(1), pp.45-55.

Nanson, G.C., 1986. Episodes of vertical accretion and catastrophic stripping: a model of disequilibrium flood-plain development. *Geological Society of America Bulletin*, *97*(12), pp.1467-1475.

Nardi, L. and Rinaldi, M., 2015. Spatio‐temporal patterns of channel changes in response to a major flood event: the case of the Magra River (central–northern Italy). *Earth Surface Processes and Landforms*, *40*(3), pp.326-339.

Newson, M.D. and Newson, C.L., 2000. Geomorphology, ecology and river channel habitat: mesoscale approaches to basin-scale challenges. *Progress in Physical Geography*, *24*(2), pp.195-217.

Nittrouer, J. A., Mohrig, D., Allison, M. A., & Peyret, A. P. B., 2011. The lowermost Mississippi River: a mixed bedrock‐alluvial channel. *Sedimentology*, *58*(7), 1914-1934.

O'Connor, J.E., Webb, R.H. and Baker, V.R., 1986. Paleohydrology of pool-and-riffle pattern development: Boulder Creek, Utah. *Geological Society of America Bulletin*, *97*(4), pp.410-420.

Olivier, J., & De Rautenbach, C. J., 2002. The implementation of fog water collection systems in South Africa. *Atmospheric Research*, *64*(1), 227-238.

Ortega, J. A., Gómez-Heras, M., Perez-López, R., & Wohl, E., 2014. Multiscale structural and lithologic controls in the development of stream potholes on granite bedrock rivers. *Geomorphology*, *204*, 588-598.

Parsons, M., McLoughlin, C. A., Kotschy, K. A., Rogers, K. H., & Rountree, M. W., 2005. The effects of extreme floods on the biophysical heterogeneity of river landscapes. *Frontiers in Ecology and the Environment*, *3*(9), 487-494.

Parsons, M., McLoughlin, C. A., Rountree, M. W., & Rogers, K. H., 2006. The biotic and abiotic legacy of a large infrequent flood disturbance in the Sabie River, South Africa. *River Research and Applications*, *22*(2), 187-201.

Petr, T., 1970. The bottom fauna of the rapids of the Black Volta River in Ghana. *Hydrobiologia*, *36*(3-4), pp.399-418.

Petts, G. and Foster, I., 1985. *Rivers and landscape*. Univ. of Technology, Loughborough, pp. 274.

Phillips, J. D., McCormack, S., Duan, J., Russo, J. P., Schumacher, A. M., Tripathi, G. N., & Pulugurtha, S., 2010. Origin and interpretation of knickpoints in the Big South Fork River basin, Kentucky–Tennessee. *Geomorphology*, *114*(3), 188-198.

Rajaguru, S.N., Gupta, A., Kale, V.S., Mishra, S., Ganjoo, R.K., Ely, L.L., Enzel, Y. and Baker, V.R., 1995. Channel form and processes of the flood-dominated Narmada River, India. *Earth Surface Processes and Landforms*, *20*(5), pp.407-421.

Reason, C. J. C., & Keibel, A., 2004. Tropical cyclone Eline and its unusual penetration and impacts over the southern African mainland. *Weather and forecasting*, *19*(5), 789-805.

Reason, C. J. C., Hachigonta, S., & Phaladi, R. F., 2005. Interannual variability in rainy season characteristics over the Limpopo region of southern Africa. *International Journal of Climatology*, *25*(14), 1835-1853.

Reason, C. J. C., Engelbrecht, F., Landman, W. A., Lutjeharms, J. R. E., Piketh, S., Rautenbach, C. D. W., & Hewitson, B. C., 2006. A review of South African research in atmospheric science and physical oceanography during 2000-2005: review article. *South African journal of science*, *102*(1 & 2), p-35.

Rhoads, B.L. and Kenworthy, S.T., 1995. Flow structure at an asymmetrical stream confluence. *Geomorphology*, *11*(4), pp.273-293.

Richards, K.S., 1976. The morphology of riffle-pool sequences. *Earth Surface Processes*, *1*(1), pp.71-88.

Richards, K.S., 1978. Simulation of flow geometry in a riffle-pool stream. *Earth surface processes*, *3*(4), pp.345-354.

Rinaldi, M., Amponsah, W., Benvenuti, M., Borga, M., Comiti, F., Lucía, A., Marchi, L., Nardi, L., Righini, M. and Surian, N., 2016. An integrated approach for investigating geomorphic response to extreme events: methodological framework and application to the October 2011 flood in the Magra River catchment, Italy. *Earth Surface Processes and Landforms*.

Robert, A., 2011. Flow resistance in alluvial channels. *Progress in Physical Geography*, *35*(6), pp.765-781.

Rountree, M. W., Heritage, G. L., Rogers, K. H., & Acreman, M. C., 2001. In-channel metamorphosis in a semiarid, mixed bedrock/alluvial river system: implications for Instream Flow Requirements. *IAHS Publications-Series of Proceedings and Reports-Intern Assoc Hydrological Sciences*, *266*, 113-124.

Roux, D.J., Nel, J.L., Ashton, P.J., Deacon, A.R., de Moor, F.C., Hardwick, D., Hill, L., Kleynhans, C.J., Maree, G.A., Moolman, J. and Scholes, R.J., 2008. Designing protected areas to conserve riverine biodiversity: lessons from a hypothetical redesign of the Kruger National Park. *Biological Conservation*, *141*(1), pp.100-117.

Sawyer, A.M., Pasternack, G.B., Moir, H.J. and Fulton, A.A., 2010. Riffle-pool maintenance and flow convergence routing observed on a large gravel-bed river. *Geomorphology*, *114*(3), pp.143-160.

Schmidt, J. C., Parnell, R. A., Grams, P. E., Hazel, J. E., Kaplinski, M. A., Stevens, L. E., & Hoffnagle, T. L., 2001. The 1996 controlled flood in Grand Canyon: flow, sediment transport, and geomorphic change. *Ecological Applications*, *11*(3), 657-671.

Schutte, I. C., 1986. The general geology of the Kruger National Park. *Koedoe*, *29*(1), 13-37.

Shoffner D, & Royall D., 2008. Hydraulic habitat composition and diversity in rural and urban stream reaches of the North Carolina piedmont (USA). River Research and Applications 24: 1082–1103.

Smithers, J. C., Schulze, R. E., Pike, A., & Jewitt, G. P. W., 2001. A hydrological perspective of the February 2000 floods: A case study in the Sabie River Catchment. *Water SA*, *27*(3), 325-332.

Stark, C.P., 2006. A self-regulating model of bedrock river channel geometry. *Geophysical Research Letters*, *33*(4).

Stear, W. M., 1985. Comparison of the bedform distribution and dynamics of modern and ancient sandy ephemeral flood deposits in the southwestern Karoo region, South Africa. *Sedimentary Geology*, *45*(3), 209-230.

Thompson, D.M., Wohl, E.E. and Jarrett, R.D., 1996. A revised velocity-reversal and sediment-sorting model for a high-gradient, pool-riffle stream. *Physical Geography*, *17*(2), pp.142-156.

Thompson, D.M., Nelson, J.M. and Wohl, E.E., 1998. Interactions between pool geometry and hydraulics. *Water Resources Research*, *34*(12), pp.3673-3681.

Thompson, D.M., 2011. The velocity-reversal hypothesis revisited. *Progress in Physical Geography*, *35*(1), pp.123-132.

Thompson, C.J., Croke, J., Fryirs, K. and Grove, J.R., 2016. A channel evolution model for subtropical macrochannel systems. *CATENA*, *139*, pp.199-213.

Tinkler, K. J., 1993. Fluvially sculpted rock bedforms in twenty mile creek, Niagara Peninsula, Ontario. *Canadian Journal of Earth Sciences*, *30*(5), 945-953.

Tooth, S., & McCarthy, T. S., 2004. Anabranching in mixed bedrock-alluvial rivers: the example of the Orange River above Augrabies Falls, Northern Cape Province, South Africa. *Geomorphology*, *57*(3), 235-262.

Torrente-Vilara, G., Zuanon, J., Leprieur, F., Oberdorff, T., & Tedesco, P. A., 2011. Effects of natural rapids and waterfalls on fish assemblage structure in the Madeira River (Amazon Basin). *Ecology of Freshwater Fish*, *20*(4), 588-597.

Van Coller, A., Rogers, K. and Heritage, G., 1997. Linking riparian vegetation types and fluvial geomorphology along the Sabie River within the Kruger National Park, South Africa. *African Journal of Ecology*, *35*(3), pp.194-212.

Van Niekerk, A. W., Heritage, G. L., & Moon, B. P., 1995. River classification for management: the geomorphology of the Sabie River in the eastern Transvaal. *South African Geographical Journal*, *77*(2), 68-76.

Van Niekerk, A. W., Heritage, G. L., Broadhurst, L. W., & Moon, B. P., 1999. Bedrock anastomosing channel systems: morphology and dynamics in the Sabie River, Mpumalanga Province, South Africa. *Varieties of Fluvial Form*, 33-51.

Van Wyk, P., & Fairall, N., 1969. The influence of the African elephant on the vegetation of the Kruger National Park. *Koedoe*, *12*(1), 57-89.

Venter, F. J., 1986. Soil patterns associated with the major geological units of the Kruger National Park. *Koedoe*, *29*(1), 125-138.

Venter, F. J., & Gertenbach, W. P. D., 1986. A cursory review of the climate and vegetation of the Kruger National Park. *Koedoe*, *29*(1), 139-148.

Vieira, M. L., 2015. *An assessment of instream flow requirements in the sabie-sand river catchment* (Doctoral dissertation, Faculty of Science, University of the Witwatersrand, Johannesburg).

Wadeson, R.A. and Rowntree, K.M., 1998. Application of the hydraulic biotope concept to the classification of instream habitats. *Aquatic Ecosystem Health & Management*, *1*(2), pp.143-157.

Wang, Z.Y., Melching, C.S., Duan, X.H. and Yu, G.A., 2009. Ecological and hydraulic studies of step-pool systems. *Journal of Hydraulic Engineering*, *135*(9), pp.705-717.

Whittaker, J.G., 1987. Sediment transport in step-pool streams. *Sediment Transport in Gravel-Bed Rivers. John Wiley and Sons New York. 1987. p 545-579, 20 fig, 40 ref.*

Wilcox, A.C. and Wohl, E.E., 2006. Flow resistance dynamics in step-pool stream channels: 1. Large woody debris and controls on total resistance. *Water Resources Research*, *42*(5).

Wilcox, A.C., Nelson, J.M. and Wohl, E.E., 2006. Flow resistance dynamics in step-pool channels: 2. Partitioning between grain, spill, and woody debris resistance. *Water Resources Research*, *42*(5).

Wildman, L.A. and MacBroom, J.G., 2005. The evolution of gravel bed channels after dam removal: Case study of the Anaconda and Union City Dam removals. *Geomorphology*, *71*(1), pp.245-262.

Williams, C. J. R., & Kniveton, D. R., 2012. Atmosphere-land surface interactions and their influence on extreme rainfall and potential abrupt climate change over southern Africa. *Climatic change*, *112*(3-4), 981-996.

Wohl, E.E., 1992. Gradient irregularity in the Herbert Gorge of northeastern Australia. *Earth surface processes and landforms*, *17*(1), pp.69-84.

Wohl, E.E. and Thompson, D.M., 2000. Velocity characteristics along a small step–pool channel. *Earth surface processes and landforms*, *25*(4), pp.353-367.

World Meteorological organisation., 2012. *Review of the 2010/2011 and 2011/2012 cyclone season: Reports of Members on significant/notable cyclone of the seasons: Report from the Republic of Mozambique*. RA I/TCC-20/Doc. 4.2(3) (24.VIII.2012). 4pp.

Yair, A., & Kossovsky, A., 2002. Climate and surface properties: hydrological response of small arid and semi-arid watersheds. *Geomorphology*, *42*(1), 43-57.

Yu, D., & Lane, S. N., 2006. Urban fluvial flood modelling using a two-dimensional diffusion-wave treatment, part 1: mesh resolution effects. *Hydrological Processes*, *20*(7), 1541-1565.

Zavadil, E. A., Stewardson, M. J., Turner, M. E., & Ladson, A. R., 2012. An evaluation of surface flow types as a rapid measure of channel morphology for the geomorphic component of river condition assessments. *Geomorphology*, *139*, 303-312.

Zimmermann, A., & Church, M., 2001. Channel morphology, gradient profiles and bed stresses during flood in a step–pool channel. *Geomorphology*, *40*(3), 311-327.